frontiers | Research Topics

Case reports in cardiovascular imaging 2023

Edited by
Riccardo Liga, Grigorios Korosoglou and Ali Yilmaz

Published in
Frontiers in Cardiovascular Medicine

ISSN 1664-8714
ISBN 978-2-8325-4997-1
DOI 10.3389/978-2-8325-4997-1

About Frontiers

Frontiers is more than just an open access publisher of scholarly articles: it is a pioneering approach to the world of academia, radically improving the way scholarly research is managed. The grand vision of Frontiers is a world where all people have an equal opportunity to seek, share and generate knowledge. Frontiers provides immediate and permanent online open access to all its publications, but this alone is not enough to realize our grand goals.

Frontiers journal series

The Frontiers journal series is a multi-tier and interdisciplinary set of open-access, online journals, promising a paradigm shift from the current review, selection and dissemination processes in academic publishing. All Frontiers journals are driven by researchers for researchers; therefore, they constitute a service to the scholarly community. At the same time, the *Frontiers journal series* operates on a revolutionary invention, the tiered publishing system, initially addressing specific communities of scholars, and gradually climbing up to broader public understanding, thus serving the interests of the lay society, too.

Dedication to quality

Each Frontiers article is a landmark of the highest quality, thanks to genuinely collaborative interactions between authors and review editors, who include some of the world's best academicians. Research must be certified by peers before entering a stream of knowledge that may eventually reach the public - and shape society; therefore, Frontiers only applies the most rigorous and unbiased reviews. Frontiers revolutionizes research publishing by freely delivering the most outstanding research, evaluated with no bias from both the academic and social point of view. By applying the most advanced information technologies, Frontiers is catapulting scholarly publishing into a new generation.

What are Frontiers Research Topics?

Frontiers Research Topics are very popular trademarks of the *Frontiers journals series*: they are collections of at least ten articles, all centered on a particular subject. With their unique mix of varied contributions from Original Research to Review Articles, Frontiers Research Topics unify the most influential researchers, the latest key findings and historical advances in a hot research area.

Find out more on how to host your own Frontiers Research Topic or contribute to one as an author by contacting the Frontiers editorial office: frontiersin.org/about/contact

Case reports in cardiovascular imaging: 2023

Topic editors

Riccardo Liga — Pisana University Hospital, Italy

Grigorios Korosoglou — GRN Klinik Weinheim, Germany

Ali Yilmaz — University Hospital Münster, Germany

Citation

Liga, R., Korosoglou, G., Yilmaz, A., eds. (2024). *Case reports in cardiovascular imaging: 2023*. Lausanne: Frontiers Media SA. doi: 10.3389/978-2-8325-4997-1

Table of contents

frontiers | Frontiers in Cardiovascular Medicine

TYPE Editorial
PUBLISHED 29 May 2024
DOI 10.3389/fcvm.2024.1424893

OPEN ACCESS

EDITED AND REVIEWED BY
Christos Bourantas,
Queen Mary University of London,
United Kingdom

*CORRESPONDENCE
Grigorios Korosoglou
gkorosoglou@hotmail.com

RECEIVED 28 April 2024
ACCEPTED 20 May 2024
PUBLISHED 29 May 2024

CITATION
Liga R and Korosoglou G (2024) Editorial: Case reports in cardiovascular imaging 2023. Front. Cardiovasc. Med. 11:1424893. doi: 10.3389/fcvm.2024.1424893

Editorial: Case reports in cardiovascular imaging 2023

Riccardo Liga[1,2] and Grigorios Korosoglou[3,4]*

[1]Department of Surgical Pathology, University of Pisa, Pisa, Italy, [2]Cardiothoracic and Vascular Department, University Hospital of Pisa, Pisa, Italy, [3]Department of Cardiology, Vascular Medicine and Pneumology, GRN Hospital Weinheim, Weinheim, Germany, [4]Cardiac Imaging Center Weinheim, Hector Foundation, Weinheim, Germany

KEYWORDS

echocardiography, cardiac magnetic resonance (CMR), cardiac computed tomography (CCT), cardiac imaging, interventional cardiology

Editorial on the Research Topic
Case reports in cardiovascular imaging: 2023

Echocardiography is considered as the "working horse" imaging technique and is used for the assessment of left-ventricular (LV), right-ventricular (RV), and valvular function as well as myocardial strain if required. While echocardiography is a bedside imaging technique, which can be performed without contrast or radiation exposure for the patients, it is dependent on the experience of the operators and on the acoustic windows. CMR, on the other hand, can provide tomographic information of myocardial function, perfusion, viability, and, if required, strain, metabolism, and valvular function, without being limited by the acoustic windows of the patients. CMR is considered the gold-standard for the assessment of chamber dimensions and function as well as the characterization and risk stratification of patients with ischemic heart disease, myocarditis, heart failure, and cardiomyopathy (1–4). Cardiac computed tomography angiography (CCTA) provides isotropic 3D visualization of cardiac structures, including moving coronary arteries with high spatial and temporal resolution and excellent image quality. Additionally, for the visualization of the coronary artery lumen, as provided by invasive coronary angiography, CCTA enables the assessment of the coronary vessel wall, including quantification of plaque volume and composition and assessment of the presence of high-risk coronary plaque features (5, 6), which have been described as precursors of plaque rupture, causing acute coronary syndromes (ACS) (7, 8). Finally, nuclear cardiac imaging techniques allow both the assessment of regional myocardial perfusion (9, 10) and the unique opportunity to perform molecular cardiac imaging with different radiotracers directed towards different molecular targets (11, 12).

Herein, we present and discuss some high-quality case reports from the area of cardiovascular imaging, aiming to enhance its role in clinical practice and contributing to improved diagnostic work-up, patient management, and, potentially, outcomes.

The role of CCTA for guiding PCI is nicely presented in the article by Su et al. on an 83-year-old man with diabetes mellitus, presenting with non-ST-elevation myocardial infarction. CCTA revealed the presence of a single coronary ostium with origin of the left and right coronary artery from the right sinus of Valsalva. The patient was successfully treated with PCI and implantation of several drug-eluting-coronary stents with a good angiographic result.

Coronary artery disease and coronary anomalies are largely represented in our case collection. Thus, the role of CCTA in the diagnosis of coronary artery disease is highlighted in the article by Korosoglou et al., where CCTA detected significant lumen narrowing in a patient with symptomatic coronary artery disease, triggering coronary revascularization by PCI. In addition, CCTA demonstrated attenuated progression of non-calcified atherosclerotic plaque during lipid-lowering treatment of the patient with bempedoic acid, which was attributed to substantial low-density-cholesterol reduction.

Although rare, coronary artery anomalies may have a significant functional and prognostic impact. In this regard, McAlpin et al. reported the case of a 14-year-old boy with a single coronary artery originating from the right coronary sinus. While the suspicion of a coronary anomaly came by transthoracic echocardiography, the final diagnosis required CCTA that also identified the inter-arterial and intramural course of the left coronary artery.

In the article by Oh et al., myocardial perfusion SPECT imaging provided functional information in a 52-year-old woman who had suffered a myocardial infarction with non-obstructive coronary arteries (MINOCA) due to coronary vasospasm at the level of a myocardial bridge, as demonstrated by intravascular ultrasound and CCTA.

Cardiac masses and tumors constitute another important field, where multi-modality cardiac imaging is often required to establish the correct diagnosis (13). The importance of multi-modal imaging in this regard was nicely demonstrated by Li et al. in a very young 23-year-old patient with a primary pericardial sarcoma. Information from CCTA, PET-CT, and CMR, the latter proving detailed visualization of cardiac and extracardiac structures, contributed to timely diagnosis, enabling optimal treatment planning.

Not only is the diagnosis of a cardiac tumor an important domain of cardiac imaging but so too is the differential diagnosis between cardiac tumors and normal anatomical structures of the heart. Thus, in the article by Akiki et al., the authors nicely demonstrated the potential of multi-modality cardiac imaging to establish the diagnosis of left atrial myxoma in a 73-year-old woman presenting with syncope. Echocardiography, CCTA, and CMR were used for pre-operative planning, and 3D printing of the tumor facilitated the use of a robotic approach for surgical removal of the tumor.

When cardiac masses are concerned, multimodality imaging may be particularly helpful for disease characterization and differential diagnosis. In this regard, the article by Kong et al. reported the case of a 69-year-old man with primary invasive cardiac angiosarcoma causing cardiac tamponade, whereby transthoracic echocardiography, chest CT, and magnetic resonance imaging were instrumental for tumor staging and for guiding patient management.

The role of multimodality imaging for the diagnosis of cardiac masses is also discussed by Yu et al., reporting on the application of advanced echocardiographic techniques and cardiac CT for the precise characterization of suspected lipomatous atrial septal hypertrophy coupled with atrial septal defect (ASD) in a 68-year-old woman.

In their article, Zhang et al. discussed the case of a 57-year-old woman with obstructive hypertrophic cardiomyopathy treated with "Echocardiography-guided Percutaneous IntraMyocardial Septal Radiofrequency Ablation" (PIMSRA, Liwen procedure). In this case, speckle tracking echocardiography was also able to detect the early improvement of regional cardiac function and the recovery of LV contractile synchronicity following treatment.

The use of nuclear cardiac imaging techniques for disease characterization is reported in two case reports. In the article by Jiang et al., molecular imaging with PET/CT using a ^{68}Ga-radiollabeled fibroblast activation protein inhibitor (FAPI) was shown to be able to detect the presence of early activated fibroblasts in a patient with unstable angina and monitor disease activity after coronary revascularization.

The clinical impact of experienced vs. non-experienced operators with echocardiography is nicely demonstrated by Caiati et al. in an 84-year-old woman who was referred to the echocardiographic laboratory for routine examination. The patient had chronic atrial fibrillation and history of heart failure and had been diagnosed with hypertensive heart disease as there was myocardial hypertrophy on the echocardiogram. The experienced view of a senior cardiologist and ultrasound contrast agent administration, however, helped to "unmask" the presence of severe apical hypertrophy of the left ventricle, establishing the correct diagnosis of apical hypertrophic cardiomyopathy.

Finally, the role of multi-modality cardiac imaging using invasive angiography, CCTA, and perfusion mapping of the lungs is nicely demonstrated by Goyal et al. in a 65-year-old man with dyspnea and history of pulmonary embolism 4 years prior to his index clinical presentation. Echocardiography showed RV-dilation with reduced function and CT demonstrated complete occlusion of the right pulmonary artery. Lung perfusion imaging demonstrated some areas of compensated perfusion in the right lung, which originated from coronary collaterals, as demonstrated by invasive coronary angiography. The patient underwent successful pulmonary thromboendarterectomy, which resulted in restoration of lung perfusion and right-ventricular function.

In conclusion, recent advances with non-invasive cardiac imaging are clinically relevant for the diagnostic-work up, timely diagnosis, and subsequent therapeutic management of patients with a multitude of cardiac disorders. All cases reported in our collection represent nice examples that demonstrate how cardiac and, if required, multimodality imaging can be incorporated into daily clinical practice to improve patient care and clinical outcomes.

Author contributions

RL: Writing – review & editing, Writing – original draft. GK: Writing – review & editing, Writing – original draft.

Conflict of interest

The authors declare that the research was conducted in the absence of any commercial or financial relationships that could be construed as a potential conflict of interest.

The author(s) declared that they were an editorial board member of Frontiers, at the time of submission. This had no impact on the peer review process and the final decision.

Publisher's note

References

1. Korosoglou G, Giusca S, Gitsioudis G, Erbel C, Katus HA. Cardiac magnetic resonance and computed tomography angiography for clinical imaging of stable coronary artery disease. Diagnostic classification and risk stratification. *Front Physiol*. (2014) 5:291. doi: 10.3389/fphys.2014.00291

2. von Knobelsdorff-Brenkenhoff F, Schuler J, Doganguzel S, Dieringer MA, Rudolph A, Greiser A, et al. Detection and monitoring of acute myocarditis applying quantitative cardiovascular magnetic resonance. *Circ Cardiovasc Imaging*. (2017) 10(2):e005242. doi: 10.1161/CIRCIMAGING.116.005242

3. Korosoglou G, Giusca S, Montenbruck M, Patel AR, Lapinskas T, Gotze C, et al. Fast strain-encoded cardiac magnetic resonance for diagnostic classification and risk stratification of heart failure patients. *JACC Cardiovasc Imaging*. (2021) 14 (6):1177–88. doi: 10.1016/j.jcmg.2020.10.024

4. Buss SJ, Breuninger K, Lehrke S, Voss A, Galuschky C, Lossnitzer D, et al. Assessment of myocardial deformation with cardiac magnetic resonance strain imaging improves risk stratification in patients with dilated cardiomyopathy. *Eur Heart J Cardiovasc Imaging*. (2015) 16(3):307–15. doi: 10.1093/ehjci/jeu181

5. Liga R, Marini C, Coceani M, Filidei E, Schlueter M, Bianchi M, et al. Structural abnormalities of the coronary arterial wall–in addition to luminal narrowing–affect myocardial blood flow reserve. *J Nucl Med*. (2011) 52(11):1704–12. doi: 10.2967/jnumed.111.091009

6. Anagnostopoulos CD, Siogkas PK, Liga R, Benetos G, Maaniitty T, Sakellarios AI, et al. Characterization of functionally significant coronary artery disease by a coronary computed tomography angiography-based index: a comparison with positron emission tomography. *Eur Heart J Cardiovasc Imaging*. (2019) 20(8):897–905. doi: 10.1093/ehjci/jey199

7. Gitsioudis G, Schussler A, Nagy E, Maurovich-Horvat P, Buss SJ, Voss A, et al. Combined assessment of high-sensitivity troponin T and noninvasive coronary plaque composition for the prediction of cardiac outcomes. *Radiology*. (2015) 276 (1):73–81. doi: 10.1148/radiol.15141110

8. Tesche C, Giesen A, Korosoglou G. Commentary: plaque features and epicardial fat volume for cardiovascular risk assessment-a key role with cardiac computed tomography? *Front Cardiovasc Med*. (2022) 9:896321. doi: 10.3389/fcvm.2022.896321

9. Gimelli A, Liga R, Duce V, Kusch A, Clemente A, Marzullo P. Accuracy of myocardial perfusion imaging in detecting multivessel coronary artery disease: a cardiac CZT study. *J Nucl Cardiol*. (2017) 24(2):687–95. doi: 10.1007/s12350-015-0360-8

10. Kalykakis GE, Antonopoulos AS, Pitsargiotis T, Siogkas P, Exarchos T, Kafouris P, et al. Relationship of endothelial shear stress with plaque features with coronary CT angiography and vasodilating capability with PET. *Radiology*. (2021) 300(3):549–56. doi: 10.1148/radiol.2021204381

11. Gimelli A, Liga R, Agostini D, Bengel FM, Ernst S, Hyafil F, et al. The role of myocardial innervation imaging in different clinical scenarios: an expert document of the European Association of Cardiovascular Imaging and Cardiovascular Committee of the European Association of Nuclear Medicine. *Eur Heart J Cardiovasc Imaging*. (2021) 22(5):480–90. doi: 10.1093/ehjci/jeab007

12. Thackeray JT. Molecular imaging using cardiac PET/CT: opportunities to harmonize diagnosis and therapy. *Curr Cardiol Rep*. (2021) 23(8):96. doi: 10.1007/s11886-021-01526-y

13. Giusca S, Kelle S, Korosoglou G. When tissue and outcomes are the issue. Cardiac magnetic resonance for patients with suspected cardiac tumours. *Eur Heart J*. (2021) 43(1):81–3. doi: 10.1093/eurheartj/ehab625

frontiers | Frontiers in Cardiovascular Medicine

TYPE Case Report
PUBLISHED 24 April 2023
DOI 10.3389/fcvm.2023.1157599

OPEN ACCESS

EDITED BY
Flavio D'Ascenzi,
University of Siena, Italy

REVIEWED BY
Gennady G. Taradin,
Donetsk National Medical University, Ukraine
Harald Becher,
University of Alberta Hospital, Canada

*CORRESPONDENCE
Carlo Caiati
carlo.caiati@uniba.it

RECEIVED 02 February 2023
ACCEPTED 03 April 2023
PUBLISHED 24 April 2023

CITATION
Caiati C, Stanca A and Lepera ME (2023) Case report: Diagnosis of apical hypertrophic cardiomyopathy that escaped clinical and echocardiographic investigations for twenty years: Reasons and clinical implications. Front. Cardiovasc. Med. 10:1157599. doi: 10.3389/fcvm.2023.1157599

Case report: Diagnosis of apical hypertrophic cardiomyopathy that escaped clinical and echocardiographic investigations for twenty years: Reasons and clinical implications

Carlo Caiati*, Alessandro Stanca and Mario Erminio Lepera

Unit of Cardiovascular Diseases, Department of Interdisciplinary Medicine, University of Bari "Aldo Moro", Bari, Italy

Background: Apical hypertrophic cardiomyopathy (ApHCM) is a rare form of hypertrophic cardiomyopathy which predominantly affects the apex of the left ventricle. The diagnosis can be challenging due to several factors, ranging from no typical clinical and electrocardiogram (EKG) findings to potential difficulties in executing and interpreting the echocardiographic examination.
Case presentation: We report the case of an 84-year-old woman who came to our echo-lab to undergo a routine echocardiogram. She had a history of permanent atrial fibrillation, paced rhythm and previous episodes of heart failure (HF), allegedly explained by a diagnosis of hypertensive heart disease that had been confirmed many times over the previous 20 years. The clinical examination and the EKG were unremarkable. The echocardiographic images were poor quality. But a senior cardiologist, expert in imaging and echocardiography, noted the lack of delineation of the endocardial border of the left ventricular (LV) apex region. Contrast echocardiography was performed and severe apical hypertrophy discovered.
Conclusion: ApHCM can be a challenging diagnosis. Contrast echocardiography must always be applied in cases of poor delineation of the LV apical endocardial border at baseline echocardiography. Timely detection and appropriate lifestyle intervention might slow the development of LV hypertrophy, and possibly minimize and delay heart failure (HF) related symptoms and arrhythmias. The prognosis remains relatively benign during long term follow-up.

KEYWORDS

apical hypertrophic cardiomyopathy, contrast echocardiography, heart failure, LV diastolic dysfunction, Doppler echocardiography

Introduction

Apical hypertrophic cardiomyopathy (ApHCM) is a form of hypertrophic cardiomyopathy, more frequently found in Asian population (up to 25% of all HCM cases) (1, 2). The prognosis is in general less severe than that of a classical HCM (1). However the complications rate has been reported at 30% being the myocardial infarction and atrial fibrillation the most frequent (1, 2), although other less frequent complications have been reported like left ventricular (LV) apical aneurism, embolic events, ventricular fibrillation, congestive heart failure (3). Although the disease is genetically transmitted,

the precise timing of diagnosis can be important since external factors can fuel the progression of the disease, strongly modulating its phenotypic expression (4, 5).

The diagnosis is based on clinical examinations, electrocardiogram (EKG) and echocardiography but each of these approaches can present limitations to such an extent that diagnosis can be missed as in our case for a long time. However critical interpretation of both the clinical symptoms and the echocardiogram can suggest the use of contrast echocardiography that can appropriately reveal the left ventricular apical abnormality. This is illustrated in the reported clinical case.

Clinical case

History

An 84-year-old woman with a history of obesity, hypertension, dyslipidaemia, carotid atherosclerosis and chronic obstructive pulmonary disease, presented to our echo-lab to undergo a routine echocardiogram. At the time, she had no complaints of chest pain, palpitations and dyspnoea at rest. There was no family history of sudden death, congestive heart failure or cardiomyopathy.

Twenty years before (in 2003) at the age of 64, after a syncopal episode, she had been implanted with a bicameral pacemaker for alleged sinoatrial node dysfunction; 9 years later the depleted battery was replaced.

About 15 years ago, (several years after pace-maker implantation) she was diagnosed with permanent atrial fibrillation and had since been on direct-acting oral anticoagulants.

In the last three years, she complained of dyspnoea following normal and less than normal physical activity (New York Heart Association [NYHA] class II-III). She also had limited mobility, due to back pain caused by multiple vertebral collapses, that further limited her physical capacity during effort. Therefore, the NYHA class was probably imprecise.

In 2020, a Holter EKG examination to verify pacemaker function identified an asymptomatic horizontal-down sloping ST-segment depression, suspicious for silent ischemia; for this reason she underwent coronary computed tomography angiography, that showed diffuse plaque involving the left anterior descending coronary artery (LAD), with >50% maximal segmental lumen narrowing. In the same year, she underwent coronary angiography; however, this did not confirm the critical LAD stenosis by Coronary Computed Angiography, so ruling out any significant coronary narrowing. Since intravascular ultrasound and coronary flow reserve were not assessed, diffuse coronary atherosclerosis could not be surely ruled out (6).

In 2022, the patient was admitted to an Internal Medicine ward, complaining of persistent fever lasting for several days and a confusional status. During hospitalization, a chest x-ray was performed which detected a consolidation in the right lung associated with an increase in inflammatory markers (C reactive protein = 17.8 mg/L), for which effective antibiotic therapy was initiated. Moreover, mild hyponatremia (129 mEq/L) was also observed and corrective treatment was administered. At discharge, a diagnosis of worsening heart failure, complicated by an acute bronchopneumonia episode, was made, although no clear explanation for this "chronic" heart failure was given. Increased dosage (50 mg/die) of a loop diuretic (furosemide) was prescribed.

Over the last twenty years, the patient had undergone several follow-up echocardiograms at qualified Hospitals, all in agreement as to the diagnosis of hypertensive heart disease.

Blood tests showed constant, modestly abnormal high pro-BNP (B-type natriuretic peptide) in the last year (**Figure 1**), which was systematically interpreted as chronic congestive heart failure caused

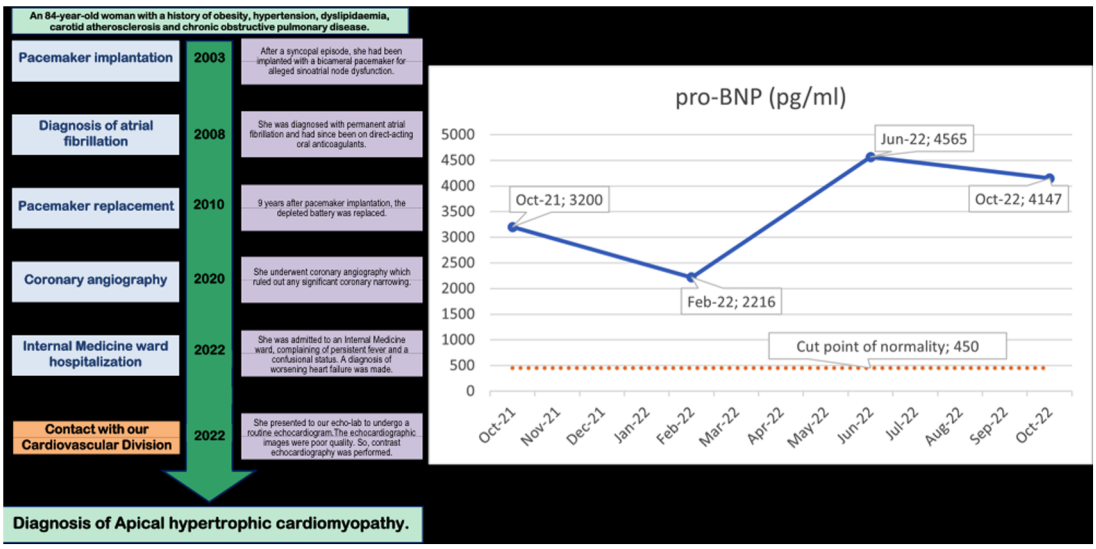

FIGURE 1
Timeline of clinical events in the 20 years before the diagnosis (on the left) and Pro-BNP values in the previous year (on the right). The Pro-BNP values are mildly but consistently abnormally high in each of the 4 evaluations.

by the hypertensive heart disease, with apparently isolated diastolic dysfunction. But this conflicted with the very mild hypertrophy of the LV. When she came to our attention for the echocardiographic evaluation her medical therapy included: apixaban 5 mg bis in die; pantoprazole 40 mg/die; bisoprolol 2,5 mg/die, furosemide 50 mg/die, canrenone 50 mg/die and digoxin 0,25 mg/die. Moreover, on the suspicion of ischemic heart disease, she had been taking rosuvastatin 10 mg/die, despite never suffering chest pain.

A timeline of the events occurring over the 20 years before the diagnosis of ApHCM is reported on the left side of the **Figure 1**.

Physicals

The patient was overweight (BMI 35.11 kg/m^2), with difficulty in walking. Physicals showed mildly increased systolic blood pressure (145/80 mmHg) (7), a well palpable apex beat in left lateral decubitus, substantially normal regarding amplitude and duration of the outward movement and without pre-systolic humps (but the patient was in atrial fibrillation [Afib]). The carotid amplitude pulse was normal but left the impression of a minimally brisk rate of rise. Jugular pulse inspection showed the absence of the x' descent, that was replaced by a significant x'v outward systolic wave followed by a very rapid y descent (secondary to significant tricuspid regurgitation). The hepato-jugular reflux (further jugular engorgement with enhancement of the top blood column after right upper abdomen compression lasting >30 s) and Kussmaul sign (increase of jugular top blood column in inspiration) were positive secondary to elevated systemic venous pressure. Auscultation elicited an irregular heart rate, the first heart sound with variable intensity and a soft systolic murmur on the xyphoid area, whose intensity remained constant after a long pause.

EKG, and chest x-ray

The resting electrocardiogram showed a paced rhythm alternating with rare native QRS complexes; the native QRS complex showed no typical for ApHCM giant T waves but only minimal atypical repolarization anomalies of the QRS in V4 (**Figure 2**).

Chest x-ray showed a slightly enlarged heart with partial calcification of the aortic arch and a thickened thoracic aorta.

Transthoracic echocardiography

The echocardiogram performed in our echo Lab was of poor quality, especially the apical window projections. It showed a mild thickening of the inter-ventricular septum (septal thickness: 12 mm; posterior wall thickness = 11 mm), with a dilated left atrium (antero-posterior LA diameter = 41 mm) and hyper-normal (74%) LV ejection fraction. Both ventricles were apparently of normal size (LV diastolic diameter: 42 mm, RV basal diameter 37 mm). There was no evidence of wall motion abnormalities or dynamic left ventricular outflow tract

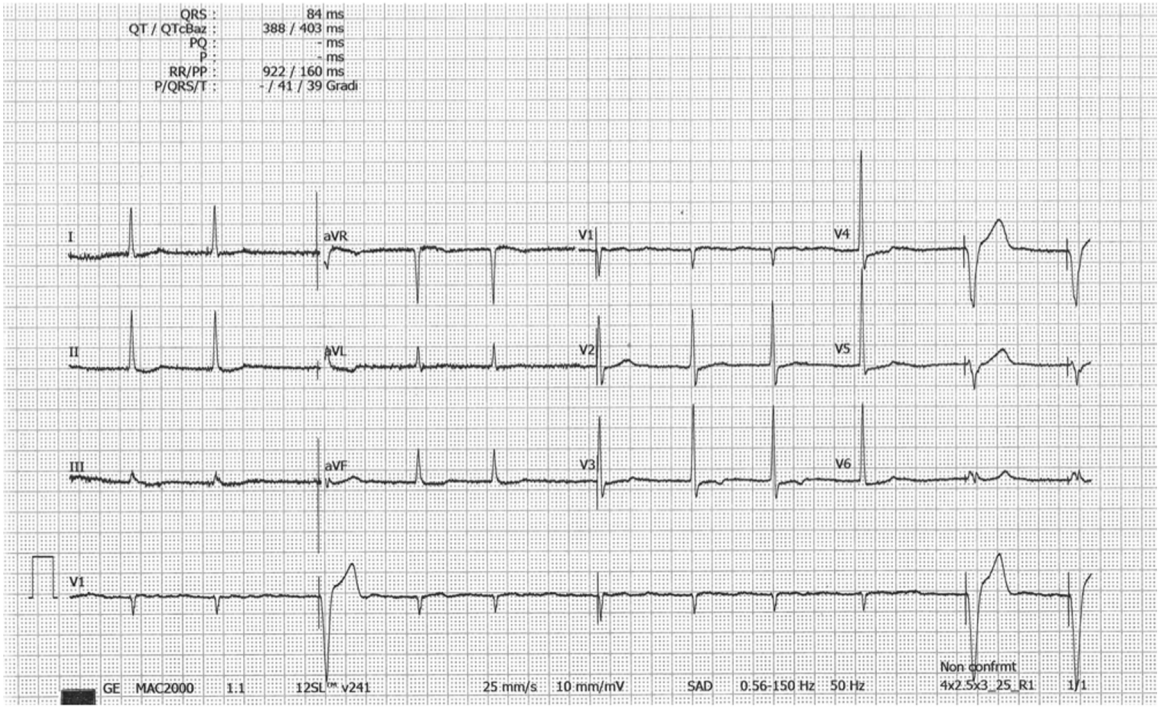

FIGURE 2
EKG tracing with no typical giant negative T waves. The rhythm is Afib; The R voltage of the QRS is modestly elevated in V3-V5 with only a shallow negative T wave in V3. Paced QRS complex. EKG = electrocardiogram; ApHCM = apical hypertrophic cardiomyopathy; Afib = atrial fibrillation.

obstruction. At first glance, the LV apical cavity did not show any abnormality, but endocardial delineation at the apex level was absent (Figure 3). In addition, there was no colour filling of the LV apex cavity even with the reduced Nyquist limit, that favours the mapping of even a markedly slow velocity flow. LV systolic function appeared hyper- normal, since at end systole, the systolic cavity was almost obliterated (the ejection fraction was not measured because of the scarce endocardial border delineation at the apex). Contrarily, LV diastolic function assessment was abnormal, revealing a possible mild elevation of left atrial and LV filling pressure. In fact, we found an elevated E/e' ratio (>12) along with a borderline venous flow abnormality (borderline rapid deceleration of the D wave), associated with left atrial dilation and mild-moderate pulmonary hypertension (45 mmHg) (normal upper value 25–30 mmHg) (Figure 4).

Regarding valve function, we found moderate-severe tricuspid regurgitation (Figure 4) and mild mitral regurgitation.

The right ventricle showed mild ventricle contractile dysfunction: mildly dilated secondary to significant tricuspid regurgitation but with normal (not hyper-normal) systolic function. The inferior vena cava and the hepatic veins were dilated, with reduced vena cava inspiratory collapse indicating pressure elevation, and in the supra-hepatic veins, systolic retrograde flow (only during inspiration) as the effect of significant tricuspid regurgitation. The significant tricuspid valve incompetence appeared to be the combination of primary tricuspid dysfunction (leaflets damage) induced by the pace-maker ventricular wire that could damage the valve at the valve crossing points, along with annular dilation induced by the mild-moderate pulmonary hypertension.

Owing to an uncertain picture of the LV apex function and morphology, since the endocardial border was not visible at that level, we decided to use contrast enhancement, using Sonoview® contrast medium, Bracco Diagnostics: each ml of the dispersion contains 8 μl of sulphur hexafluorane in the microbubbles, equivalent to 45 micrograms (8). The duration of enhancement after a bolus is longer than 3 min, so we injected 1 ml of bolus solution, allowing the duration of the enhancement to cover 3 min of scanning. The contrast very clearly depicted the endocardial border of the apex cavity as a hyper reflective line that delimited a restricted apex cavity, partially filled with contrast medium. The restricted LV apical cavity showed a typical "ace-of-spades"-like configuration, with severe apical hypertrophy (maximal thickness = 3.6 cm) (Figure 3) and hyper-normal ejection fraction (74%). Thus, a reliable diagnosis of apical HCM could be made.

Discussion

The main particularity of this case is that a diagnosis of ApHCM was not made for decades, and the unexpected progressively worsening HF was not appropriately explained. A unique convergence of several factors regarding clinical, EKG

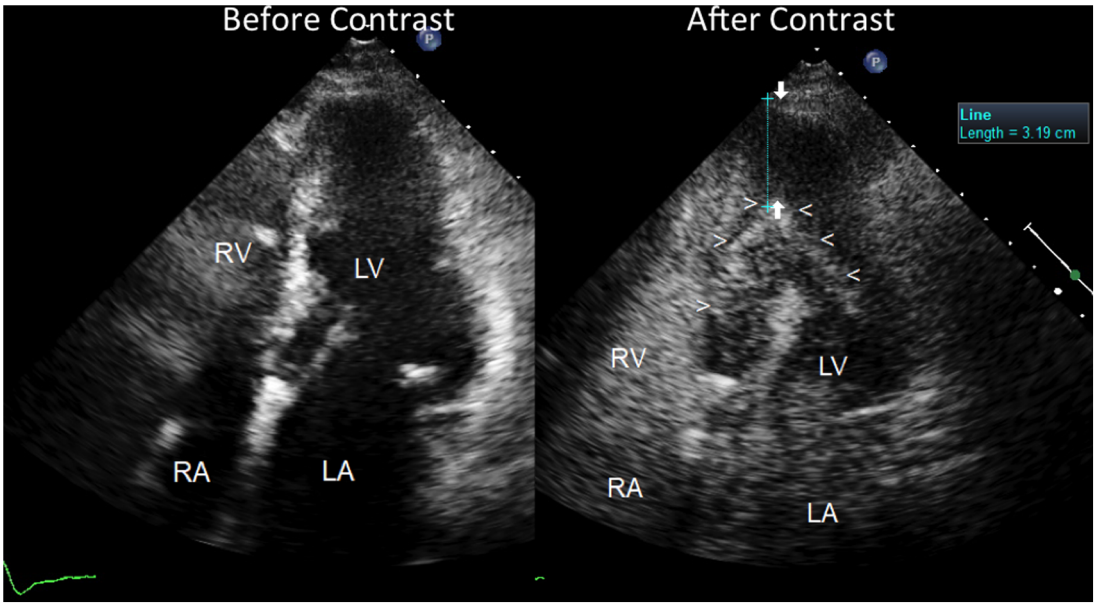

FIGURE 3
Severe apical left ventricular hypertrophy, as assessed by contrast enhanced transthoracic echocardiography. Four chamber view before (on the left) and after ultrasound contrast injection (on the right). Before contrast, the LV apical region does not show any clear delineation of the endocardial border but reveals a fairly homogeneous low backscatter echo-structure resembling a blood pool. No evident abnormality of the LV apical region can be noted but just poor quality imaging of the apical region with scarce delineation of the endocardium; the pace-maker leads can be noted in the right atrial cavity. On the contrary, after contrast injection (Sonoview® 1 cc in bolus) (on the right), a perfect delineation of the true apical endocardium is very clearly depicted as a hyper reflective line of backscatter (arrowheads). The severe hypertrophy of the LV apical wall can be noted and measured, as indicated by arrows (>3 cm thickness). The left atrium is dilated. The right atrial cavities are filled with contrast medium. LV = left ventricle; RV = right ventricle; RA = right atrium; LA = left atrium.

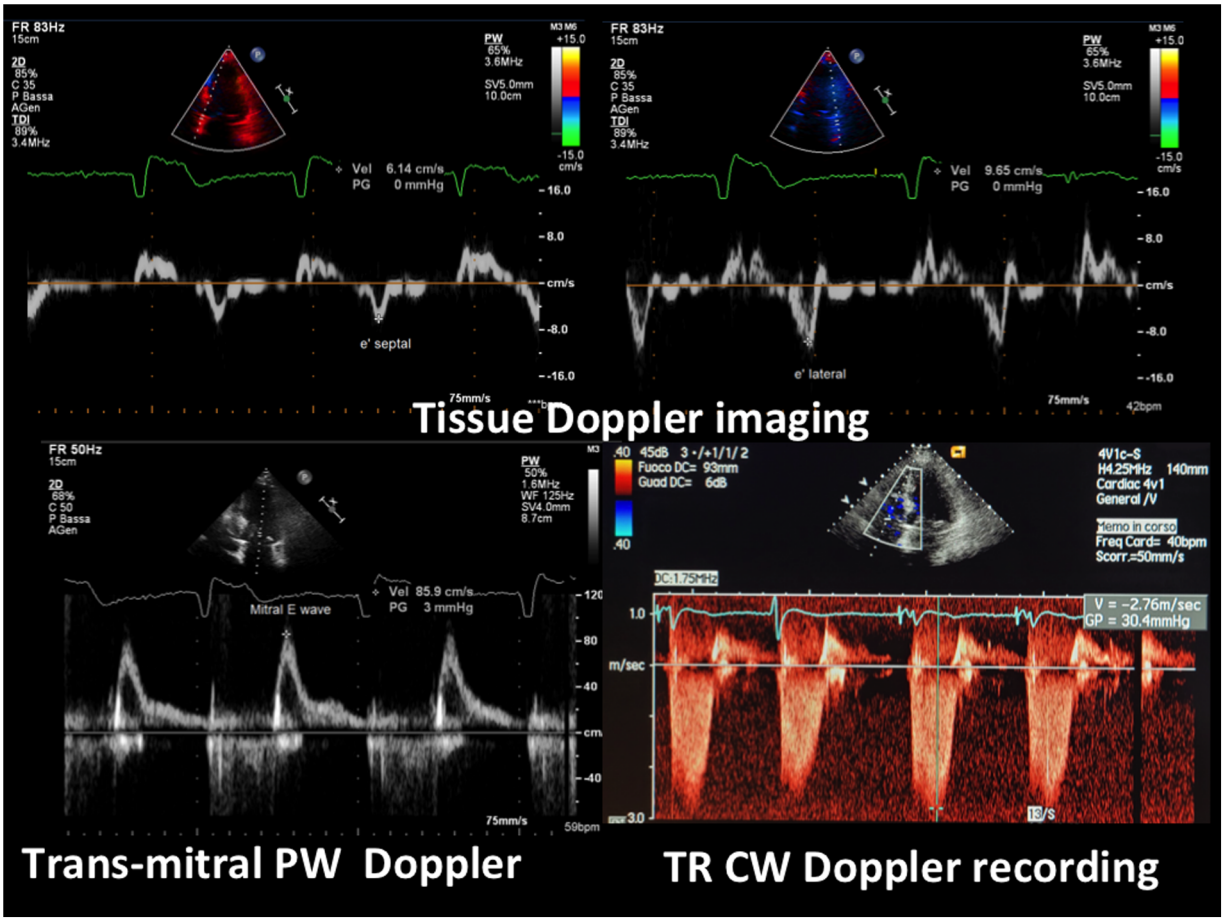

FIGURE 4
E/e' and pulmonary pressure evaluation by transthoracic Doppler. At the top, tissue Doppler imaging of the movement of the septal (on the left, e' septal wave) and of the lateral mitral annulus (on the right, e' lateral wave); at the bottom (on the left) transmitral blood flow Doppler recording (mitral E wave) (the A wave is lacking since the rhythm is atrial fibrillation). The E/e' ratio is elevated, indicating a high mean left atrial pressure confirmed by the elevated pulmonary pressure, as assessed by the maximal velocity of the TR jet (>2.7 cm/s) (bottom right). PW = pulsed Doppler; CW = continuous Doppler; TR = tricuspid regurgitation.

and echocardiography findings conspired to hamper the proper diagnosis, and misdiagnosis possibly hastened the disease progression owing to inappropriate drugs prescription and the lack of a more profound modulation of appropriate nutrigenomic and the associated epigenetic interventions (4, 5). Nonetheless, the patient was an octogenarian, confirming the relatively benign disease expression of this variant of hypertrophic cardiomyopathy (1).

Considering the difficulty in diagnosing ApHCM, we believe the main problem lies in executing and interpreting the echocardiograms (9). The non typical EKG findings may have contributed to the misdiagnosis (10). Indeed typical "giant" T waves are found in only 47% of patients with ApHCM and they are also less frequently observed in patients outside Japan (11). Finally, poorly accurate bedside investigations, especially before Afib onset (even if not specific) may also have contributed to the delayed diagnosis (12).

Echocardiography. In the literature, descriptions of the numerous caveats in the execution and interpretation of echocardiograms in this situation are lacking, especially in patients with a poor ultrasound window. In interpreting LV function and morphology during echo, the first step should be to check the endocardial border delineation, in particular at the level of the apex region. It is well known that the LV endocardial border can be incompletely delineated, especially in poor windows, since in this view the ultrasound beam is parallel to the endocardium and, therefore, fails to reflect enough ultrasound for effective visualization of the endocardial surface (13). During the scanning, the rapid sequence of the frames can give the false impression that the endocardial border is there and that the poor quality images are the cause of the poor endocardial definition. However, the bottom line is that all cases with poor endocardial border definition at the LV apex must be further investigated by contrast echocardiography, especially in difficult windows (8). A survey reported that in 31.7% of cases, echocardiography initially failed to diagnose ApHCM, later found at cardiac magnetic resonance imaging (CMRI) (9). In situations of unclear LV endocardial delineation, in particular at the apex, contrast echo is mandatory (14). That is the main indication for using contrast medium to enhance LV endocardial

border delineation by echocardiography. CMRI can have possibly useful application for the diagnosis of ApHCM (15). However CMRI may implies additional risks, time delays, and costs (16). In particular a major drawback of CMRI is that it has got genotoxic effects as demonstrated by the significantly higher level of DNA double-strand breaks measured in human lymphocytes after exposure even with a 1.5 T machine as compared with pre exposure level (17). This cancerogenic effect is compounded by the possible gadolinium induced nephrogenic systemic fibrosis (18). Contrast echocardiography on the other hand is totally safe, so repeatable, showing the same diagnostic potential as CMRI to evaluate LV wall thickness and function with very favorable cost-effective analysis (16). So it is a preferable test for assessing hypertrophic cardiomyopathy and in general LV function and LV wall thickness in difficult patients. Moreover in ApHCM there is the need to assess coronaries, task that can be accomplished with enhanced echo Doppler that allows direct, functional evaluation of coronary stenosis in the left main and the whole left anterior descending coronary artery along with the integrative evaluation of coronary flow reserve in the distal LAD (19, 20); coronary stenosis detection with this functional approach appears even better than the morphologic approach by coronary computed tomography as preliminary demonstrated (21).

Another important aspect of our case is the presence of significant LV diastolic dysfunction, that went unexplained and was wrongly attributed to hypertensive heart disease. The evaluation of diastolic dysfunction in Afib can be challenging (22, 23). In our case unequivocal findings were present: firstly, dilation of the LA, that was the reason for the precocious Afib (**Figure 3**) associated with an E/e' > 12 (**Figure 4**) and secondarily, mild-moderate pulmonary hypertension (45 mmHg systolic) (**Figure 4**). Pulmonary venous flow Doppler recording, although extremely important for assessing LV diastolic function, is less reliable because atrial contraction is lacking in Afib (24).

The E/e' is a clear, validated index reflecting even in atrial fibrillation patients the increase of mean atrial pressure when the ratio gets higher than 12 (22, 23); it is expressed by the mitral E wave peak velocity that is normalized by the mitral annulus protodiastolic descent (e', evaluated by tissue Doppler imaging). As a consequence of elevated LV diastolic and left atrial pressure, the patient developed secondary pulmonary hypertension (**Figure 4**). The elevated pulmonary pressure was accurately evaluated by means of tricuspid regurgitation maximal velocity, a very reliable, validated Doppler finding (25). Then pulmonary hypertension either created or worsened the tricuspid regurgitation by means of tricuspid annulus dilation. Any increase in right ventricle afterload is handled by progressive dilation of the ventricle and this implies tricuspid annulus dilation owing to the specific anatomic features of that annulus (26).

This elevated left atrial pressure was also the reason for the persistently elevated proBNP in the previous year, as reported (27) (**Figure 1**). This was compounded by the dilation and elevated pressure in the right atrium secondary to the tricuspid regurgitation.

Over the years the patient was treated for heart failure symptoms, mainly with diuretics (Furosemide), at increased dosage to 50 mg/day after the last episode of heart failure. Neither angiotensin converting enzyme (ACE) inhibitors nor angiotensin II receptor blockers nor aldosterone inhibitors were prescribed. However, by reducing the circulating blood volume the use of loop diuretics can stimulate the renin angiotensin system and both directly and indirectly (by renin and angiotensin), the sympathetic outflow, especially without any ACE inhibition (28). The ensuing hormonal activation can further stimulate LV hypertrophy and myocardial fibrosis. Hypertension (the patient was moderately hypertensive), together with elevated circulating aldosterone, are associated with stimulation of cardiac fibroblasts and resultant augmented fibrosis in the hypertrophic tissue structure of the LV (29).

It is ironic that even though ACE inhibition drugs are widely used in hypertension, they were not used when specific ACE inhibition was potentially needed and worth trying (30). On the contrary, she was prescribed Digoxin for several years, that possibly further worsened the LV diastolic dysfunction (31).

Moreover, the LV diastolic dysfunction could have accelerated progression of the apical LV hypertrophy through stimulating the immune system, creating a vicious circle and worsening the disease. Left ventricular diastolic dysfunction, in fact, has been associated to the release of pro-inflammatory cytokines, prolonged hypoxemia, and excessive activation of neuroendocrine and autonomic nerve function, further aggravating the hormonal storms that foster myocardial hypertrophy and fibrosis (32). Experimental evidence has shown that blockade of interleukin 6, a typical inflammatory cytokine, attenuates left ventricular hypertrophy (33).

Finally, the patient was moderately overweight and this, with the ensuing hyperinsulinemia, could have further fueled the progression of the LV hypertrophy (34).

In conclusion, accurate and timing diagnosis with contrast echocardiography can prompt more precocious interventions in order to possibly prevent or delay the onset of the ApHCM complications; strain-independent factors (fibrosis and hypertrophy) are the more important target of the therapeutic interventions: weight reduction in obese patients with appropriate diet and normalization of hyperglycemia along with blood pressure normalization may reduce LV fibrosis/hypertrophy by several mechanisms (34) including modulating genes expression by a nutrigenomic effect (4); then ACE inhibition pharmacologic treatment could also possibly reduce myocardial fibrosis (35); other ancillary interventions are to avoid drugs that has got inotropic effect like digitalis and *implantable cardioverter-defibrillator* application (when indicated) that act on life threatening arrhythmias. Moreover, since ApHCM less frequently exhibits clear genetic familiarity, both European Society of Cardiology and American Heart Association HCM guidelines provide no ApHCM specific genotyping or family screening recommendations. Nevertheless, our opinion is to recommend serial cardiological evaluations, including EKG and echocardiography integrated with contrast enhancement in case of poor LV endocardial delineation, for the first-degree relatives of the patient, and to intensify follow-up in case of symptoms or apparent abnormalities thanks to the harmless effect of ultrasound energy.

Conclusion

ApHCM can be a challenging diagnosis. Contrast echocardiography must always be applied in cases of poor delineation of the LV apical endocardial border at baseline echocardiography. Timely detection and appropriate lifestyle intervention might reduce the severity of LV hypertrophy and minimize and delay HF related symptoms and arrhythmias. The prognosis is seen to remain relatively benign after long term follow-up (20 years).

Data availability statement

The raw data supporting the conclusions of this article will be made available by the authors, without undue reservation.

Ethics statement

Ethical review and approval was not required for the study on human participants in accordance with the local legislation and institutional requirements. The patients/participants provided their written informed consent to participate in this study. Written informed consent was obtained from the individual(s) for the publication of any potentially identifiable images or data included in this article.

Author contributions

All authors contributed to the article and approved the submitted version.

Acknowledgments

The authors would like to thank Mary V. Pragnell, B.A., for invaluable support in revising the manuscript language.

Conflict of interest

The authors declare that the research was conducted in the absence of any commercial or financial relationships that could be construed as a potential conflict of interest.

Publisher's note

All claims expressed in this article are solely those of the authors and do not necessarily represent those of their affiliated organizations, or those of the publisher, the editors and the reviewers. Any product that may be evaluated in this article, or claim that may be made by its manufacturer, is not guaranteed or endorsed by the publisher.

References

1. Eriksson MJ, Sonnenberg B, Woo A, Rakowski P, Parker TG, Wigle ED, et al. Long-term outcome in patients with apical hypertrophic cardiomyopathy. *J Am Coll Cardiol.* (2002) 39(4):638–45. doi: 10.1016/S0735-1097(01)01778-8

2. Carter AR, Santos Ferreira DL, Taylor AE, Lawlor DA, Davey Smith G, Sattar N, et al. Role of the metabolic profile in mediating the relationship between body mass Index and left ventricular mass in adolescents: analysis of a prospective cohort study. *J Am Heart Assoc.* (2020) 9(20):e016564. doi: 10.1161/JAHA.120.016564

3. Hughes RK, Knott KD, Malcolmson J, Augusto JB, Mohiddin SA, Kellman P, et al. Apical hypertrophic cardiomyopathy: the variant less known. *J Am Heart Assoc.* (2020) 9(5):e015294. doi: 10.1161/JAHA.119.015294

4. Wolf CM. Hypertrophic cardiomyopathy: genetics and clinical perspectives. *Cardiovasc Diagn Ther.* (2019) 9(Suppl 2):S388–415. doi: 10.21037/cdt.2019.02.01

5. Arad M, Seidman JG, Seidman CE. Phenotypic diversity in hypertrophic cardiomyopathy. *Hum Mol Genet.* (2002) 11(20):2499–506. doi: 10.1093/hmg/11.20.2499

6. Lee BK, Lim HS, Fearon WF, Yong AS, Yamada R, Tanaka S, et al. Invasive evaluation of patients with angina in the absence of obstructive coronary artery disease. *Circulation.* (2015) 131(12):1054–60. doi: 10.1161/CIRCULATIONAHA.114.012636

7. Williams B, Mancia G, Spiering W, Agabiti Rosei E, Azizi M, Burnier M, et al. ESC/ESH guidelines for the management of arterial hypertension. *Eur Heart J.* (2018) 39(33):3021–104. doi: 10.1093/eurheartj/ehy339

8. Senior R, Andersson O, Caidahl K, Carlens P, Herregods MC, Jenni R, et al. Enhanced left ventricular endocardial border delineation with an intravenous injection of SonoVue, a new echocardiographic contrast agent: a European multicenter study. *Echocardiography.* (2000) 17(8):705–11. doi: 10.1111/j.1540-8175.2000.tb01223.x

9. Yan L, Wang Z, Xu Z, Li Y, Tao Y, Fan C. Two hundred eight patients with apical hypertrophic cardiomyopathy in China: clinical feature, prognosis, and comparison of pure and mixed forms. *Clin Cardiol.* (2012) 35(2):101–6. doi: 10.1002/clc.20995

10. Koga Y, Katoh A, Matsuyama K, Ikeda H, Hiyamuta K, Toshima H, et al. Disappearance of giant negative T waves in patients with the Japanese form of apical hypertrophy. *J Am Coll Cardiol.* (1995) 26(7):1672–8. doi: 10.1016/0735-1097(95)00377-0

11. Paluszkiewicz J, Krasinska B, Milting H, Gummert J, Pyda M. Apical hypertrophic cardiomyopathy: diagnosis, medical and surgical treatment. *Kardiochir TorakoChirurgia Pol.* (2018) 15(4):246–53. doi: 10.5114/kitp.2018.80922

12. Webb JG, Sasson Z, Rakowski H, Liu P, Wigle ED. Apical hypertrophic cardiomyopathy: clinical follow-up and diagnostic correlates. *J Am Coll Cardiol.* (1990) 15(1):83–90. doi: 10.1016/0735-1097(90)90180-W

13. Thanigaraj S, Perez JE. Apical hypertrophic cardiomyopathy: echocardiographic diagnosis with the use of intravenous contrast image enhancement. *Journal of the American Society of Echocardiography: Official Publication of the American Society of Echocardiography.* (2000) 13(2):146–9. doi: 10.1016/S0894-7317(00)90026-9

14. Olszewski R, Timperley J, Cezary S, Monaghan M, Nihoyannopoulis P, Senior R, et al. The clinical applications of contrast echocardiography. *Eur J Echocardiogr.* (2007) 8(3):s13–23. doi: 10.1016/j.euje.2007.03.021

15. Moon JC, Fisher NG, McKenna WJ, Pennell DJ. Detection of apical hypertrophic cardiomyopathy by cardiovascular magnetic resonance in patients with non-diagnostic echocardiography. *Heart.* (2004) 90(6):645–49. doi: 10.1136/hrt.2003.014969

16. Kurt M, Shaikh KA, Peterson L, Kurrelmeyer KM, Shah G, Nagueh SF, et al. Impact of contrast echocardiography on evaluation of ventricular function and clinical management in a large prospective cohort. *J Am Coll Cardiol.* (2009) 53(9):802–10. doi: 10.1016/j.jacc.2009.01.005

17. Fiechter M, Stehli J, Fuchs TA, Dougoud S, Gaemperli O, Kaufmann PA. Impact of cardiac magnetic resonance imaging on human lymphocyte DNA integrity. *Eur Heart J.* (2013) 34(30):2340–5. doi: 10.1093/eurheartj/eht184

18. Mendichovszky IA, Marks SD, Simcock CM, Olsen OE. Gadolinium and nephrogenic systemic fibrosis: time to tighten practice. *Pediatr Radiol.* (2008) 38(5):489–96. quiz 602–3. doi: 10.1007/s00247-007-0633-8

19. Caiati C, Zedda N, Cadeddu M, Chen L, Montaldo C, Iliceto S, et al. Detection, location, and severity assessment of left anterior descending coronary artery stenoses by means of contrast-enhanced transthoracic harmonic echo Doppler. *Eur Heart J.* (2009) 30(14):1797–806. doi: 10.1093/eurheartj/ehp163

20. Caiati C, Lepera M, Pollice P, Favale S. Non invasive detection of accelerated stenotic flow in the entire left anterior descending coronary artery provides insight into the causes of impaired coronary flow reserve: a study conducted with enhanced transthoracic convergent color Doppler echocardiography. *J Am Coll Cardiol*. (2020) 75(11 Supplement 1):1784. doi: 10.1016/S0735-1097(20)32411-6

21. Caiati C, Scardapane A, Iacovelli F, Pollice P, Achille TI, Favale S, et al. Coronary flow and reserve by enhanced transthoracic Doppler trumps coronary anatomy by computed tomography in assessing coronary artery stenosis. *Diagnostics (Basel)*. (2021) 11(2):245. doi: 10.3390/diagnostics11020245

22. Arques S. Clinical relevance of the spectral tissue Doppler E/e' ratio in the management of patients with atrial fibrillation: a comprehensive review of the literature. *J Atr Fibrillation*. (2018) 11(2):2038. doi: 10.4022/jafib.2038

23. Nagueh SF, Appleton CP, Gillebert TC, Marino PN, Oh JK, Smiseth OA, et al. Recommendations for the evaluation of left ventricular diastolic function by echocardiography. *J Am Soc Echocardiogr*. (2009) 22(2):107–33. doi: 10.1016/j.echo.2008.11.023

24. Caiati C, Argentiero A, Forleo C, Favale S, Lepera ME. Predictors of exercise capacity in dilated cardiomyopathy with focus on pulmonary venous flow recorded with transesophageal eco-Doppler. *J Clin Med*. (2021) 10(24):5954. doi: 10.3390/jcm10245954

25. Parasuraman S, Walker S, Loudon BL, Gollop ND, Wilson AM, Lowery C, et al. Assessment of pulmonary artery pressure by echocardiography—a comprehensive review. *IJC Heart & Vasculature*. (2016) 12:45–51. doi: 10.1016/j.ijcha.2016.05.011

26. Utsunomiya H, Itabashi Y, Mihara H, Berdejo J, Kobayashi S, Siegel RJ, et al. Functional tricuspid regurgitation caused by chronic atrial fibrillation. *Circulation: Cardiovascular Imaging*. (2017) 10(1):e004897. doi: 10.1161/CIRCIMAGING.116.004897

27. Davutoglu V, Celik A, Aksoy M, Sezen Y, Soydinc S, Gunay N. Plasma NT-proBNP is a potential marker of disease severity and correlates with symptoms in patients with chronic rheumatic valve disease. *Eur J Heart Fail*. (2005) 7(4):532–6. doi: 10.1016/j.ejheart.2004.07.006

28. Opie LH, Pfeffer MA. Inhibitors of the renin-angiotensin-aldosterone system. In: Opie LH, Gersh BJ, editors. *Drugs for the heart*. Philadelfia, PA: Elsevier Saunders (2013). p. 119–68.

29. Weber KT, Brilla CG. Pathological hypertrophy and cardiac interstitium. Fibrosis and renin-angiotensin-aldosterone system. *Circulation*. (1991) 83 (6):1849–65. doi: 10.1161/01.CIR.83.6.1849

30. Gersh BJ, Opie LH. Which therapy for which condition? In: Opie LH, Gersh BJ, editors. *Drugs for the heart*. Philadelfia, PA: Elsevier Saunders (2013). p. 463–541.

31. Teerlink JR, Sliwa K, Opie LH. Heart failure. In: Opie LH, Gersh BJ, editors. *Drugs for the heart*. Philadelfia, PA: Elsevier Saunders (2013). p. 169–223.

32. Mocan M, Mocan Hognogi LD, Anton FP, Chiorescu RM, Goidescu CM, Stoia MA, et al. Biomarkers of inflammation in left ventricular diastolic dysfunction. *Dis Markers*. (2019) 2019:7583690. doi: 10.1155/2019/7583690

33. Hada Y, Uchida HA, Mukai T, Kojima F, Yoshida M, Takeuchi H, et al. Inhibition of interleukin-6 signaling attenuates aortitis, left ventricular hypertrophy and arthritis in interleukin-1 receptor antagonist deficient mice. *Clin Sci (Lond)*. (2020) 134(20):2771–87. doi: 10.1042/CS20201036

34. Phanzu BK, Natuhoyila AN, Vita EK, Kabangu J-RM, Longo-Mbenza B. Association between insulin resistance and left ventricular hypertrophy in asymptomatic, black, sub-saharan African, hypertensive patients: a case–control study. *BMC Cardiovasc Disord*. (2021) 21(1):1. doi: 10.1186/s12872-020-01829-y

35. Edavettal JM, Gardner JD. New insight into the regression of cardiac fibrosis. *American Journal of Physiology-Heart and Circulatory Physiology*. (2022) 323(1): H201–H3. doi: 10.1152/ajpheart.00306.2022

frontiers | Frontiers in Cardiovascular Medicine

TYPE Case Report
PUBLISHED 30 May 2023
DOI 10.3389/fcvm.2023.1188095

OPEN ACCESS

EDITED BY
Antonios Karanasos,
Hippokration General Hospital, Greece

REVIEWED BY
Hiroki Teragawa,
JR Hiroshima Hospital, Japan
Rocco Antonio Montone,
Agostino Gemelli University Polyclinic (IRCCS), Italy

*CORRESPONDENCE
Myung Ho Jeong
✉ myungho@chollian.net

†These authors have contributed equally to this work

RECEIVED 16 March 2023
ACCEPTED 10 May 2023
PUBLISHED 30 May 2023

CITATION
Oh S, Hyun DY, Cho S-G, Hong YJ, Kim JH, Ahn Y and Jeong MH (2023) Case report: A fatal case of myocardial infarction due to myocardial bridge and concomitant vasospasm: the role of stress gated SPECT.
Front. Cardiovasc. Med. 10:1188095.
doi: 10.3389/fcvm.2023.1188095

Case report: A fatal case of myocardial infarction due to myocardial bridge and concomitant vasospasm: the role of stress gated SPECT

Seok Oh[1†], Dae Young Hyun[1†], Sang-Geon Cho[2], Young Joon Hong[1,3], Ju Han Kim[1,3], Youngkeun Ahn[1,3] and Myung Ho Jeong[1,3*]

[1]Department of Cardiology, Department of Internal Medicine, Chonnam National University Hospital, Gwangju, Republic of Korea, [2]Department of Nuclear Medicine, Chonnam National University Hospital, Gwangju, Republic of Korea, [3]Department of Cardiology, Department of Internal Medicine, Chonnam National University Medical School, Gwangju, Republic of Korea

Introduction: Although most cases of myocardial bridge (MB) are clinically benign, sometimes it can be one of potential threats of myocardial infarction (MI) and life-threatening arrhythmia. In the present study, we present a case of ST-segment elevation MI caused by MB and concomitant vasospasm.
Case Presentation: A 52-year-old woman was brought to our tertiary hospital due to resuscitated cardiac arrest. Because the 12-lead electrocardiogram indicated ST-segment elevation MI, coronary angiogram was promptly commenced, which showed near-total occlusion at the middle portion of left anterior descending coronary artery (LAD). After intracoronary nitroglycerin administration, this occlusion was dramatically relieved, however, systolic compression at this site remained, indicative of myocardial bridge (MB). Intravascular ultrasound also showed eccentric compression with a "half-moon" sign, which is consistent with MB. Coronary computed tomography also showed a bridged coronary segment surrounded by myocardium at the middle portion of LAD. To assess the severity and extent of myocardial damages and ischemia, myocardial single photon emission computed tomography (SPECT) was additionally conducted, showing a moderate fixed perfusion defect around the cardiac apex, suggesting MI. After receiving optimal medical therapy, the patient's clinical symptoms and signs were improved then the patient was discharged from the hospital successfully and uneventfully.
Conclusion: We demonstrated a case of MB-induced ST-segment elevation MI which was confirmed with its perfusion defects via myocardial perfusion SPECT. There have been proposed a number of diagnostic modalities to examine its anatomic and physiologic significance. Among them, myocardial perfusion SPECT can be available as one of useful modalities to evaluate the severity and extent of myocardial ischemia in patients with MB.

KEYWORDS

cardiac imaging techniques, myocardial bridging, myocardial infarction, coronary angiography, SPECT CT

Abbreviations
CAG, coronary angiogram; CCB, calcium channel blocker; CCTA, coronary computed tomography; CVS, coronary vasospasm; I-NTG, intracoronary nitroglycerin; IVUS, intravascular ultrasound; LAD, left anterior descending coronary artery; MB, myocardial bridge; MI, myocardial infarction; MINOCA, with non-obstructive coronary arteries; MLA, minimum lumen diameter; SPECT, single photon emission computed tomography.

1. Introduction

Myocardial bridge (MB) is a congenital coronary anomaly manifested by coronary artery segment tunnelling through the myocardial bands (1), and this term was first mentioned in 1961 in a case report about angiographic narrowing during the systole (2). Although many clinicians tend to consider it to be a benign condition, sometimes it can be clinically fatal (3, 4). In other words, MB may contribute to the development of acute coronary syndrome such as myocardial infarction (MI) or cardiac arrest (5–7). Especially, coronary vasospasm (CVS) may act as a trigger factor for these situations in patients with MB (7). We present a case of ST-segment elevation MI triggered by CVS within the site of MB.

2. Case presentation

A 52-year-old Korean woman with essential hypertension was admitted to our cardiovascular center because of resuscitated cardiac arrest as the chief complaint. Several hours before the presentation, the patient experienced squeezing chest pain and was suddenly collapsed then received bystander cardiopulmonary resuscitation. During the transportation via ambulance, the patient had received electrical defibrillation for documented ventricular fibrillation (**Supplementary Figure S1**). There was no documentation of previous cardiovascular events. On the physical examination, temperature was 36.5°C, heart rate was 90 beats per minute, respiratory rate was 20 beats per minute, and blood pressure was 120/90 mmHg. A 12-lead electrocardiogram showed abnormal ST-segment elevation with pathologic Q-waves in precordial leads (**Figure 1**). In the laboratory test, high-sensitivity troponin-I was elevated to 1.332 ng/ml (reference: 0–0.050 ng/ml). Since we initially concluded a diagnosis of ST-segment elevation MI, the catheterization laboratory was activated then emergent coronary angiogram (CAG) was promptly planned for percutaneous coronary intervention.

Initial CAG was performed via the right femoral artery at the catheterization laboratory. It revealed near-total occlusion at the middle portion of left anterior descending coronary artery (LAD) with reduced antegrade coronary flow (**Figure 2A**). After intracoronary nitroglycerin (I-NTG) administration, however, this stenosis was dramatically relieved (**Figure 2B**), but there was found systolic compression at the same site, suggestive of MB (**Figures 2C,D**, **Supplementary Video S1**). In quantitative coronary analysis, the systolic diameter was 0.84 mm and the diastolic diameter was 1.17 mm, which meant that the diameter change from diastole to systole was about 28.2% (**Supplementary Figure S2**). For the further evaluation, intravascular ultrasound (IVUS) study was examined with a guidance system (Eagle Eye® Platinum RX Digital IVUS Catheter, Volcano Corporation, Rancho Cordova, CA, USA). In IVUS, eccentric compression was seen in the MB segment with a half-moon-like echo-lucent space between the MB segment and epicardial tissue (**Figures 2E,F**, **Supplementary Video S2**). There was no definite evidence of atherosclerotic plaque formation within the MB segment. The cross-sectional area at this segment was 4.99 mm^2 during the diastole, and 3.42 mm^2 during the systole (**Supplementary Figure S3**). In multiple-slice coronary computed tomography angiography (CCTA), there was seen a coronary segment surrounded by myocardium at the middle portion of LAD (**Figure 2G**). We concluded that the final diagnosis of this patient was MI with non-obstructive coronary arteries (MINOCA). The patient was transferred to the intensive care unit for the hemodynamic monitoring.

To determine its functional significance, Tc-99 m methylisobutyl isonitrile single photon emission computed tomography (SPECT) was additionally conducted. It demonstrated a medium-sized, moderate fixed perfusion defect around the apex, downstream to the bridging segment of the LAD, suggesting MI (**Figure 3**). The cardiac SPECT/CCTA hybrid imaging also confirmed excellent correlation between the extent of perfusion defects and the anatomical location of MB (**Figure 4A**), which was also correlated with CAG finding (**Figure 4B**).

As the patient received optimal antiplatelet agents, high-intensity statins, and non-dihydropyridine calcium channel blockers (CCBs), the patient's clinical symptoms and signs were improved. The patient was discharged from the hospital then has remained symptom-free on follow-up outpatient visits.

3. Discussion and conclusion

MB is one of normal variants of coronary artery which is manifested by intramuscular course of a coronary artery. Although the true prevalence of MB is not fully understood, its angiographic detection seems not uncommon with the detection rates varying from 0.5–12% in the resting CAG to about 40% in I-NTG administration or coronary reactivity testing (8). Since most patients with MBs have no clinical symptoms, many clinicians are reluctant to manage it with intensive medical treatments then just tend to recommend simple observation with not much clinical significance. Although most cases with MBs are clinically benign (7), as suggested in the present case, sometimes it can be one of potential threats of MI and life-threatening arrhythmia (9, 10). According to an observational retrospective study, MB seems to be a potential cause of MI, and its prevalence was significantly higher in patients with MINOCA than in their counterparts (10). Moreover, since MB itself is one of independent risk factors for ischemia-induced myocardial fibrosis and MINOCA (11), it also act as a crucial factor contributing to the onset of fatal arrhythmia (12).

There have been proposed a number of diagnostic modalities to examine its anatomic and physiologic significance (13, 14). Invasive modalities include CAG, and intracoronary imaging/physiology studies. CAG may demonstrate the diameter change between systole and diastole within the segment of MB. "Milking effect" is one of characteristic findings with a significant (≥70%) reduction in minimum lumen diameter (MLA) during the systole and persistent ≥35% decrease in MLA (15). After I-NTG

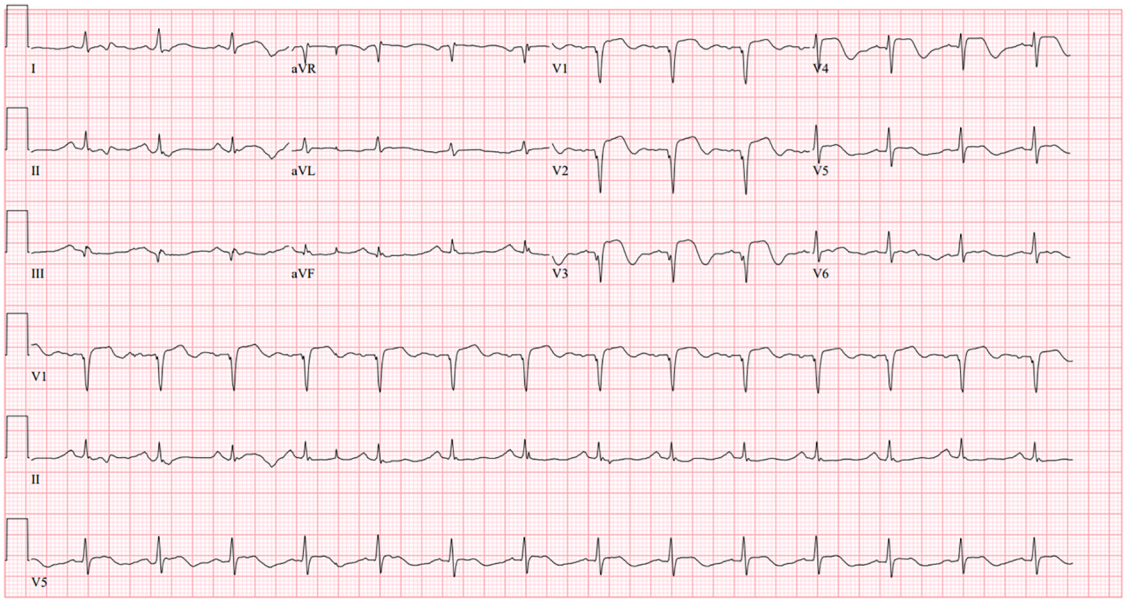

FIGURE 1
Initial 12-lead electrocardiogram: A 12-lead electrocardiogram showed abnormal ST-segment elevation with pathologic Q-waves in precordial leads.

administration, systolic compression can be accentuated by vasodilation of non-bridged coronary segments (16). As shown in the present case, IVUS can show the characteristic "half-moon" sign which is an echo-lucent space between the MB segment and epicardial tissue. Atherosclerotic plaque can also be seen proximal to MB in IVUS. Coronary physiologic studies such as fractional flow reserve can be useful, but its role of MB has remained challenging (14).

Non-invasive modalities include CCTA, stress gated SPECT, and stress echocardiogram. CCTA is able to identify bridging

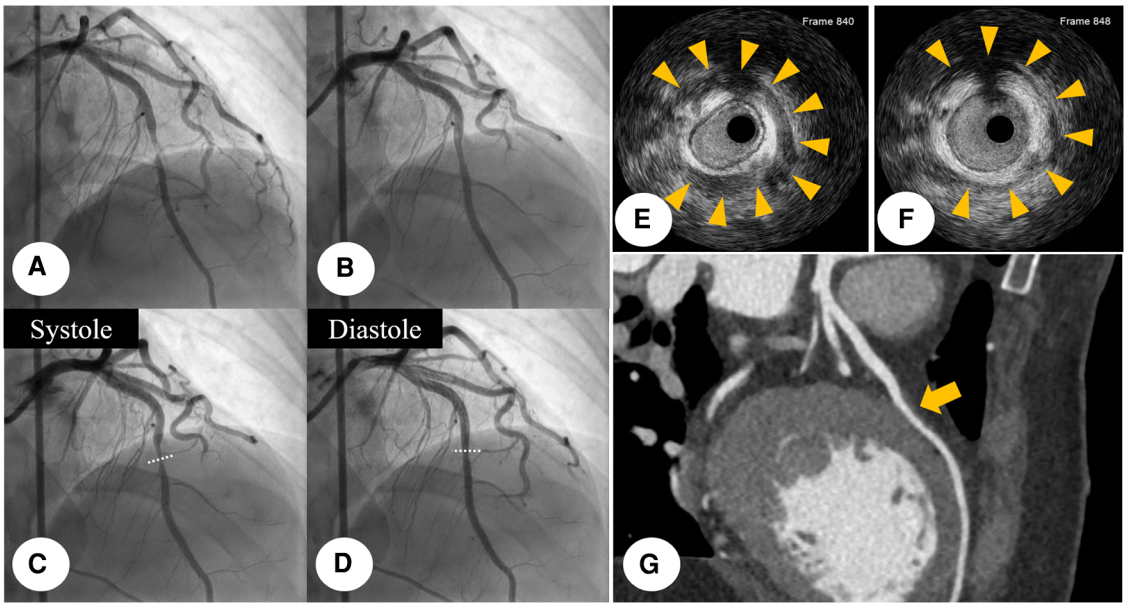

FIGURE 2
Initial CAG finding: initial CAG demonstrated near-total occlusion (yellowish arrow) at the middle portion of LAD with reduced antegrade coronary flow. (**A**) This stenosis was dramatically relieved (yellowish arrow), after I-NTG administration (**B**) After I-NTG administration, systolic compression was seen at the middle portion of LAD, which means MB. (**C**,**D**) IVUS was further examined with a guidance system (Eagle Eye® Platinum RX Digital IVUS Catheter, Volcano Corporation, Rancho Cordova, CA, USA), demonstrating eccentric compression with a half-moon-like echo-lucent space between the MB segment and epicardial tissue. (**E**,**F**) Multiple-slice CCTA imaging showed a bridged coronary segment surrounded by myocardium at the middle portion of LAD (yellowish arrow). (**G**) CAG, coronary angiogram; CCTA, coronary computed tomography angiography; I-NTG, intracoronary nitroglycerin; LAD, left anterior descending coronary artery; MB, myocardial bridge.

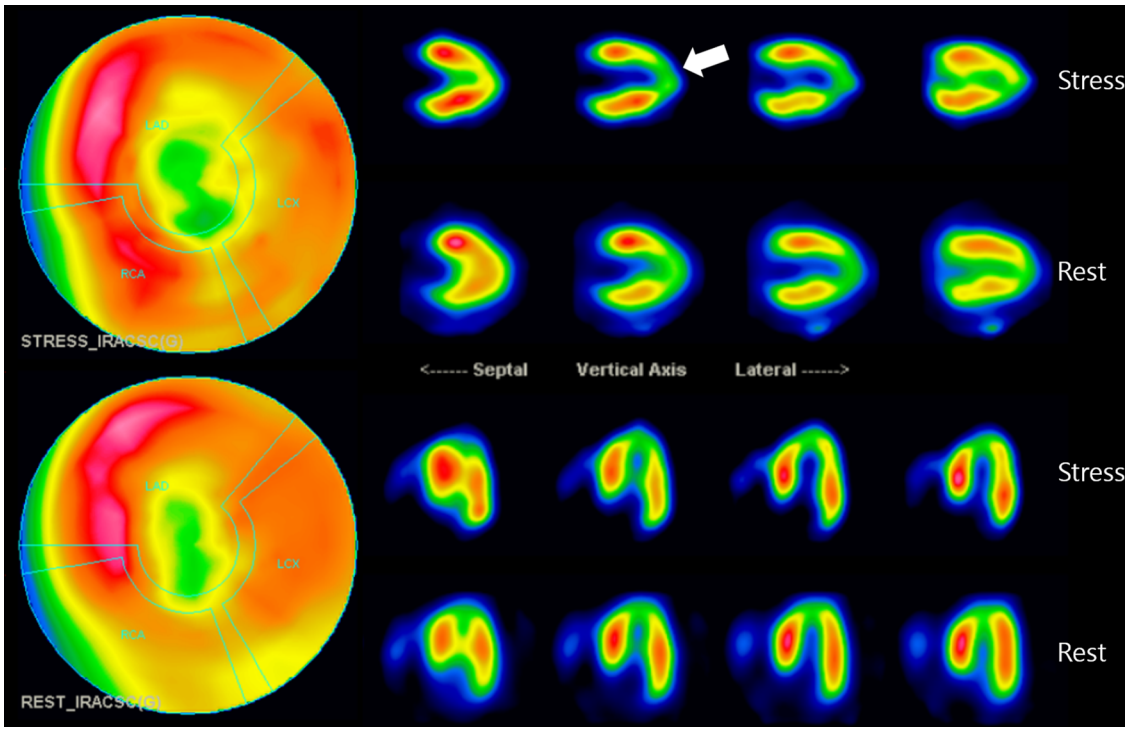

FIGURE 3
Myocardial perfusion SPECT imaging: SPECT scan showed medium-sized, non-transmural infarction around the apex (whitish arrow). This defect correlates to the downstream myocardium to the bridging segment of the mid-LAD, as marked by arrows. LAD, left anterior descending coronary artery; SPECT, single photon emission computed tomography.

segment surrounded by myocardium (17), whereas stress gated SPECT can visualize myocardial perfusion defects then quantify the degree of myocardial ischemia (18). In the present case, we utilized the myocardial perfusion SPECT. Although most cases of MB can be found in anatomical imaging modalities, functional imaging like myocardial perfusion SPECT can also be feasible and useful to evaluate its functional significance in the form of perfusion defects (19). Lee and his colleagues demonstrated that high-grade MB could induce perfusion defects on territories of LAD and its branches in dipyridamole TI-201 SPECT findings (20). Such findings may reflect the degree of luminal narrowing by systolic contraction (18). A retrospective study by Huang

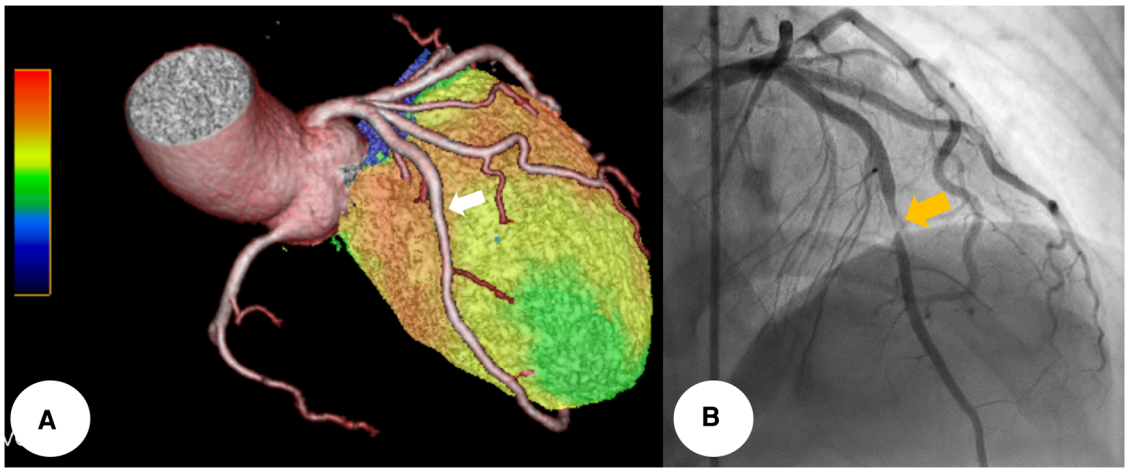

FIGURE 4
The cardiac SPECT/CCTA hybrid imaging also confirmed excellent correlation between the extent of perfusion defects and the anatomical location of MB, which was well correlated with CAG finding (whitish arrow and yellowish arrow) (**A**,**B**). CCTA, coronary computed tomography angiography; MB, myocardial bridge; SPECT, single photon emission computed tomography.

et al. showed abnormal myocardial perfusion in patients with MB at the middle portion of LAD (21).

The treatment options can be subdivided into two categories: (A) pharmacological therapy; (B) interventional therapy. In the pharmacological therapy, beta-blocker is the mainstay treatment which can relieve the hemodynamic disturbance caused by MB through its negative chronotropic effect (15). CCBs are also available with similar pharmacologic mechanisms of beta-blockers. Like in this case, they may be more beneficial in patients with MB and concomitant CVS (13). In the literature review, there have been no available comparative studies of beta-blocker vs. CCB in patients with MB. In contrast, pure vasodilators such as long-acting nitrates should be avoided or applied with caution because they can worsen symptoms by accentuating systolic compression of the MB segment (22). If refractory to pharmacological therapy, interventional therapy should be considered. Interventional therapy includes percutaneous coronary intervention with stenting for the bridged coronary segment, supra-arterial myotomy, or coronary artery bypass grafting.

Meanwhile, we should know that this case shows MINOCA with concomitant presence of MB and CVS. MB seems to be closely related to CVS (11, 23, 24). That is, patients having MB tended to have a higher proportion of CVS compared to those not having MB (11, 25). Although not fully accountable, it is plausible that sustained shear stress (i.e., contraction-relaxation effect) of the site of MB may induce the alteration in endothelial function (11, 23), resulting in coronary vasomotor disorders. Since patients with both of them tend to have a higher risk of adverse cardiac events such as readmission for recurrent angina pectoris (11, 25), therefore, coronary reactivity testing may be a useful diagnostic tool to elicit CVS then verify these high-risk patients (26).

In the present case, we detected the fatal case of MB-induced MINOCA through multimodality imaging tools. While there are a number of useful diagnostic modalities, myocardial perfusion SPECT can be available as one of useful modalities to evaluate the severity and extent of myocardial ischemia in patients with MB.

Data availability statement

The original contributions presented in the study are included in the article/**Supplementary Material**, further inquiries can be directed to the corresponding author.

Ethics statement

The studies involving human participants were reviewed and approved by Chonnam National University Hospital. Written informed consent was obtained from the patient for the publication of any potentially identifiable images or data included in this article.

Author contributions

SO and DH: drafted the manuscript. SO, DH: designed the study methodology. SO, DH, SC: collected the data. YH, JK, YA, and MJ: reviewed and edited the manuscript. All authors contributed to the article and approved the submitted version.

Acknowledgments

We sincerely thank SO, DH, and MJ for providing and interpreting CAG images. We also thank SC for providing and interpreting myocardial perfusion SPECT images.

Conflict of interest

The authors declare that the research was conducted in the absence of any commercial or financial relationships that could be construed as a potential conflict of interest.

Publisher's note

Supplementary material

The Supplementary Material for this article can be found online at: https://www.frontiersin.org/articles/10.3389/fcvm.2023.1188095/full#supplementary-material

References

1. Alegria JR, Herrmann J, Holmes DR Jr., Lerman A, Rihal CS. Myocardial bridging. *Eur Heart J*. (2005) 26(12):1159–68. doi: 10.1093/eurheartj/ehi203

2. Angelini P, Trivellato M, Donis J, Leachman D R. Myocardial bridges: a review. *Prog Cardiovasc Dis*. (1983) 26(1):75–88. doi: 10.1016/0033-0620(83)90019-1

3. Ripa C, Melatini MC, Olivieri F, Antonicelli R. Myocardial bridging: a 'forgotten' cause of acute coronary syndrome—a case report. *Int J Angiol*. (2007) 16(3):115–8. doi: 10.1055/s-0031-1278262

4. Thej MJ, Kalyani R, Kiran J. Atherosclerosis and myocardial bridging: not a benign combination. An autopsy case report. *J Cardiovasc Dis Res*. (2012) 3 (2):176–8. doi: 10.4103/0975-3583.95380

5. Abe T, Jujo K, Matsukage T. Myocardial bridging may shed light on one aspect of unexplained myocardial infarction with non-obstructive coronary arteries. *Eur Heart J Acute Cardiovasc Care*. (2022) 11(6):508–9. doi: 10.1093/ehjacc/zuac074

6. Husmann L, Nkoulou R, Wolfrum M, Kaufmann PA. Myocardial bridging causing infarction and ischaemia. *Eur Heart J*. (2011) 32(7):790. doi: 10.1093/eurheartj/ehq423

7. Ki YJ. Myocardial bridging presenting as myocardial ischaemia induced cardiac arrest: a case report. *BMC Cardiovasc Disord*. (2021) 21(1):178. doi: 10.1186/s12872-021-01975-x

8. Tarantini G, Migliore F, Cademartiri F, Fraccaro C, Iliceto S. Left anterior descending artery myocardial bridging: a clinical approach. *J Am Coll Cardiol*. (2016) 68(25):2887–99. doi: 10.1016/j.jacc.2016.09.973

9. Mizuno A, Nishi Y, Niwa K. Deferring coronary stenting for myocardial bridging by fractional flow reserve and optical coherence tomography. *J Invasive Cardiol*. (2012) 24(2):E27–9.

10. Matta A, Nader V, Canitrot R, Delmas C, Bouisset F, Lhermusier T, et al. Myocardial bridging is significantly associated to myocardial infarction with non-obstructive coronary arteries. *Eur Heart J Acute Cardiovasc Care*. (2022) 11(6):501–7. doi: 10.1093/ehjacc/zuac047

11. Montone RA, Gurgoglione FL, Del Buono MG, Rinaldi R, Meucci MC, Iannaccone G, et al. Interplay between myocardial bridging and coronary spasm in patients with myocardial ischemia and non-obstructive coronary arteries: pathogenic and prognostic implications. *J Am Heart Assoc*. (2021) 10(14):e020535. doi: 10.1161/jaha.120.020535

12. Kazbanov IV, ten Tusscher KH, Panfilov AV. Effects of heterogeneous diffuse fibrosis on arrhythmia dynamics and mechanism. *Sci Rep*. (2016) 6:20835. doi: 10.1038/srep20835

13. Corban MT, Hung OY, Eshtehardi P, Rasoul-Arzrumly E, McDaniel M, Mekonnen G, et al. Myocardial bridging: contemporary understanding of pathophysiology with implications for diagnostic and therapeutic strategies. *J Am Coll Cardiol*. (2014) 63(22):2346–55. doi: 10.1016/j.jacc.2014.01.049

14. Aleksandric SB, Djordjevic-Dikic AD, Dobric MR, Giga VL, Soldatovic IA, Vukcevic V, et al. Functional assessment of myocardial bridging with conventional and diastolic fractional flow reserve: vasodilator versus inotropic provocation. *J Am Heart Assoc*. (2021) 10(13):e020597. doi: 10.1161/JAHA.120.020597

15. Bourassa MG, Butnaru A, Lesperance J, Tardif JC. Symptomatic myocardial bridges: overview of ischemic mechanisms and current diagnostic and treatment strategies. *J Am Coll Cardiol*. (2003) 41(3):351–9. doi: 10.1016/s0735-1097(02)02768-7

16. Ferreira AG Jr., Trotter SE, Konig B Jr., Decourt LV, Fox K, Olsen EG. Myocardial bridges: morphological and functional aspects. *Br Heart J*. (1991) 66(5):364–7. doi: 10.1136/hrt.66.5.364

17. Kim PJ, Hur G, Kim SY, Namgung J, Hong SW, Kim YH, et al. Frequency of myocardial bridges and dynamic compression of epicardial coronary arteries: a comparison between computed tomography and invasive coronary angiography. *Circulation*. (2009) 119(10):1408–16. doi: 10.1161/CIRCULATIONAHA.108.788901

18. Gawor R, Kusmierek J, Plachcinska A, Bienkiewicz M, Drozdz J, Piotrowski G, et al. Myocardial perfusion GSPECT imaging in patients with myocardial bridging. *J Nucl Cardiol*. (2011) 18(6):1059–65. doi: 10.1007/s12350-011-9406-8

19. Singh D, Vadi SK, Parmar M, Sood A, Mehrotra S, Mittal BR. Role of (99 m)Tc-sestamibi gated SPECT/CT myocardial perfusion imaging in the management of patients with myocardial bridging and its correlation with coronary angiography. *J Cardiol Cases*. (2017) 15(4):136–40. doi: 10.1016/j.jccase.2016.12.006

20. Lee YS, Moon DH, Shin JW, Park SW, Park SJ, Lee HK. Dipyridamole TI-201 SPECT imaging in patients with myocardial bridging. *Clin Nucl Med*. (1999) 24(10):759–64. doi: 10.1097/00003072-199910000-00006

21. Huang WS, Chang HD, Yang SP, Tsao TP, Cheng CY, Cherng SC. Abnormal 201Tl myocardial single photon emission computed tomography in energetic male patients with myocardial bridge. *Nucl Med Commun*. (2002) 23(11):1123–8. doi: 10.1097/00006231-200211000-00013

22. Hongo Y, Tada H, Ito K, Yasumura Y, Miyatake K, Yamagishi M. Augmentation of vessel squeezing at coronary-myocardial bridge by nitroglycerin: study by quantitative coronary angiography and intravascular ultrasound. *Am Heart J*. (1999) 138(2 Pt 1):345–50. doi: 10.1016/s0002-8703(99)70123-7

23. Herrmann J, Higano ST, Lenon RJ, Rihal CS, Lerman A. Myocardial bridging is associated with alteration in coronary vasoreactivity. *Eur Heart J*. (2004) 25(23):2134–42. doi: 10.1016/j.ehj.2004.08.015

24. Kim JW, Seo HS, Na JO, Suh SY, Choi CU, Kim EJ, et al. Myocardial bridging is related to endothelial dysfunction but not to plaque as assessed by intracoronary ultrasound. *Heart*. (2008) 94(6):765–9. doi: 10.1136/hrt.2007.115980

25. Nam P, Choi BG, Choi SY, Byun JK, Mashaly A, Park Y, et al. The impact of myocardial bridge on coronary artery spasm and long-term clinical outcomes in patients without significant atherosclerotic stenosis. *Atherosclerosis*. (2018) 270:8–12. doi: 10.1016/j.atherosclerosis.2018.01.026

26. Montone RA, Rinaldi R, Del Buono MG, Gurgoglione F, La Vecchia G, Russo M, et al. Safety and prognostic relevance of acetylcholine testing in patients with stable myocardial ischaemia or myocardial infarction and non-obstructive coronary arteries. *EuroIntervention*. (2022) 18(8):e666–76. doi: 10.4244/eij-d-21-00971

frontiers | Frontiers in Cardiovascular Medicine

TYPE Case Report
PUBLISHED 08 June 2023
DOI 10.3389/fcvm.2023.1204736

OPEN ACCESS

EDITED BY
Julian A. Luetkens,
University Hospital Bonn, Germany

REVIEWED BY
Daniel Kuetting,
University Hospital Bonn, Germany
Rodrigo Salgado,
Antwerp University Hospital & Holy Heart Lier, Belgium

*CORRESPONDENCE
S. Chris Malaisrie
✉ chris.malaisrie@nm.org

RECEIVED 12 April 2023
ACCEPTED 19 May 2023
PUBLISHED 08 June 2023

CITATION
Goyal A, Avery R, Cuttica MJ, Flaherty JD, Malaisrie SC and Mylvaganam R (2023) Case report: Multimodality imaging of unusual coronary to pulmonary collaterals in chronic thromboembolic pulmonary hypertension. Front. Cardiovasc. Med. 10:1204736. doi: 10.3389/fcvm.2023.1204736

Case report: Multimodality imaging of unusual coronary to pulmonary collaterals in chronic thromboembolic pulmonary hypertension

Ansh Goyal[1], Ryan Avery[2], Michael J. Cuttica[3], James D. Flaherty[4], S. Chris Malaisrie[1]* and Ruben Mylvaganam[3]

[1]Department of Cardiac Surgery, Bluhm Cardiovascular Institute, Northwestern University Feinberg School of Medicine and Northwestern Memorial Hospital, Chicago, IL, United States, [2]Department of Radiology, Northwestern University Feinberg School of Medicine and Northwestern Memorial Hospital, Chicago, IL, United States, [3]Department of Pulmonary and Critical Care, Northwestern University Feinberg School of Medicine and Northwestern Memorial Hospital, Chicago, IL, United States, [4]Department of Cardiology, Bluhm Cardiovascular Institute, Northwestern University Feinberg School of Medicine and Northwestern Memorial Hospital, Chicago, IL, United States

We present unusual coronary-pulmonary collaterals in a 65-year-old CTEPH patient. Perfusion mapping of a dual-energy computed tomography (DECT) study revealed areas of right lung that were minimally perfused despite unilateral occlusion of the right pulmonary artery, leading to the discovery of coronary-pulmonary collaterals *via* invasive coronary angiography. Pulmonary thromboendarterectomy removed the clot en-bloc. Post-surgery DECT and catheterization confirmed restoration of pulmonary arterial circulation and excellent hemodynamic response. Here, suggestion of perfusion to a proximally obstructed lung with DECT helped to document the presence of rarely documented coronary-pulmonary artery collaterals.

KEYWORDS

CTEPH, DECT, pulmonary endarterectomy, coronary angiogram, pulmonary angiography, collaterals, chronic thromboembolic pulmonary hypertension

Introduction

Chronic thromboembolic pulmonary hypertension (CTEPH) is classified as group 4 pulmonary hypertension where unresolved thromboembolic disease obstructs the pulmonary artery. The resultant lung ischemia commonly leads to bronchial arterial collateralization thought to lower pulmonary vascular resistance and reduce mortality (1). While CTEPH is frequently studied with CT-PA and ventilation-perfusion scans, dual-energy CT (DECT) scans are an emerging evaluation tool among others including photon counting CT or rapid kV switching dual-energy CT (2–4). DECT depends on dual sensor-based simultaneous computed tomography scans at two different tube voltages with contrast iodine. This allows for subsequent image processing based on material decomposition detected as attenuation differences at different energy levels to calculate perfusion blood volume (PBV) at each voxel and accordingly visualize contrast uptake based on a given color scale. Depending on phase of contrast uptake, perfusion

defects are visualized such as in V/Q imaging during the arterial phase, while imaging timed later can reveal perfusion due to collaterals (5). A DECT study is dose neutral when compared to a standard CTA, though some studies have shown some differences depending on employed technique and differences in normalization of image quality, signal to noise ratio and dose length product (6–8). Here, images were acquired with a dual energy-dual source scanner with 2 separate 64-row detectors and image postprocessing was completed using Syngo DE Lung PBV, Siemens Healthcare software, which uses the three-material decomposition theory of iodine, air and soft-tissue to calculate PBV. Ultimately, patients with CTEPH may be candidates for surgical cure with pulmonary thromboendarterectomy based on image-guided assessment and clinical status (9). The purpose of this case study is to describe utility of DECT-PBV to evaluate pulmonary embolism and its functional consequences as well as illustrate its role for the first time in characterizing the rarely documented coronary-pulmonary collaterals in a unilateral CTEPH patient.

Case presentation

We present a 65-year-old former 40-pack year smoker with a medical history of chronic obstructive pulmonary disease requiring supplemental oxygen, leading to atrial fibrillation, diastolic heart failure, and chronic thromboembolic pulmonary hypertension (CTEPH) who was referred to our institution for advanced surgical management of CTEPH. On admission, the patient was experiencing increased dyspnea and significant oxygen desaturation, necessitating transfer to our institution for further evaluation and diagnostics.

The patient was in his usual state of health until 4 years prior when he developed right lower extremity swelling and dyspnea and was diagnosed with a deep vein thrombosis (DVT) and pulmonary embolism (PE). Review of these historical records demonstrated extensive pulmonary embolic material beginning in the right main pulmonary artery extending into segmental and subsegmental arteries. He was initiated on warfarin and remained adherent with therapeutic INR's.

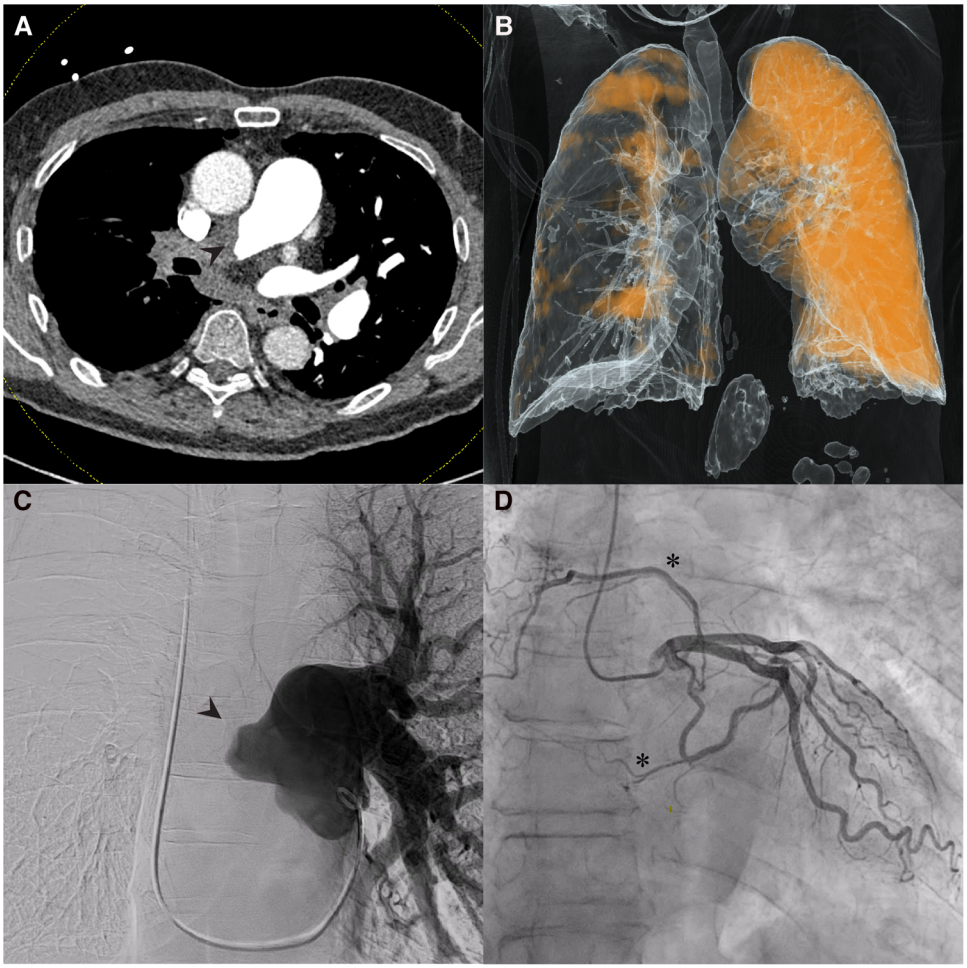

FIGURE 1
Dual-Energy computed tomography (DECT), pulmonary and coronary angiography. (A) Coronal DECT image demonstrating obstruction of right pulmonary artery (arrowhead); (B) Perfusion mapping demonstrates limited perfusion of right lung from unknown systemic supply at time of imaging. (C) Pulmonary angiography confirmed complete obstruction of right pulmonary circulation (arrowhead); (D) Coronary angiography revealed multiple systemic coronary-pulmonary collaterals from the left circumflex artery (asterisks).

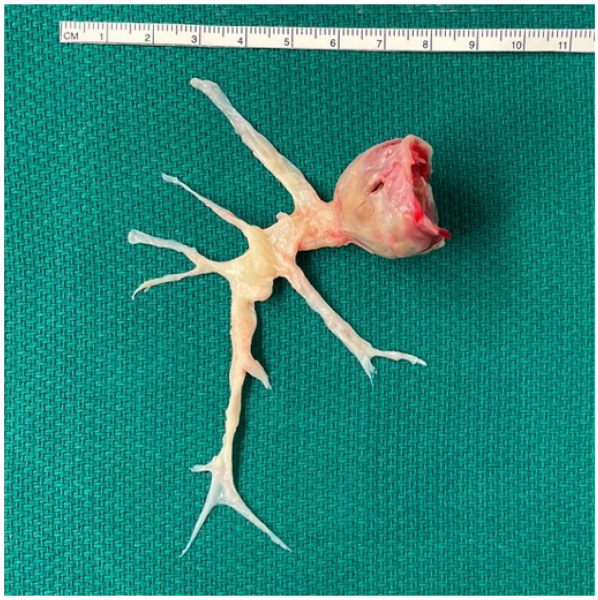

FIGURE 2
Surgical specimen. Entire clot removed en-bloc *via* thromboendarterectomy.

Transthoracic echocardiography revealed a normal sized left ventricle with an ejection fraction of 64%. The right ventricle was moderately dilated with decreased systolic function, there was interventricular flattening in both systole and diastole, the right atrium was severely enlarged, and estimated right ventricular systolic pressures were elevated. RV basal diameter was 4.45 cm, RA volume was 94.3 ml, TAPSE was 1.71 cm, and S' prime was 9.79 cm/s.

Dual-energy computed tomography (DECT) redemonstrated unilateral complete occlusion of right pulmonary arterial circulation with thrombus propagation into the proximal right pulmonary artery. No filling defects in the left pulmonary arterial system were visualized. Despite the apparent complete obstruction of the right pulmonary artery, perfused blood volume (PBV) mapping of the dual energy CT study revealed areas of the right lung that were still minimally perfused (**Figure 1 A,B**).

Pulmonary angiography with left and right heart catheterization was undertaken for surgical candidacy and planning. Right heart catheterization revealed a right atrial pressure of 4mmHg, mean pulmonary artery pressure of 40mmHg, pulmonary wedge pressure of 4mmHg, cardiac output of 3.5, cardiac index of 1.8 and pulmonary vascular resistance of 10.3 wood units. Pulmonary angiography clearly demonstrated complete obstruction of the right pulmonary artery (**Figure 1C**). Coronary angiography revealed the presence of coronary to pulmonary collaterals traveling to the pulmonary circulation from the left circumflex artery (**Figure 1D**). An aortogram was not clinically indicated as systemic collateral flow has been classically described and is not routinely investigated in CTEPH. With the delayed timing of the DECT images, it is likely that the perfusion mapping in the right hemithorax represents collateral flow through the coronary-pulmonary collaterals seen on the coronary angiography, bronchial collaterals, or both. There was no evidence the patient experienced coronary steal syndrome or angina given the presence of these coronary-pulmonary collaterals.

The patient underwent successful pulmonary thromboendarterectomy, Cox-Maze 3, and left atrial appendage occlusion without complication. Briefly, a primary median sternotomy was performed, bypass was initiated, and aortic cross clamp was applied. The right pulmonary artery was opened, and the entire clot was removed *en bloc* from all 10 segments of the right pulmonary artery under hypothermic circulatory arrest (**Figure 2**). The left pulmonary artery was inspected and found to have no significant clot consistent with pre-operative imaging. After bypass flows were resumed, an atrial clip was placed at the base left atrial appendage externally and atriotomies were performed to complete the Cox-Maze 3 procedure.

Post-surgery DECT confirmed patency of the right pulmonary artery and restoration of segmental and subsegmental pulmonary arterial circulation (**Figure 3A,B**). Pathology from the cast was negative for malignancy. Catheterization revealed an excellent hemodynamic response to surgery with a right atrial pressure of 3 mmHg (delta −1 mmHg), mean pulmonary artery pressure of 22 mmHg (delta −18 mmHg), cardiac output of 3.9 (delta +0.4), cardiac index of 2.0 (delta +0.2) and pulmonary vascular resistance of 4.9 wood units (delta −5.4 wood units). Repeat echocardiography revealed RV basal diameter of 3.84 cm (delta −0.61 cm), RA volume of 52.5 ml (delta −41.8 ml), TAPSE of 0.84 cm (delta −0.87 cm), and S' of 7.87 cm/s (delta −1.92 cm/s).

Discussion

We highlight that DECT-derived PBV mapping is a uniquely powerful tool to characterize the pulmonary vasculature, and to some extent the systemic vasculature, of patients and should receive more widespread consideration for evaluation of CTEPH because it allows for simultaneous assessment of pulmonary vessel obstruction and arterial perfusion to confirm diagnoses and guide clinical decision-making (**Figure 4**). First, significant focal perfusion to a proximally obstructed lung was revealed, eventually leading to a diagnosis of unilateral CTEPH. Unilateral CTEPH is independently a rarely discovered entity, seemingly documented only in case reports in patients with underlying thrombophilic disorders (10, 11). Whether the unilateral nature of this patient's disease contributed in some manner to the development of the coronary-pulmonary collaterals in this patient without a thrombophilia is unknown. Second, the DECT study revealed greater than expected perfusion to the obstructed lung. As a result, when invasive angiography was pursued, special attention was paid to elucidate the source of collateral flow, leading to the discovery of the rarely documented coronary-pulmonary artery collaterals.

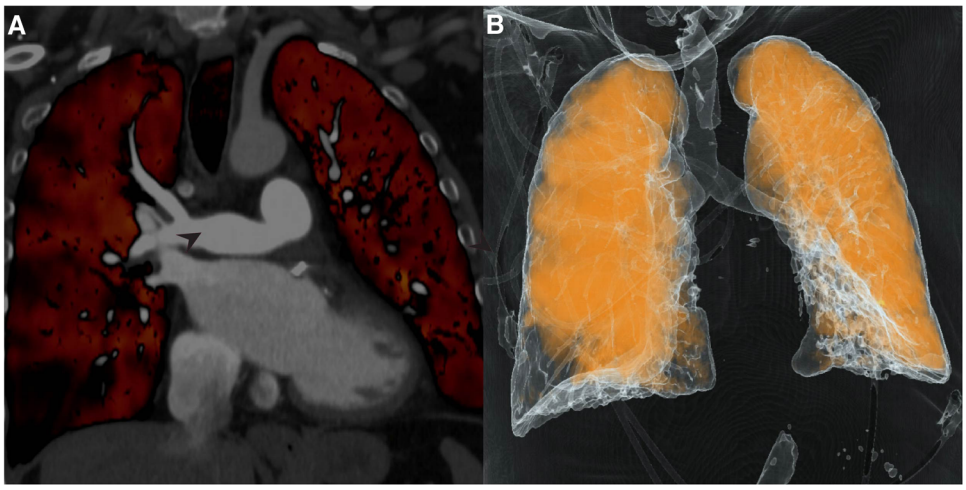

FIGURE 3
Dual-Energy computed tomography (DECT). (A) Repeat DECT demonstrates patent pulmonary artery post-thromboendarterectomy; (B) Perfusion mapping reveals significantly improved perfusion of right lung.

The physiological and molecular mechanisms underpinning angiogenesis and development of coronary-pulmonary collaterals are unclear. The contribution of systemic to pulmonary collaterals and the two-compartment model of pathophysiology in CTEPH remains to be elucidated. Thus far, while documentation of these collaterals in CTEPH patients has remained limited, research has suggested that the prevalence of coronary-pulmonary collaterals in CTEPH may be higher than previously thought (12–15). Bronchopulmonary collaterals in CTEPH have been more commonly documented and are suggested to promote bronchial dilation, lower post-operative pulmonary vascular resistance, and ultimately reduce post-operative mortality (1). Ultimately, it may be that bronchial collateralization contributed to some of the perfusion findings; however, the location of the discovered coronary-pulmonary collaterals vs. the PBV/perfusion map suggests they were a significant contributor as well. These coronary-pulmonary collaterals may share pathophysiology similar to bronchial-pulmonary collaterals, decrease pulmonary arterial resistance, and may also develop due to hypoxic factors. Our institution has adopted a delayed phase imaging protocol with the use of DECT to help understand and identify collateral flow.

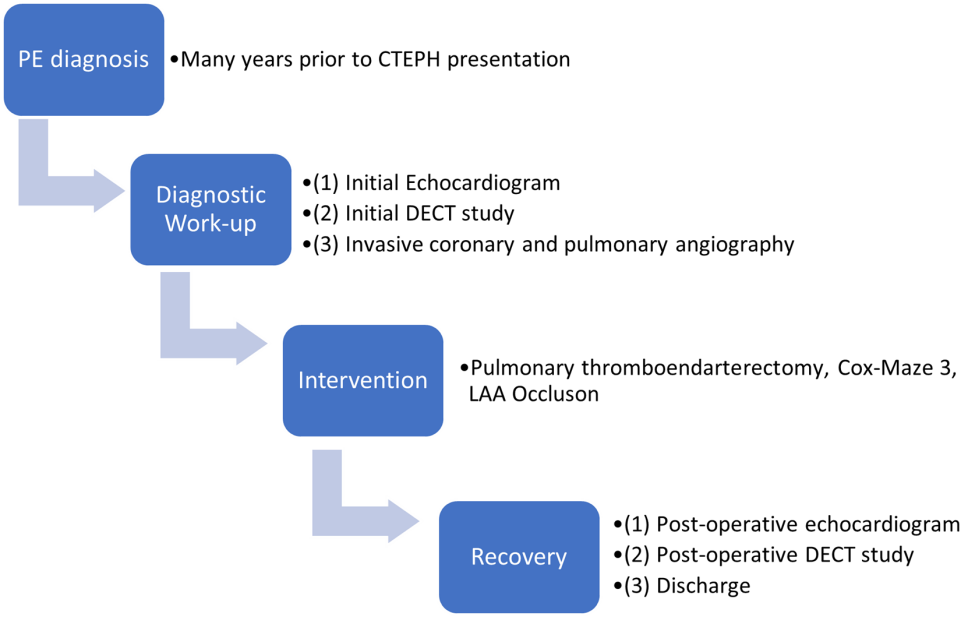

FIGURE 4
Timeline of events associated with the care episode.

Ethics statement

Written informed consent was obtained from the participant/patient(s) for the publication of this case report.

Data availability statement

The original contributions presented in the study are included in the article, further inquiries can be directed to the corresponding author.

Author contributions

AG made substantial contributions to the conception/design, data analysis/interpretation of data, and drafting of article. RM made substantial contributions to the conception/design, data analysis/interpretation of data, critical revision of article. RA, MJC, JDF and SCM made substantial contributions to conception/design and critical revision of article. All authors approve the final version of this manuscript to be published and agree to be accountable for their contributions of the work in ensuring that questions related to the accuracy or integrity of the work are appropriately investigated and resolved.

Conflict of interest

The authors declare that the research was conducted in the absence of any commercial or financial relationships that could be construed as a potential conflict of interest.

Publisher's note

References

1. Delcroix M, Vonk Noordegraaf A, Fadel E, Lang I, Simonneau G, Naeije R. Vascular and right ventricular remodelling in chronic thromboembolic pulmonary hypertension. *Eur Respir J.* (2013) 41(1):224–32. doi: 10.1183/09031936.00047712

2. Heinrich M, Uder M, Tscholl D, Grgic A, Kramann B, Schäfers HJ. CT Scan findings in chronic thromboembolic pulmonary hypertension: predictors of hemodynamic improvement after pulmonary thromboendarterectomy. *Chest.* (2005) 127(5):1606–13. doi: 10.1378/chest.127.5.1606

3. Hong YJ, Shim J, Lee SM, Im DJ, Hur J. Dual-Energy CT for pulmonary embolism: current and evolving clinical applications. *Korean J Radiol.* (2021) 22 (9):1555–68. doi: 10.3348/kjr.2020.1512

4. Abdellatif W, Ebada MA, Alkanj S, Negida A, Murray N, Khosa F, et al. Diagnostic accuracy of dual-energy CT in detection of acute pulmonary embolism: a systematic review and meta-analysis. *Can Assoc Radiol J.* (2021) 72(2):285–92. doi: 10.1177/0846537120902062

5. Petritsch B, Kosmala A, Gassenmaier T, Weng AM, Veldhoen S, Kunz AS, et al. Diagnosis of pulmonary artery embolism: comparison of single-source CT and 3rd generation dual-source CT using a dual-energy protocol regarding image quality and radiation dose. *Rofo.* (2017) 189(6):527–36. Diagnostik der akuten Lungenarterienembolie: Vergleich von Single-Source CT und Dritt-Generation Dual-Source CT unter Einsatz eines Dual-Energy Protokolls—Bildqualität und Strahlenexposition. doi: 10.1055/s-0043-103089

6. Krauss B, Grant KL, Schmidt BT, Flohr TG. The importance of spectral separation: an assessment of dual-energy spectral separation for quantitative ability and dose efficiency. *Invest Radiol.* (2015) 50(2):114–8. doi: 10.1097/rli.0000000000000109

7. Faby S, Kuchenbecker S, Sawall S, Simons D, Schlemmer HP, Lell M, et al. Performance of today's Dual energy CT and future multi energy CT in virtual non-contrast imaging and in iodine quantification: a simulation study. *Med Phys.* (2015) 42(7):4349–66. doi: 10.1118/1.4922654

8. Henzler T, Fink C, Schoenberg SO, Schoepf UJ. Dual-energy CT: radiation dose aspects. *AJR Am J Roentgenol.* (2012) 199(5 Suppl):S16–25. doi: 10.2214/ajr.12.9210

9. Kim NH. Assessment of operability in chronic thromboembolic pulmonary hypertension. *Proc Am Thorac Soc.* (2006) 3(7):584–8. doi: 10.1513/pats.200605-106LR

10. Hon S, Channick RN, Farber HW. Unilateral chronic thromboembolic pulmonary disease: a mimic of pulmonary artery agenesis. *Am J Respir Crit Care Med.* (2020) 201(10):e74–5. doi: 10.1164/rccm.201905-0997IM

11. Laczika K, Lang IM, Quehenberger P, Mannhalter C, Muhm M, Klepetko W, et al. Unilateral chronic thromboembolic pulmonary disease associated with combined inherited thrombophilia. *Chest.* (2002) 121(1):286–9. doi: 10.1378/chest.121.1.286

12. Lee NS, Auger WR, Pretorius V, Blanchard DG, Daniels LB. Coronary artery-to-pulmonary artery collaterals in chronic thromboembolic pulmonary hypertension. *Circ Cardiovasc Imaging.* (2014) 7(6):962–6. doi: 10.1161/circimaging.114.002368

13. Lee NS, Blanchard DG, Knowlton KU, McDivit AM, Pretorius V, Madani MM, et al. Prevalence of coronary artery-pulmonary artery collaterals in patients with chronic thromboembolic pulmonary hypertension. *Pulm Circ.* (2015) 5(2):313–21. doi: 10.1086/681225

14. Haghbayan H, Coomes EA, Gunaratne K. A man in his 40s with coronary-to-pulmonary artery collateralizations. *JAMA Cardiol.* (2020) 5(3):356. doi: 10.1001/jamacardio.2019.5289

15. Kim MS, Jung JI, Chun HJ. Coronary to pulmonary artery fistula: morphologic features at multidetector CT. *Int J Cardiovasc Imaging.* (2010) 26(Suppl 2):273–80. doi: 10.1007/s10554-010-9711-3

frontiers | Frontiers in Cardiovascular Medicine

TYPE Case Report
PUBLISHED 04 August 2023
DOI 10.3389/fcvm.2023.1203832

OPEN ACCESS

EDITED BY
Edoardo Conte,
University of Milan, Italy

REVIEWED BY
Valeria Pergola,
University Hospital of Padua, Italy
Angelo Ratti,
University of Milan, Italy

*CORRESPONDENCE
Grigorios Korosoglou
grigorios.korosoglou@grn.de

RECEIVED 11 April 2023
ACCEPTED 29 June 2023
PUBLISHED 04 August 2023

CITATION
Korosoglou G, Giesen A, Geiss E and Stach K (2023) Case report: Strong low-density-cholesterol reduction accompanied by shrinkage of low-attenuation coronary plaque during lipid-lowering treatment with bempedoic acid—serial evaluation by coronary computed tomography angiography. Front. Cardiovasc. Med. 10:1203832. doi: 10.3389/fcvm.2023.1203832

Case report: Strong low-density-cholesterol reduction accompanied by shrinkage of low-attenuation coronary plaque during lipid-lowering treatment with bempedoic acid—serial evaluation by coronary computed tomography angiography

Grigorios Korosoglou[1,2,3]*, Alexander Giesen[1,2], Eva Geiss[4] and Ksenija Stach[4]

[1]Department of Cardiology, Vascular Medicine & Pneumology, GRN Hospital Weinheim, Weinheim, Germany, [2]Weinheim Imaging Center, Hector Foundation, Weinheim, Germany, [3]University of Heidelberg, Heidelberg, Germany, [4]Fifth Department of Medicine, University Medical Centre Mannheim, University of Heidelberg, Mannheim, Germany

Here, we present a patient with coronary artery disease and prior percutaneous coronary interventions. This patient had to discontinue taking multiple statins and ezetimibe due to intolerance with musculoskeletal complaints and nausea. Monotherapy with bempedoic acid was well tolerated and was exceptionally effective at lipid lowering, enabling patients to achieve the low-density lipoprotein target of <55 mg/dl, as recommended by current guidelines. In addition, serial coronary computed tomography angiography performed upon clinical indications, during 20 months of lipid-lowering treatment with bempedoic acid, demonstrated signs of favorable plaque component modification, with shrinkage of the low-attenuation plaque component compared to baseline findings.

KEYWORDS

coronary artery disease, non-calcified plaque, hyperlipidemia, statin intolerance, bempedoic acid

Introduction

Lipid-lowering therapy constitutes the cornerstone for the treatment of atherosclerotic cardiovascular disease. In this regard, extensive clinical and experimental evidence showed that low-density lipoprotein (LDL) is pivotal in the process of atherogenesis within the arterial wall (1). Therefore, current guidelines recommend a reduction of LDL-cholesterol of >50% from baseline and an LDL goal of <55 mg/dl in patients at very high risk for atherosclerotic cardiovascular disease both in primary and secondary prevention (2).

From a diagnostic point of view, coronary computed tomography angiography (CCTA) has emerged as the central non-invasive imaging technique not only for the detection of anatomically significant coronary artery disease (CAD) (3) but also for the evaluation of atherosclerotic plaque composition within the arterial wall (4, 5). In this regard, total low-attenuation plaque burden was reported as the most robust predictor of death and

myocardial infarction, beyond stenosis severity in patients with CAD (4, 5). Statins, which are the primary lipid-lowering medications, were previously shown to enhance the progression of coronary artery calcification by repeated calcium-scoring scans (6). Recently, this effect was verified by serial CCTA scans, showing that statins result in slower plaque progression and transformation toward high-density calcium (7).

Recently, the non-statin lipid-lowering drug, bempedoic acid, was introduced and tested in high-risk patients under maximally tolerated statins and in statin-intolerant groups, exhibiting a good safety profile and effectiveness in terms of LDL reduction (8). However, data are scarce in terms of its potential effects on atherosclerotic plaque progression by serial CCTA studies.

Case presentation

A 66-year-old female patient was initially referred to our outpatient center in March 2017 with suspected CAD due to exertional angina (CCS class II) and dyspnea. The patient had a history of arterial hypertension, which was treated with 5 mg ramipril per day, and hyperlipidemia, which was treated for 2 years with 10 mg simvastatin (initial LDL-cholesterol of 162 mg/dl). The ECG showed normal findings, and echocardiography revealed mild myocardial hypertrophy and normal ventricular diameters and function (LV ejection fraction of 62%).

Due to clinical symptoms and an intermediate pre-test probability of 16% (9), vasodilator stress cardiac magnetic resonance (CMR) was performed, the result of which exhibited myocardial perfusion abnormalities in the septal and inferior walls. No myocardial scars were detected through late gadolinium enhancement. Due to inducible myocardial ischemia in two myocardial segments, accompanied by persistent symptoms, coronary angiography was performed, confirming high-grade lesions in the left anterior descending artery (LAD) and right coronary artery (RCA). Percutaneous coronary intervention (PCI) was performed in both arteries, resulting in complete resolution of anginal symptoms thereafter.

Lipid-lowering treatment was changed to 20 mg of atorvastatin per day, resulting in an LDL-cholesterol of 101 mg/dl in July 2017 and 118 mg/dl in October 2017. Since the target value of <70 mg/dl recommended by previous guidelines (10) could not be achieved, 10 mg of ezetimibe was added to the lipid-lowing medication, without significantly affecting LDL-cholesterol, which was measured at 113 mg/dl during April 2018. **Figure 1** shows the serial LDL-cholesterol values between March 2017 and December 2022.

In June 2018, the patient started experiencing unsteadiness, weakness, hypoesthesia symptoms, and muscle pain in both legs. An electrophysiology examination of the peripheral muscles remained without detectable neurologic abnormalities, and statin-induced muscle symptoms (SAMS) were suspected. Atorvastatin (20 mg per day) was changed to pravastatin (10 mg per day) leading to clinical improvement of SAMS. However, LDL-cholesterol remained high, measuring 143 mg/dl in October 2018 (**Figure 1**).

In March 2019, the patient was referred to rheumatologists due to a recurrence of SAMS. Hereby, small fiber neuropathy (SFN) associated with anti-Mi-2 autoantibody-positive myositis was diagnosed. Since SFN encompasses several etiologies, such as diabetes, anti-retroviral, hypothyroidism, and hyperlipidemia, and has also been associated with statin therapy (11, 12), treatment with pravastatin was discontinued. SAMS further improved, and the patient was continued on treatment with 10 mg of ezetimibe per day. During this period from March 2019 to December 2020, LDL-cholesterol remained above the desired target value, ranging between 102 and 124 mg/dl (**Figure 1**).

In March 2021, the patient reported new onset of atypical angina accompanied by exertional dyspnea. In addition, ezetimibe intolerance was suspected due to nausea. The ECG and echocardiography showed stable findings, and CCTA was performed to exclude the progression of CAD, including in-stent

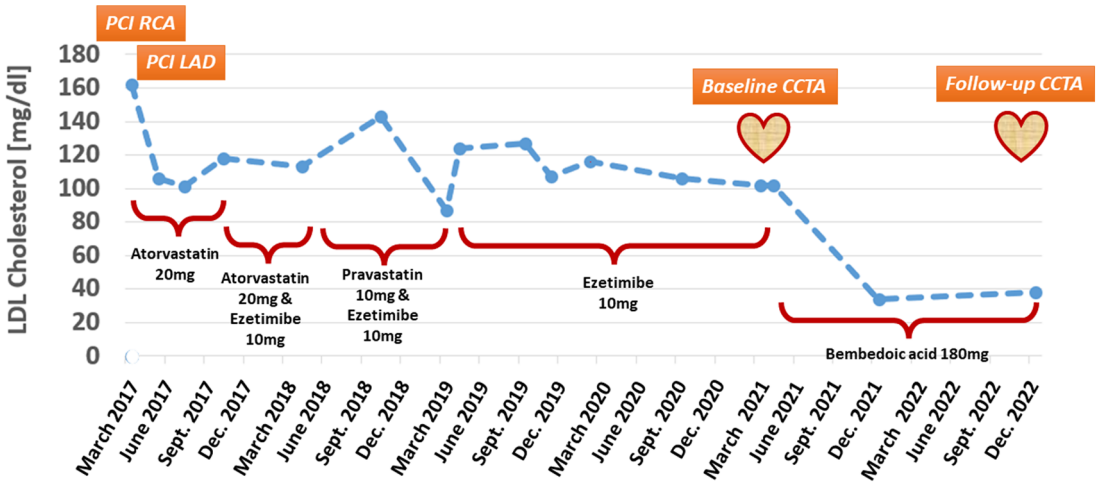

FIGURE 1
LDL-cholesterol during treatment with different lipid-lowering medications, including simvastatin, atorvastatin, pravastatin, ezetimibe, and bempedoic acid.

restenosis. CCTA was performed in a third-generation dual-source CT (SOMATOM Force, Siemens Healthineers, Forchheim, Germany), exhibiting patent stents in the LAD and RCA and any other high-grade stents. In the distal RCA, a moderate stenosis was detected, composed of non-calcified calcified components [**Figures 2A**, **C**, **E**, pointing to low-attenuation (red arrows) and calcified (green arrows) plaque components]. The plaque and both its calcified and non-calcified components were located directly at the crux of the RCA, resulting in a moderate ~50%–70% diameter stenosis [coronary artery disease reporting and data system (CAD-RADS) 2.0 score of 3]. Repeated stress CMR showed normal perfusion, so invasive angiography was deferred. In addition, treatment with ezetimibe was discontinued due to recurrent episodes of nausea, and treatment with bempedoic acid was initiated. In November 2021, during a single treatment with bempedoic acid, the LDL-cholesterol was measured at 34 mg/dl and remained at 38 mg/dl on December 2022. Since the LDL target was now reached based on current guidelines (2), treatment with bempedoic acid was continued, and treatment with PSCK9 inhibitors was deferred.

In addition, a follow-up CCTA examination was performed on December 2022 (20 months after the initial CCTA) in our facility using the same third-generation dual-source CT scanner due to recurrent atypical symptoms. CCTA revealed patency of the stents in the LAD and the proximal RCA. Interestingly, the moderate lesion detected in the distal RCA in the baseline scan now revealed signs of plaque stabilization, exhibiting similar calcified plaque (green arrows in **Figures 2B**, **D**, **F**), whereas the low-attenuation plaque component was hardly detectable (small red arrows). In addition, the resultant lumen narrowing was now considered to be just mild, causing about 25%–50% diameter stenosis (CAD-RADS 2.0 score of 2). The patient was continued on treatment with 180 mg of bempedoic acid daily, and her subsequent clinical course in the next 4 months was uneventful.

Discussion

This is to our knowledge the first case in the current literature, reporting on favorable plaque component modification by serial CCTA studies and shrinkage of low-attenuation plaque components in a patient, where lipid-lowering monotherapy with bempedoic acid achieved substantial LDL reduction, which could not be achieved by multiple statins and ezetimibe due to SAMS-associated intolerance effects.

Bempedoic acid, a non-statin lipid-lowering drug, which prevents cholesterol synthesis by inhibiting the action of the adenosine triphosphate (ATP) citrate lyase, a cytosolic enzyme upstream of 3-hydroxy-3-methylglutarylcoenzyme A reductase, is associated with a low incidence of muscle-related adverse events (13). In monotherapy of patients with statin intolerance, bempedoic acid reduces LDL levels by 23%, whereas LDL reduction may exceed about 40% in combination with ezetimibe (14). In addition, the recent CLEAR Outcomes study showed that treatment with

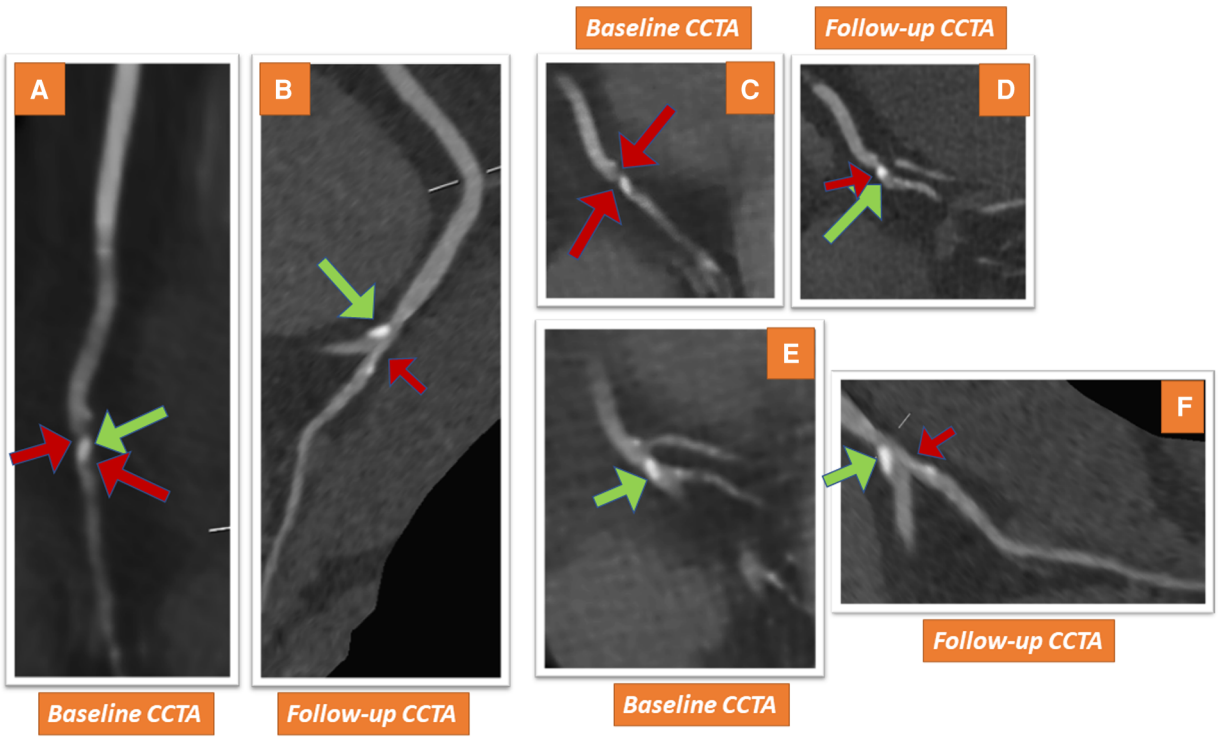

FIGURE 2
CCTA shows a non-calcified plaque and calcified components in the distal RCA of the patient (red and green arrows in A–C, pointing to low-attenuation and calcified plaque components, respectively). The lesion detected in the distal RCA reveals signs of favorable plaque component modification with follow-up CCTA after 20 months, exhibiting similar calcified plaque (green arrows in D–F), whereas low-attenuation plaque components are now hardly detectable (red arrows in D–F).

bempedoic acid in statin-intolerant patients was associated with a lower risk of major adverse cardiovascular events, for the composite endpoint death from cardiovascular cause, non-fatal myocardial infarction, non-fatal stroke, and coronary revascularization (15). Previous studies reported the ability of bempedoic acid to reduce the high-sensitive C-reactive protein (hs-CRP) (8, 16), as a biomarker of low-grade inflammation, involved in atherosclerotic disease progression. This may add anti-inflammatory effects to the lipid-lowering potential of bempedoic acid.

Our case report highlights the potential of bempedoic acid for effective lipid lowering in a patient with statin and ezetimibe intolerance. In addition, its potential for the reduction of non-calcified burden components is described by serial CCTA images. It should be noted, however, that the patient had been on treatment with statins and ezetimibe for a considerable time before the initiation of treatment with bempedoic acid, which may have confounded the effects on plaque burden and composition, as described in this context. In addition, it needs to be noted that bempedoic acid was considered before the initiation of PCSK9 treatment due to the patient's preference for oral over subcutaneous therapy and due to cost issues. Indeed, the current reimbursement system in Germany requires proof of administration of all possible sorts of lipid-lowing treatment, including statins, ezetimibe, and bempedoic acid prior to the approval of treatment with PCSK9 inhibitors. In our case, bempedoic acid reduced LDL-cholesterol by over 80% compared to the initial LDL values. Notably, relatively high inter-individual heterogeneity in LDL lowering from 0 to over 80% has been described in previous studies (17). Similar effects have previously been reported for statins, which may be the consequence of genetic polymorphisms modulating cholesterol homeostasis (18). Thus, our patient seems to be a hyper-responder to bempedoic acid in this context, where the substance achieved highly effective LDL reduction as well as favorable plaque modification. Future studies like the ongoing LOCATE trial (https://drks.de/search/de/trial/DRKS00031954) are now warranted to investigate the potential of bempedoic acid and other lipid-lowering or anti-inflammatory drugs on plaque modification within multi-center serial CCTA studies.

Data availability statement

The raw data supporting the conclusions of this article will be made available by the authors, without undue reservation.

Ethics statement

Ethical review and approval were not required for the study on human participants in accordance with the local legislation and institutional requirements. The patients/participants provided their written informed consent to participate in this study and for the publication of any potentially identifiable images or data included in this article in line with COPE guidelines.

Author contributions

GK and KS designed the study, performed the analysis, wrote and reviewed the manuscript, and provided important intellectual input. AG and EG reviewed the manuscript and provided important intellectual input. All authors contributed to the article and approved the submitted version.

Funding

For the publication fee, we acknowledge the financial support from Deutsche Forschungsgemeinschaft, through the funding program "Open Access Publikationskosten," and Heidelberg University.

Conflict of interest

The authors declare that the research was conducted in the absence of any commercial or financial relationships that could be construed as a potential conflict of interest.

Publisher's note

All claims expressed in this article are solely those of the authors and do not necessarily represent those of their affiliated organizations, or those of the publisher, the editors and the reviewers. Any product that may be evaluated in this article, or claim that may be made by its manufacturer, is not guaranteed or endorsed by the publisher.

References

1. Boren J, Chapman MJ, Krauss RM, Packard CJ, Bentzon JF, Binder CJ, et al. Low-density lipoproteins cause atherosclerotic cardiovascular disease: pathophysiological, genetic, and therapeutic insights: a consensus statement from the European Atherosclerosis Society Consensus Panel. *Eur Heart J.* (2020) 41(24):2313–30. doi: 10.1093/eurheartj/ehz962

2. Mach F, Baigent C, Catapano AL, Koskinas KC, Casula M, Badimon L, et al. 2019 ESC/EAS guidelines for the management of dyslipidaemias: lipid modification to reduce cardiovascular risk. *Eur Heart J.* (2020) 41(1):111–88. doi: 10.1093/eurheartj/ehz455

3. Group DT, Maurovich-Horvat P, Bosserdt M, Kofoed KF, Rieckmann N, Benedek T, et al. CT or invasive coronary angiography in stable chest pain. *N Engl J Med.* (2022) 386(17):1591–602. doi: 10.1056/NEJMoa2200963

4. Williams MC, Kwiecinski J, Doris M, McElhinney P, D'Souza MS, Cadet S, et al. Low-attenuation noncalcified plaque on coronary computed tomography angiography predicts myocardial infarction: results from the multicenter SCOT-HEART trial (Scottish computed tomography of the HEART). *Circulation.* (2020) 141(18):1452–62. doi: 10.1161/CIRCULATIONAHA.119.044720

5. Giusca S, Schutz M, Kronbach F, Wolf D, Nunninger P, Korosoglou G. Coronary computer tomography angiography in 2021—acquisition protocols, tips and tricks and heading beyond the possible. *Diagnostics.* (2021) 11(6). doi: 10.3390/diagnostics11061072

6. Dykun I, Lehmann N, Kalsch H, Mohlenkamp S, Moebus S, Budde T, et al. Statin medication enhances progression of coronary artery calcification: the Heinz

Nixdorf Recall Study. *J Am Coll Cardiol*. (2016) 68(19):2123–5. doi: 10.1016/j.jacc.2016.08.040

7. van Rosendael AR, van den Hoogen IJ, Gianni U, Ma X, Tantawy SW, Bax AM, et al. Association of statin treatment with progression of coronary atherosclerotic plaque composition. *JAMA Cardiol*. (2021) 6(11):1257–66. doi: 10.1001/jamacardio.2021.3055

8. Goit R, Saddik SE, Dawood SN, Rabih AM, Niaj A, Raman A, et al. Bempedoic acid's use as an adjunct in lowering low-density lipoprotein cholesterol in patients with coronary artery disease: a systematic review. *Cureus*. (2022) 14(10):e29891. doi: 10.7759/cureus.29891

9. Knuuti J, Wijns W, Saraste A, Capodanno D, Barbato E, Funck-Brentano C, et al. 2019 ESC guidelines for the diagnosis and management of chronic coronary syndromes. *Eur Heart J*. (2020) 41(3):407–77. doi: 10.1093/eurheartj/ehz425

10. Catapano AL, Graham I, De Backer G, Wiklund O, Chapman MJ, Drexel H, et al. 2016 ESC/EAS guidelines for the management of dyslipidaemias. *Eur Heart J*. (2016) 37(39):2999–3058. doi: 10.1093/eurheartj/ehw272

11. Devigili G, Tugnoli V, Penza P, Camozzi F, Lombardi R, Melli G, et al. The diagnostic criteria for small fibre neuropathy: from symptoms to neuropathology. *Brain*. (2008) 131(Pt 7):1912–25. doi: 10.1093/brain/awn093

12. Lo YL, Leoh TH, Loh LM, Tan CE. Statin therapy and small fibre neuropathy: a serial electrophysiological study. *J Neurol Sci*. (2003) 208(1–2):105–8. doi: 10.1016/S0022-510X(02)00396-9

13. Saeed A, Ballantyne CM. Bempedoic acid (ETC-1002): a current review. *Cardiol Clin*. (2018) 36(2):257–64. doi: 10.1016/j.ccl.2017.12.007

14. Ray KK, Bays HE, Catapano AL, Lalwani ND, Bloedon LT, Sterling LR, et al. Safety and efficacy of bempedoic acid to reduce LDL cholesterol. *N Engl J Med*. (2019) 380(11):1022–32. doi: 10.1056/NEJMoa1803917

15. Nissen SE, Lincoff AM, Brennan D, Ray KK, Mason D, Kastelein JJP, et al. Bempedoic acid and cardiovascular outcomes in statin-intolerant patients. *N Engl J Med*. (2023) 388(15):1353–64. doi: 10.1056/NEJMoa2215024

16. Ridker PM, Lei L, Ray KK, Ballantyne CM, Bradwin G, Rifai N. Effects of bempedoic acid on CRP, IL-6, fibrinogen and lipoprotein(a) in patients with residual inflammatory risk: a secondary analysis of the CLEAR harmony trial. *J Clin Lipidol*. (2023) 17(2):297–302. doi: 10.1016/j.jacl.2023.02.002

17. Warden BA, Cardiology BA, Purnell JQ, Duell PB, Fazio S. Real-world utilization of bempedoic acid in an academic preventive cardiology practice. *J Clin Lipidol*. (2022) 16(1):94–103. doi: 10.1016/j.jacl.2021.11.013

18. Karlson BW, Wiklund O, Palmer MK, Nicholls SJ, Lundman P, Barter PJ. Variability of low-density lipoprotein cholesterol response with different doses of atorvastatin, rosuvastatin, and simvastatin: results from VOYAGER. *Eur Heart J Cardiovasc Pharmacother*. (2016) 2(4):212–7. doi: 10.1093/ehjcvp/pvw006

frontiers | Frontiers in Cardiovascular Medicine

TYPE Case Report
PUBLISHED 14 August 2023
DOI 10.3389/fcvm.2023.1237951

OPEN ACCESS

EDITED BY
Riccardo Liga,
Pisana University Hospital, Italy

REVIEWED BY
Mila Stajevic,
University of Belgrade, Serbia
Lorenzo Monti,
University of Milan, Italy

*CORRESPONDENCE
Yukun Cao
yukuncao@hust.edu.cn
Heshui Shi
heshuishi@hust.edu.cn

†These authors have contributed equally to this work

RECEIVED 10 June 2023
ACCEPTED 31 July 2023
PUBLISHED 14 August 2023

CITATION
Li X, Cao Y, Shao G, Cui Y, Li Y, Zhang K, Liu X and Shi H (2023) Multimodality imaging assessment of primary pericardial rhabdomyosarcoma: a case report. Front. Cardiovasc. Med. 10:1237951. doi: 10.3389/fcvm.2023.1237951

Multimodality imaging assessment of primary pericardial rhabdomyosarcoma: a case report

Xingxuan Li[1], Yukun Cao[2*†], Guozhu Shao[2], Yue Cui[2], Yumin Li[2], Kailu Zhang[2], Xiaoqing Liu[2] and Heshui Shi[2*†]

[1]Cancer Center, Union Hospital, Tongji Medical College, Huazhong University of Science and Technology, Wuhan, China, [2]Department of Radiology, Union Hospital, Tongji Medical College, Huazhong University of Science and Technology, Wuhan, China

Primary pericardial sarcomas are rare and lethal diseases. To date, only a few cases of primary pericardial sarcomas, such as rhabdomyosarcoma (RMS), have been reported. Since the unusual location of RMS in the pericardium makes it challenging to diagnose, precise diagnostic procedures are required. In this study, we present the case of a 23-year-old man who experienced postprandial obstruction and atypical precordial pain that lasted for a week. Echocardiography revealed a heterogeneous isoechoic pericardial mass with a significant pericardial effusion. Contrast-enhanced CT revealed a massive pericardial effusion along with an irregular, defined, heterogeneously enhancing mass that was located between the pericardium and diaphragm. PET-CT imaging showed an intense FDG uptake in the pericardial mass. Furthermore, cardiac MRI demonstrated malignant characteristics of the pericardial mass and provided a detailed visualization of its exact anatomical connection with both cardiac and extracardiac structures. Finally, a pathologic examination of a puncture biopsy specimen confirmed the diagnosis of primary pericardial RMS. Our case emphasizes the importance of multimodal imaging for the differential diagnosis and evaluation of cardiac involvement, while providing clinicians with crucial information for clinical treatment and decision-making.

KEYWORDS

cardiac tumor, rhabdomyosarcoma, cardiac magnetic resonance, PET-CT, echocardiography

Background

Despite being rare, cardiac masses remain a significant part of cardio-oncology in clinical practice. These masses include benign tumors, primary or secondary malignant tumors, and tumor-like masses. The prevalence of primary cardiac tumors is reported to range from 0.001% to 0.3% (1). However, primary pericardial tumors are much rarer than primary cardiac tumors, accounting for only 0.001% to 0.007% (2). These tumors are predominantly malignant, with more than half of cases seen in younger patients, typically between the ages of 20 and 30, and are associated with a poor prognosis (3). The gold standard for treating malignant pericardial tumors is complete surgical resection. However, because of the aggressive nature of the tumors, more than 40% of patients may present with metastatic conditions (1).

With the advent of multimodal imaging, it is now possible to comprehensively identify the etiology of cardiac masses in many cases, in conjunction with clinical information (4). In this article, we report a case to highlight the importance of multimodal imaging in precise diagnosis and management of a rare primary pericardial sarcoma.

Case presentation

A 23-year-old male patient was referred to our hospital clinic due to symptoms of postprandial obstruction and atypical precordial pain that persisted for one week (**Supplementary Table S1**). He had no significant medical history relevant and no past interventions. On presentation, physical examination revealed a heart rate of 61 beats per minute, a blood pressure of 122/62 mmHg, and normal oxygen saturation. Chest auscultation revealed clear lungs and no cardiac murmur, and there was no lower extremity edema or jugular vein dilatation.

The resting electrocardiogram indicated sinus rhythm and ST-segment elevation (**Supplementary Figure S1**). Initial blood tests revealed mild elevation in B-type natriuretic peptide (BNP) at 188 pg/ml (normal range <100 pg/ml), aspartate aminotransferase at 67 U/L (normal range 8–40 U/L), and lactate dehydrogenase at 306 U/L (normal range 109–245 U/L). The levels of D-dimer, fibrinogen degradation products, and a tumor marker known as neuron-specific enolase were highly elevated at 7.95 mg/L (normal range <0.5 mg/L), 28.8 ug/ml (normal range <5 ug/ml) and 24.67 ug/L (normal range <16.3 ug/L), respectively.

Given his unusual symptoms and laboratory results, transthoracic echocardiography (TTE) and chest contrast-enhanced computed tomography (CT) were recommended. The TTE revealed a heterogeneous isoechoic pericardial mass with massive pericardial effusion (**Figure 1A**). Color Doppler flow imaging demonstrated minimal blood flow signals along the margins of the mass (**Figure 1B**). The dimensions of the atria and ventricles appeared to be within the normal range, and the morphology and function of the cardiac valves were unremarkable. The CT scan revealed a 6.5 cm × 7.8 cm × 6.3 cm irregular mass between the pericardium and diaphragm and significant pericardial effusion (up to 40 mm) (**Figures 1C–E**). Additionally, a 1.0 cm enlarged lymph node was detected in the right cardio-diaphragmatic angle (**Figure 1F**).

A F18-fluorodeoxy glucose-positron emission tomography (18F-FDG PET-CT) scan was recommended to provide additional information about the mass and evaluate its metabolic activity. The PET-CT scan revealed hypermetabolic activity located between the pericardium and diaphragm, with a standard uptake value (SUVmax) ranging from 5.4 to 15.9 (**Figure 2**). Additionally, hypermetabolic activity was detected in the lymph nodes of the right cardio-diaphragmatic angle, with SUVmax values of 5.9–7.3. No hypermetabolic lesions were detected in other parts of the body.

Multiparametric cardiac magnetic resonance imaging (CMR) further showed signal features suggestive for a malignant nature of the pericardial mass. Specifically, in accordance with CT, CMR showed an irregular defined mass between the pericardium and diaphragm, adjoining with enlarged lymph nodes in the right cardio-diaphragmatic angle and massive pericardial effusion (**Figure 3**). In cine imaging using a steady-state free-precession

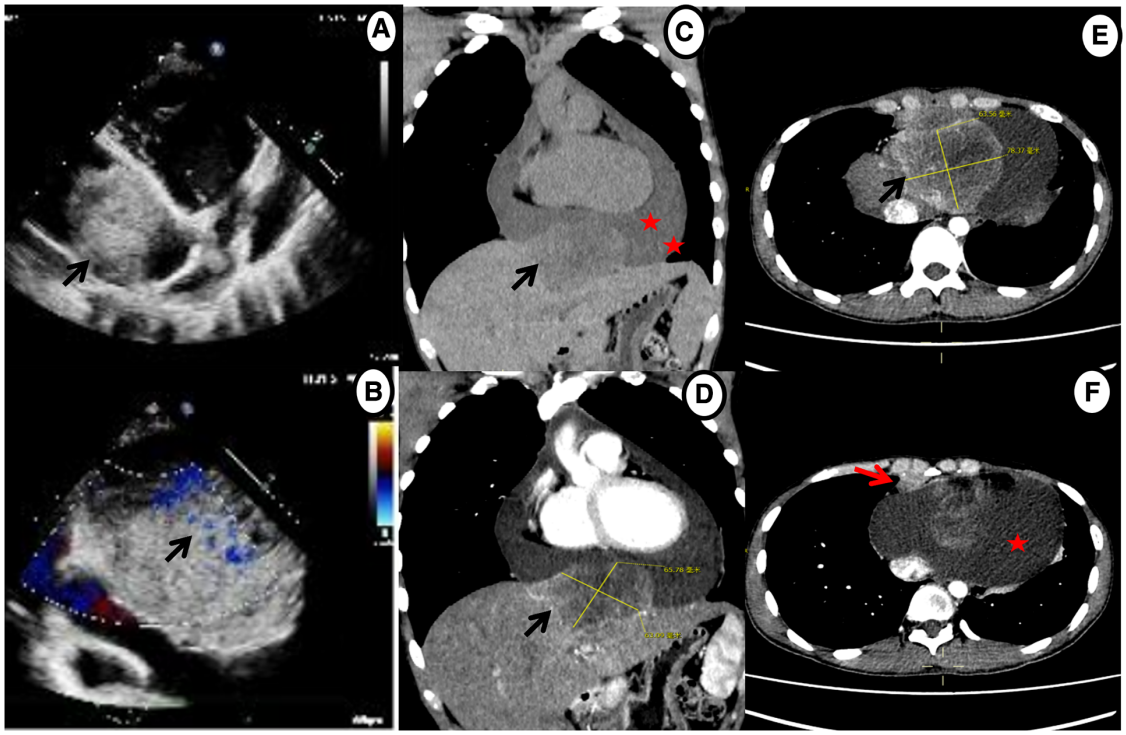

FIGURE 1
Echocardiography and chest contrast-enhanced CT demonstrating a massive mass (black arrow) and pericardial effusion (star). (A,B) Echocardiography shows a mass in the pericardium with a small amount of blood flow signals. (C–E) CT reveals an irregular, heterogeneously enhancing mass between pericardium and diaphragm with massive pericardial effusion. (F) Axial contrast-enhanced CT shows enlarged enhancing lymph nodes in the right cardio-diaphragmatic angle (red arrow).

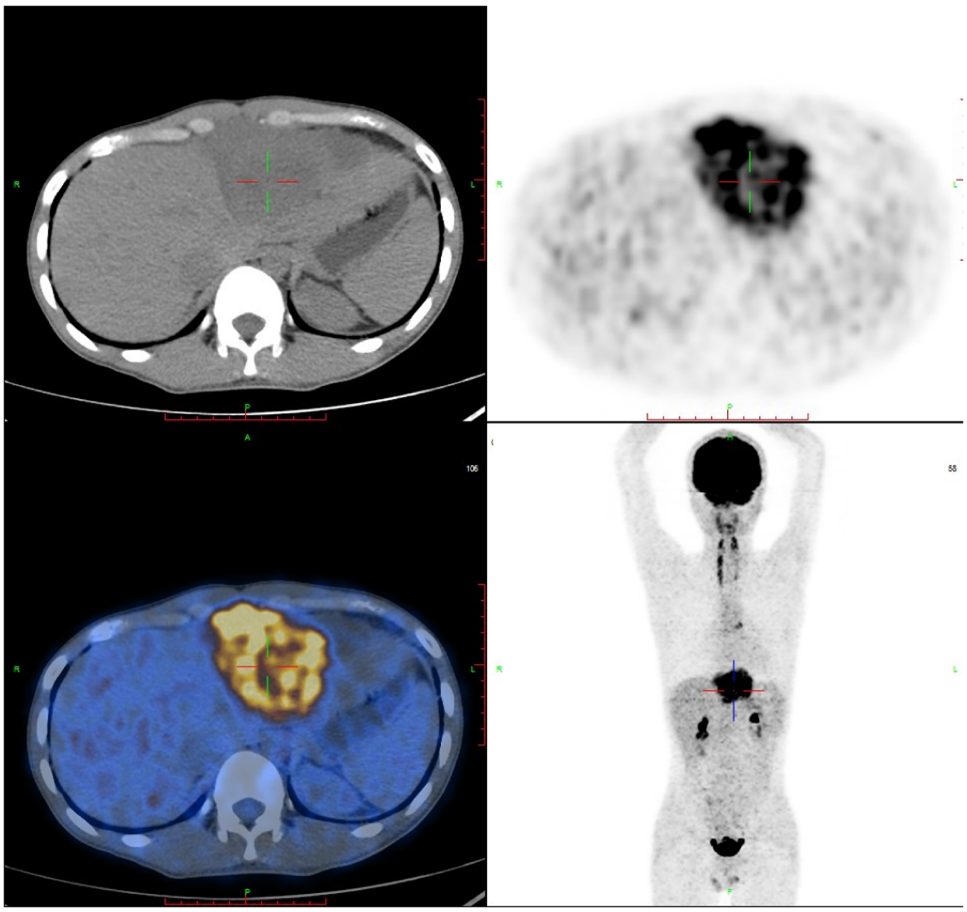

FIGURE 2
FDG-PET reveals hypermetabolic activity located between the pericardium and diaphragm, with a standard uptake value (SUVmax) ranging from 5.4–15.9, and no abnormal lesions are found in other parts of the body. FDG-PET, Fluorine-18 fluorodeoxyglucose positron emission tomography.

sequence, slight motion amplitude was observed in the large pericardial mass. However, there was no effect on the contractility of the global myocardium (**Supplementary Video S1–S2**). The relaxation of the inferior wall of the biventricle was slightly limited due to the compression of the adjacent myocardium by the mass (**Supplementary Video S3**). The analysis of cardiac function revealed preserved biventricular systolic function, with left ventricular ejection fraction at 69% and right ventricular ejection fraction at 63%. Despite the normal LV ejection fraction but elevated BNP, tissue tracking technology was used to conduct myocardial strain analysis (**Supplementary Figure S2**). The results indicated a decrease in the global longitudinal strain of the left ventricle (−11%; reference range: −15%–18%), while the global radial (34%; reference range: 30%–37%) and circumferential (−24%; reference range: −21%–25%) strains remained normal. These findings suggest the possibility of subtle segment contractile dysfunction due to the presence of a pericardial inflammation or a mass between the myocardium and pericardium. A conventional plain scanning sequence demonstrated a slightly hypointense appearance on T1w-imaging and a heterogeneously hyperintense appearance on T2w-imaging of the mass (**Figures 3A,B**, **4A,B**). The presence of heterogeneously strongly elevated T1 (1,700–2,500 ms) and T2 values (120–172 ms) within the mass was also documented using T1 and T2 mapping images (**Figures 4D,E**). However, the native T1 (908 ms), T2 (46 ms) and extracellular volume (25%) values of left ventricular myocardium were approximately normal. Resting first-pass perfusion showed that there was a complete perfusion defect within the mass related to avascularity (**Supplementary Video S4**). On late gadolinium enhancement (LGE) imaging, there was no LGE core within the mass, surrounded by slightly heterogeneously high signal enhancement (**Figures 3C,D**, **4C**). Diffusion MRI revealed that the mass was homogeneously bright on diffusion weighted imaging (DWI) and dark on apparent diffusion coefficient (ADC) (**Figures 3E,F**), suggestive of reduced diffusivity possibly owing to hypercellularity.

In addition, a CT-guided percutaneous needle biopsy was conducted, and subsequently, histopathological analysis of the tissue sample supported the diagnosis of pericardial sclerosing rhabdomyosarcoma (RMS) (**Supplementary Figure S3**). The immunohistochemical results were as follows: CD99 (+), Desmin (+), MyoD1 (diffusely strong+), Myogenin (focal+), Vimentin(+), WT1 (Paranuclear+), D2-40 (+), CD56 (+), FLi-1 (+), ALK (+), MDM2 (+), CDK4 (+), P16 (focal+), S100 (partly mild+), Ki67

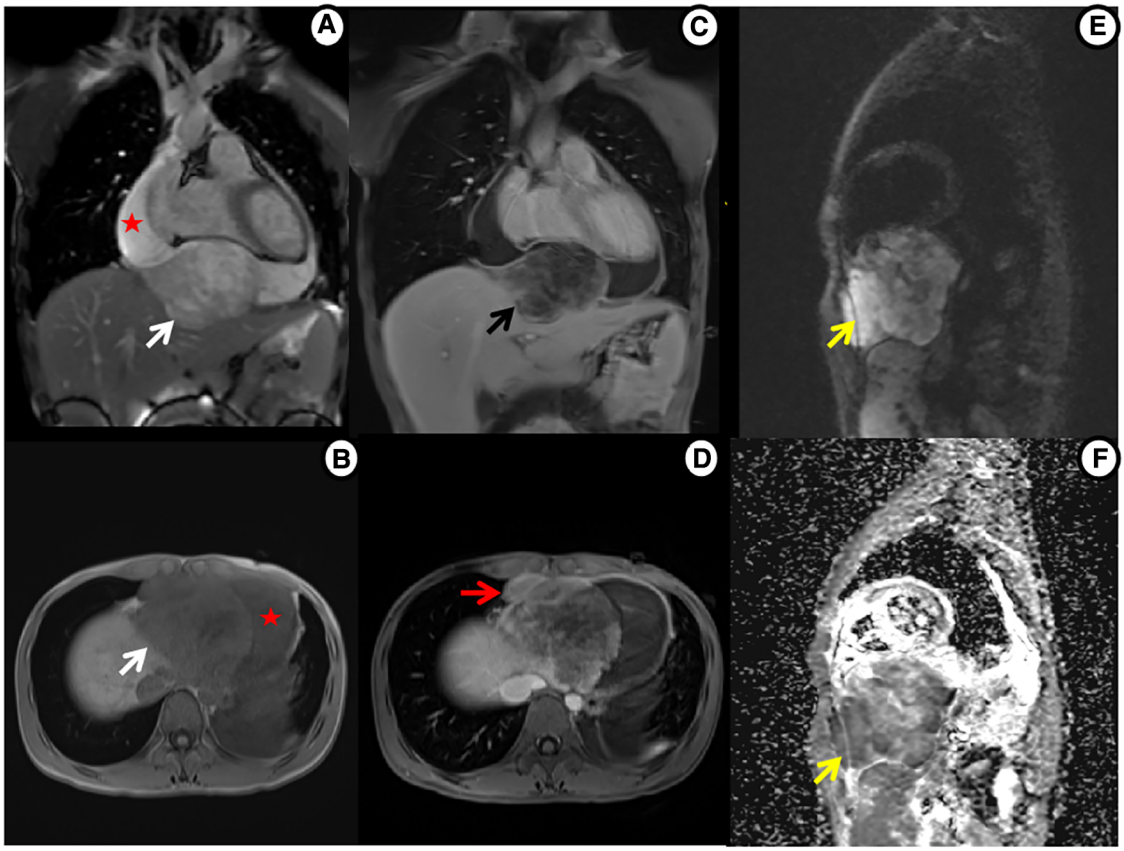

FIGURE 3
Cardiac MRI shows mass tissue characterization. (A) Cine imaging: heterogeneously hyperintense mass (white arrow) and large pericardial effusion (star). (B) Precontrast T1WI: slightly hypointense mass. (C) Postcontrast T1WI: non-enhanced core within mass, surrounded by slightly heterogeneous enhancement (black arrow). (D) Postcontrast T1WI: enlarged enhanced lymph nodes (red arrow). (E,F) Diffusion MRI: bright mass on DWI and dark on ADC (yellow arrow).

(LI: approximately 30%). Due to the tumor's size, location, and malignancy grade, the patient was referred to the oncology department of our hospital for conservative chemotherapy. However, during the eight-month follow-up after treatment, both the mass and lymph nodes in the right cardio-diaphragmatic angle showed modest enlargement (**Supplementary Figure S4**).

Discussion

Primary pericardial sarcomas are a rare and fatal type of cancer, accounting for about 10% of all primary cardiac sarcomas (5). Unlike other sarcomas, RMS tumors in the pericardium typically arise from the myocardium and have a propensity to involve multiple areas within the heart. However, primary pericardial involvement in patients is extremely rare (1). These cases are most frequently observed in infants and children, and there are no documented instances of RMS in young adult patients thus far (2, 3).

Due to its association with pericardial effusion, pericarditis, or invasion of adjacent structures, the clinical symptoms and signs of pericardial RMS are usually nonspecific. As a result, patients often present with a variety of symptoms, such as chest pain, dyspnea, and palpitations, often accompanied by pericardial effusion (6). In the current case, the patient reported feeling of obstruction after eating and atypical precordial pain, which was likely associated with the tumor's involvement of the adjacent diaphragm and pericardium. The ECG showed ST-segment elevation, which could be attributed to pericarditis caused by the mass invading the inferior pericardium, myocardial ischemia, or nonspecific physiological factors. Because of its rapid growth rate prior to clinical manifestation, RMS is challenging to treat and carries a grim prognosis. The gold standard of sarcoma treatment is surgery; however, the effectiveness of surgical removal is dependent on the tumor's anatomical location and metastasis. In primary pericardial RMS, the standard therapy in recent decades has been a combination of surgery, chemotherapy, and radiation therapy. Nonetheless, immediate surgical intervention was not recommended for the patient due to the following reasons: extensive tumor invasion of the diaphragm and potential lymph node metastasis in the right cardio-diaphragmatic angle. As a result, the patient underwent primary systemic chemotherapy after admission.

TTE has the capability to assess the impact of mass on both cardiac function and morphology. Additionally, it is also able to identify space-occupying lesions. However, TTE has several

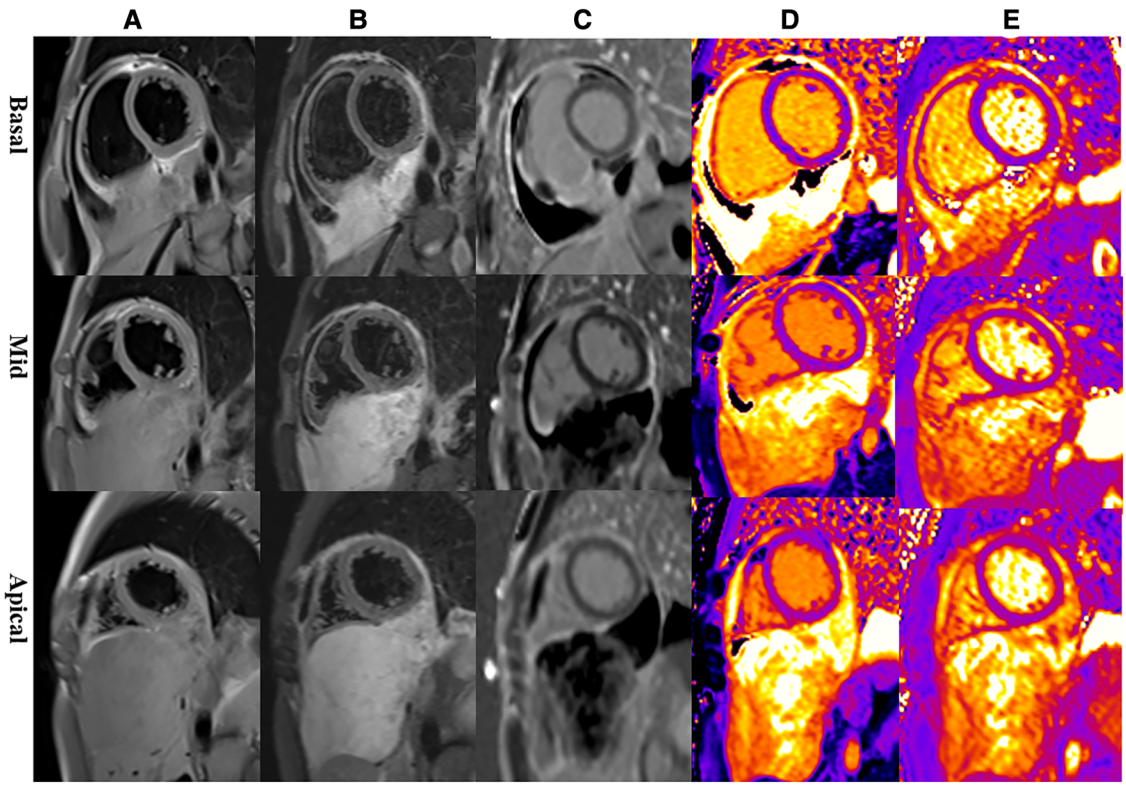

FIGURE 4
Representative magnetic resonance images of the basal, mid, and apical short-axis slices. (A) Dark-blood T1-weighted images show isointense mass. (B) Dark-blood T2-weighted images show strongly hyperintense mass. (C) Late gadolinium enhancement sequences reveal that there is peripheral heterogeneous uptake and a spared central core. (D) Native T1 mapping depicts evidently elevated T1 values in the mass. (E) T2 mapping depicts evidently elevated T2 values in the mass.

limitations, including a lower signal-to-noise ratio, weak acoustic windows, and through-plane motion artifacts. Cardiac CT offers valuable insights into the morphology of tumors with exceptional spatial and temporal resolution. PET provides a precise evaluation of the metabolic activity of tumors by using 18F-FDG. FDG-PET assists in staging malignancies and also aids in the identification of possible myocardial and pericardial involvement. It is a valuable tool for assessing early responses to cancer treatment, planning radiation therapy, and determining optimal biopsy location (7). Nevertheless, a limitation of FDG-PET is the requirement for dietary preparation, particularly in patients with intra-myocardial tumors and those with a history of radiation exposure (8).

Cardiac MRI is a highly valuable diagnostic imaging technique for assessing and follow-up in patients with cardiac masses (9). It offers multiplanar imaging with a wide field of view, without exposing patients to ionizing radiation. Additionally, it allows for the assessment of cardiac functional and anatomical characteristics, as well as myocardial tissue characterization (10). This information is critical for the early diagnosis and timely treatment of patients. **Supplementary Table S2** presents a summary of the clinical and imaging features reported in primary pericardial sarcomas from published case reports (9–21). Our analysis reveals that these tumors tend to be large, with irregular or ill-defined borders, particularly when their size exceeds 5 cm (14, 15, 17, 18). Furthermore, central areas of necrosis or hemorrhage may be evident, and there is often a significant degree of pericardial effusion or hemopericardium. Its enhancement features are closely associated with vascularity and pathological components (10, 12, 21). The patient showed ECG abnormalities and BNP elevation. Myocardial strain analysis revealed a decrease in the global longitudinal strain of the left ventricle, while the native T1, T2, and extracellular volume values of the left ventricular myocardium were within normal range. Hence, we postulate that the elevation of BNP is associated with abnormal left ventricular myocardial strain.

In our case, the enhanced CT and PET imaging revealed atypical features of heterogeneous attenuation, enhancement, and hypermetabolic activity. However, these findings complicate the process of making a differential diagnosis of the tumor. After a thorough review of the pericardial RMS patient's multiparametric CMR imaging, the following features have been identified: (1) heterogeneous hypointensity on T1-weighted images and hyperintensity on T2-weighted images indicate tumor tissue characteristics and part necrosis; (2) T1 and T2 mapping images with elevated T1 and T2 values reveal specific fibrosis and edema within the mass; (3) resting first-pass perfusion imaging shows a complete hypointense defect, indicating avascularity within the mass; (4) slightly heterogeneous LGE is associated with fibrosis and partial necrosis; (5) bright DWI and dark ADC in diffusion

MRI suggest malignant tendencies; (6) cine and conventional plain scan sequences contribute to the description of its association with cardiac and extracardiac structures. Nonetheless, regarding the CMR features of pericardial RMS, only two cases have been reported, and the CMR images are deficient in providing elaborate details. In addition, it is a rare malignant tumor mostly found in children and not adults; therefore, limited data hinders our understanding of the multiparametric features of pericardial RMS in adults.

Conclusion

Pericardial RMS is an exceptionally uncommon disease with an unfavorable result. Early diagnosis and timely intervention could potentially improve the prognosis. We described a case of atypical presentation of pericardial RMS and its multimodal imaging features. Multimodality imaging techniques, particularly cardiac MRI, allow for the evaluation of the size, borders, and tissue characteristics of the cardiac mass. It also helps in distinguishing its relationship with cardiac and extracardiac structures, quantifying its vascularity and degree of enhancement, and assessing its impact on cardiac structure and function. Nonetheless, further experience is necessary to gain a better understanding of the imaging characteristics of primary malignant pericardial tumors.

Data availability statement

The original contributions presented in the study are included in the article/**Supplementary Material**, further inquiries can be directed to the corresponding authors.

Ethics statement

The studies involving humans were approved by Medical Ethics Committee, Union Hospital, Tongji Medical College, Huazhong University of Science and Technology. The studies were conducted in accordance with the local legislation and institutional requirements. Written informed consent for participation in this study was provided by the participants' legal guardians/next of kin. Written informed consent was obtained from the individual(s) for the publication of any potentially identifiable images or data included in this article.

Author contributions

YC and HS contributed to the conception and design of the study. XL and YC collected the data and wrote the first draft of the manuscript. GS, YC, YL, XL, and KZ wrote sections of the manuscript. All authors contributed to the article and approved the submitted version.

Funding

This study was funded by Hubei Province Key Laboratory of Molecular Imaging (02.03.2018-90) and Union Hospital, Huazhong University of Science and Technology (02.03.2019-101).

Conflict of interest

The authors declare that the research was conducted in the absence of any commercial or financial relationships that could be construed as a potential conflict of interest.

Publisher's note

Supplementary material

The Supplementary Material for this article can be found online at: https://www.frontiersin.org/articles/10.3389/fcvm.2023.1237951/full#supplementary-material

References

1. Tyebally S, Chen D, Bhattacharyya S, Mughrabi A, Hussain Z, Manisty C, et al. Cardiac tumors JACC cardiooncology state-of-the-art review. *Jacc Cardiooncol*. (2020) 2:293–311. doi: 10.1016/j.jaccao.2020.05.009

2. Restrepo CS, Vargas D, Ocazionez D, Martínez-Jiménez S, Cuellar SLB, Gutierrez FR. Primary pericardial tumors. *RadioGraphics*. (2013) 33:1613–30. doi: 10.1148/rg.336135512

3. Ramlawi B, Leja MJ, Abu Saleh WK, Al Jabbari O, Benjamin R, Ravi V, et al. Surgical treatment of primary cardiac sarcomas: review of a single-institution experience. *Ann Thorac Surg*. (2016) 101:698–702. doi: 10.1016/j.athoracsur.2015.07.087

4. Maleszewski JJ, Anavekar NS, Moynihan TJ, Klarich KW. Pathology, imaging, and treatment of cardiac tumours. *Nat Rev Cardiol*. (2017) 14:536–49. doi: 10.1038/nrcardio.2017.47

5. Maleszewski JJ, Basso C, Bois MC, Glass C, Klarich KW, Leduc C, et al. The 2021 WHO classification of tumors of the heart. *J Thorac Oncol*. (2022) 17:510–8. doi: 10.1016/j.jtho.2021.10.021

6. Panda SP, Chinnaswamy G, Vora T, Prasad M, Bansal D, Kapoor G, et al. Diagnosis and management of rhabdomyosarcoma in children and adolescents: ICMR consensus document. *Indian J Pediatr*. (2017) 84:393–402. doi: 10.1007/s12098-017-2315-3

7. Rahbar K, Seifarth H, Schafers M, Stegger L, Hoffmeier A, Spieker T, et al. Differentiation of malignant and benign cardiac tumors using 18F-FDG PET/CT. *J Nucl Med*. (2012) 53:856–63. doi: 10.2967/jnumed.111.095364

8. Osborne MT, Hulten EA, Murthy VL, Skali H, Taqueti VR, Dorbala S, et al. Patient preparation for cardiac fluorine-18 fluorodeoxyglucose positron emission tomography imaging of inflammation. *J Nucl Cardiol*. (2017) 24:86–99. doi: 10.1007/s12350-016-0502-7

9. Motwani M, Kidambi A, Herzog BA, Uddin A, Greenwood JP, Plein S. MR Imaging of cardiac tumors and masses: a review of methods and clinical applications. *Radiology*. (2013) 268:26–43. doi: 10.1148/radiol.13121239

10. Salerno M, Sharif B, Arheden H, Kumar A, Axel L, Li DB, et al. Recent advances in cardiovascular magnetic resonance techniques and applications. *Circ Cardiovasc Imaging*. (2017) 10:e003951. doi: 10.1161/circimaging.116.003951

11. Liu JH, Wang Z, Yang Y, Xiong Y, Wang W, Qiu JX, et al. Multimodal diagnostic workup of primary pericardial mesothelioma: a case report. *Front Cardiovasc Med*. (2021) 8:758988. doi: 10.3389/fcvm.2021.758988

12. Jeong D, Patel A, Francois CJ, Gage KL, Fradley MG. Cardiac magnetic resonance imaging in oncology. *Cancer Control*. (2017) 24:147–60. doi: 10.1177/107327481702400207

13. Luo Y, Gong K, Xie T, Liu R, Guo H, Wang L, et al. Case report: a young man with giant pericardial synovial sarcoma. *Front Cardiovasc Med*. (2022) 9:829328. doi: 10.3389/fcvm.2022.829328

14. Krywanczyk AR, Tan CD, Rodriguez ER. A clinico-pathologic approach to the differential diagnosis of pericardial tumors. *Curr Cardiol Rep*. (2021) 23:119. doi: 10.1007/s11886-021-01548-6

15. Maleszewski JJ, Bois MC, Bois JP, Young PM, Stulak JM, Klarich KW. Neoplasia and the heart pathological review of effects with clinical and radiological correlation. *J Am Coll Cardiol*. (2018) 72:202–27. doi: 10.1016/j.jacc.2018.05.026

16. Li XD, Chen Y, Liu JY, Xu L, Li Y, Liu DT, et al. Cardiac magnetic resonance imaging of primary cardiac tumors. *Quant Imaging Med Surg*. (2020) 10:294–313. doi: 10.21037/qims.2019.11.13

17. Anand AK, Khanna A, Sinha SK, Mukherjee U, Walia JS, Singh AN. Pericardial synovial sarcoma. *Clin Oncol*. (2003) 15:186–8. doi: 10.1016/s0936-6555(02)00215-7

18. Schumann C, Kunze M, Kochs M, Hombach V, Rasche V. Pericardial synovial sarcoma mimicking pericarditis in findings of cardiac magnetic resonance imaging. *Int J Cardiol*. (2007) 118:e83–84. doi: 10.1016/j.ijcard.2007.01.029

19. Timoteo AT, Branco LM, Bravio I, Pinto E, Timoteo T, Matos P, et al. Primary angiosarcoma of the pericardium: case report and review of the literature. *Kardiol Pol*. (2010) 68:802–5.

20. Matsakas EP, Lazaros GA, Panou FK, Karavidas AI, Papalimberi EP, Scotis ID, et al. Primary pericardial fibrosarcoma presenting as "near" cardiac tamponade. *Clin Cardiol*. (2002) 25:83–5. doi: 10.1002/clc.4950250210

21. Wang JG, Wei ZM, Liu H, Li YJ. Primary pleomorphic liposarcoma of pericardium. *Interact Cardiovasc Thorac Surg*. (2010) 11:325–7. doi: 10.1510/icvts.2010.239723

22. Tutak E, Satar M, Ozbarlas N, Uguz A, Yapicioglu H, Narli N, et al. A newborn infant with intrapericardial rhabdomyosarcoma: a case report. *Turk J Pediatr*. (2008) 50:179–81.

23. Jeudy J, Kirsch J, Tavora F, Burke AP, Franks TJ, Mohammed TL, et al. From the radiologic pathology archives cardiac lymphoma: radiologic-pathologic correlation. *Radiographics*. (2012) 32:1369–80. doi: 10.1148/rg.325115126

24. Mongé MC, Walterhouse DO, Kalapurakal JA, Rigsby CK, Backer CL. Resection of intrapericardial rhabdomyosarcoma in a child. *World J Pediatr Congenit Heart Surg*. (2016) 7:108–11. doi: 10.1177/2150135115581387

frontiers | Frontiers in Cardiovascular Medicine

TYPE Case Report
PUBLISHED 23 August 2023
DOI 10.3389/fcvm.2023.1245213

OPEN ACCESS

EDITED BY
Riccardo Liga,
Pisana University Hospital, Italy

REVIEWED BY
Amitoj Singh,
University of Arizona, United States
Ofir Koren,
Cedars Sinai Medical Center, United States

*CORRESPONDENCE
Yi Yu
yuyi01@xinhuamed.com.cn
Yi-Gang Li
liyigang@xinhuamed.com.cn

†These authors have contributed equally to this work

RECEIVED 23 June 2023
ACCEPTED 07 August 2023
PUBLISHED 23 August 2023

CITATION
Yu Y, Ding M, Chen J-L, Wang T, Chen Y-H, Yang X-M, Chen S-Y, Wang Y-P and Li Y-G (2023) Multimodality imaging in diagnosing lipomatous atrial septal hypertrophy with atrial septal defect: a case report.
Front. Cardiovasc. Med. 10:1245213.
doi: 10.3389/fcvm.2023.1245213

Multimodality imaging in diagnosing lipomatous atrial septal hypertrophy with atrial septal defect: a case report

Yi Yu[1*†], Ming Ding[2†], Jin-Lan Chen[1], Ting Wang[1], Yu-Han Chen[1], Xiao-Min Yang[1], Su-Yun Chen[3], Yue-Peng Wang[1] and Yi-Gang Li[1*]

[1]Department of Cardiology, Xinhua Hospital Affiliated to School of Medicine, Shanghai Jiao Tong University, Shanghai, China, [2]Department of Radiology, Xinhua Hospital Affiliated to School of Medicine, Shanghai Jiao Tong University, Shanghai, China, [3]Department of Nuclear Medicine, Xinhua Hospital Affiliated to School of Medicine, Shanghai Jiao Tong University, Shanghai, China

Background: Lipomatous atrial septal hypertrophy (LASH) with atrial septal defect (ASD) is a rare congenital anomaly. Although LASH is a histologically benign cardiac lesion characterized by excessive fat deposition in the interatrial septum that spares the fossa ovale, it has been associated with supraventricular arrhythmias or sick sinus syndrome. Application of multimodal imaging is crucial for accurate diagnosis, appropriate treatment of LASH with ASD, and follow-up.
Case summary: A 68-year-old female patient presented with recurrent chest tightness and palpitation. Multimodal imaging revealed the characterizations of LASH and ASD. Two-dimensional transesophageal echocardiography showed a "dumbbell"-shaped involvement of the cephalad and caudal regions with sparing of a single secundum ASD. The septum with a brightness feature is an uncommon condition characterized by the deposition of unencapsulated fat cells in the atrial septum. Real-time four-dimensional transesophageal echocardiography reflected the lipomatous hypertrophy of the atrial septum and an oval-shaped ASD. Cardiac computer tomography angiography later confirmed this finding. The patient achieved a good clinical response with an ASD percutaneous occlusion guided by intracardiac echocardiography (ICE).
Conclusion: This case demonstrates a LASH combined with ASD. Multimodality imaging can provide an accurate diagnosis and may guide the procedure for precise occlusion.

KEYWORDS

lipomatous atrial septal hypertrophy, atrial septal defect, multimodality imaging, transesophageal echocardiography, case report

Introductions

Lipomatous atrial septal hypertrophy (LASH) with atrial septal defect (ASD) is a rare abnormality. LASH is a histologically benign cardiac lesion characterized by excessive fat deposition in the interatrial septum that spares the fossa ovale (1–3). The prevalence rate of LASH was reported at approximately 2.2% in patients referred for a multislice computed tomography (CT) scan and 8% in patients undergoing transesophageal echocardiography (TEE) (1). Only a few cases of LASH were found to be related to hemodynamic alterations (congestive heart failure, superior vena cava obstruction), and surgical intervention should only be reserved for patients who show marked superior vena cava or right atrium obstruction (4–8). Although LASH has been associated with

supraventricular arrhythmias (9, 10) or sick sinus syndrome (11), there are few reports in the literature on patients with both LASH and ASD (9, 12). Advances in multimodal imaging techniques may aid in diagnosing, treating, and following up LASH with ASD (13).

Case presentation

A 68-year-old female patient with a 10-year history of hypertension was hospitalized in our department due to recurrent chest tightness and palpitation for half a month, accompanied by limb edema and dizziness. She had a history of multiple ground-glass nodules in both lungs, pulmonary bullae in the lower lobe of the right lung, esophageal papilloma, reflux esophagitis, gastric body submucosal eminence, and erosive gastritis. On presentation, she was afebrile, with a heart rate of 75 beats per minute, a blood pressure of 175/90 mmHg, and normal oxygen saturation.

An electrocardiogram documented that the patient had sinus arrhythmia and intermittent atrial premature beats, with short atrial tachycardia. The levels of serum N-terminal pro-B-type natriuretic peptide (NT-proBNP) (20.59 pg/ml) were elevated. The glycosylated hemoglobin level was 6.5%. Transthoracic echocardiography showed a secundum ASD with a size of 12 mm × 13.2 mm, and the interatrial septum was significantly thickened (19.4 mm). The right atrium and right ventricle were dilated, with a pulmonary-to-systemic flow ratio (Qp/Qs) of 2.0. There was mild tricuspid regurgitation, and the systolic pulmonary artery pressure was ≈49.8 mm Hg. The global left ventricle ejection fraction measured using the Simpson method was 63.4%, and grade I diastolic dysfunction was detected.

Two-dimensional transesophageal echocardiography revealed a "dumbbell"-shaped involvement of the cephalad and caudal regions with sparing of a single secundum ASD with a size of 9 mm × 13.2 mm. The maximal thickness of the interatrial septum was 20.7 mm, and the thinnest atrial septum was 1.6 mm from the view at 0°–180°. The atrial septum presented with a brightness feature, a rare condition characterized by the deposition of unencapsulated fat cells in this area (**Figures 1A, B**). There was no obstruction in the superior and inferior vena cava. A two-dimensional color Doppler ultrasound evidenced a left-to-right shunt through ASD (**Figures 1C,D**). The diagnosis of LASH with ASD was established based on the above findings. Real-time four-dimensional transesophageal echocardiography (RT4D-TEE) confirmed the lipomatous hypertrophy of the atrial septum and an oval-shaped ASD (**Figure 1E** and **Supplementary Movie I**). In addition, a color Doppler ultrasound of RT4D-TEE demonstrated the defect appeared foraminal in a location with a significant left-to-right shunt, suggesting a "foraminal" or "fossa" ASD (**Figure 1F** and **Supplementary Movie II**).

A cardiac computer tomography angiography (CCTA) scan was performed to further characterize the atrial septum and evaluate the status of the coronary artery. The CCTA images demonstrated a 9 mm × 13 mm defect on the atrial septum (**Figures 2A,B**). The volume rendering image of the CCTA scan showed a non-enhancing, smooth, well-marginated mass with an appearance similar to subcutaneous fat (**Figures 2C,D**). In addition, the CCTA scan revealed a myocardial bridge in the middle of the left anterior descending artery.

Myocardial perfusion imaging was performed to evaluate metabolic activity. Results showed no hypermetabolic lesions or abnormal myocardial blood perfusion in the heart. The left ventricular systolic and diastolic functions were normal.

The patient underwent an ASD percutaneous occlusion under the guidance of intracardiac echocardiography (ICE) (**Supplementary Movie III**). During the operation, the LASH with ASD could be visualized by ICE from different angles. After balloon sizing, an 18 mm septal occluder device (Pushi, Shanghai) was successfully deployed (**Figures 3A,B** and **Supplementary Movie IV**). The occluder embraced the thick lipomatous cephalad rim and the thin "normal" caudal rim of the fossa ovalis. The left-to-right shunt disappeared, and no procedural complications, such as erosion or embolization, were observed. The patient was asymptomatic postoperation and followed up in an outpatient clinic (**Supplementary Figures 1A–C**). The atrial septum no longer increased in thickness. The systolic pulmonary artery pressure was ≈25.8 mmHg after ASD closure.

Discussion

The patient was examined using multimodality imaging, including two-dimensional TEE (2D-TEE), RT4D-TEE, and CCTA. The diagnostic features of LASH with ASD include the following: (1) initial 2D-TEE imaging showed a "dumbbell"-shaped involvement of the cephalad and caudal regions with sparing of a single secundum ASD, (2) RT4D-TEE demonstrated lipomatous hypertrophy of the atrial septum and an oval-shaped ASD with a significant left-to-right shunt, and (3) CCTA images demonstrated the defect structure of the atrial septum and showed a non-enhancing, smooth, well-marginated mass with an appearance similar to subcutaneous fat.

The pathognomonic "dumbbell" shape is due to hypertrophy of the septum primum and secundum with sparing of the fossa ovalis (12). Echocardiographic features of LASH include a diffuse, echo-dense globular thickening anteroinferior or posterosuperior, and the magnitude of fat accumulation is >15 mm in thickness (14). As we all know, most cases of LASH are benign; nevertheless, patients with significant hypertrophy may develop obstruction of right atrial filling, dyspnea, or symptoms similar to congestive heart failure (15). A massive LASH larger than 20 mm may alter the nearby atrial musculature, leading to disturbed atrial conduction, resulting in arrhythmias (16–18). Heyer et al. (19) and Breuer et al. (6) reported that the obstruction of the right atrium by massive septal hypertrophy potentially requires surgical resection. In addition, older age and obesity are contributors to the pathogenesis of LASH; both are risk factors for the development of atrial fibrillation. However, there are few reports in the literature on patients with both LASH and ASD (9). Moir et al. (20) reported a case of successful percutaneous transcatheter closure using an FSO device for combined LASH

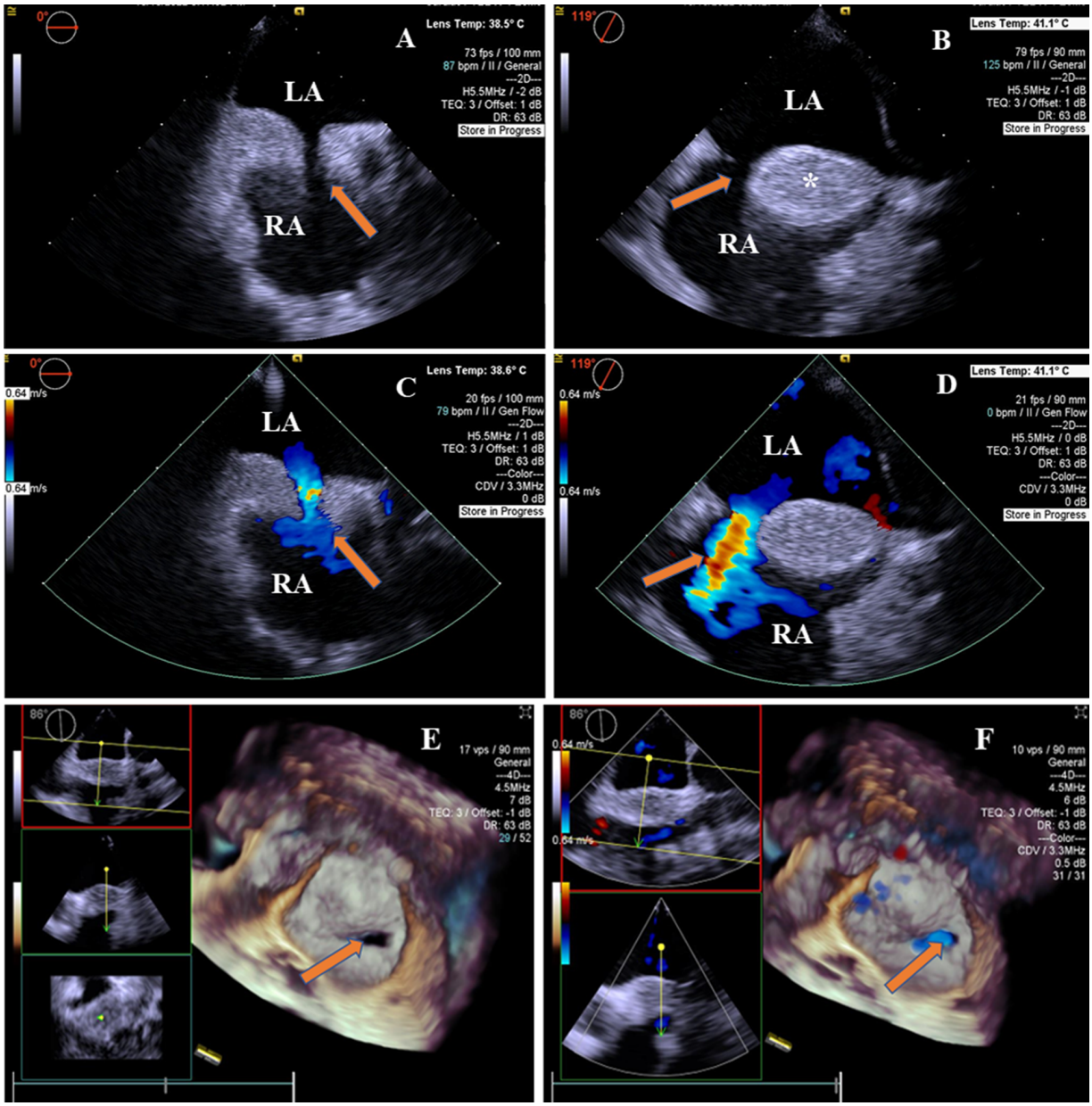

FIGURE 1
2D-TEE and 4D-TEE images revealed lipomatous hypertrophy of the atrial septum with atrial septal defect. (**A**) On 2D-TEE imaging, a single secundum ASD (arrow) and interatrial septum thickened to 20.7 mm in diameter were observed from 0° view. The septum with brightness features is characterized by the deposition of unencapsulated fat cells in the atrial septum. (**B**) 2D-TEE further documented a "dumbbell"-shaped involvement of the cephalad and caudal regions with sparing of the fossa ovalis (arrow) from 119° view. The interatrial septal fatty infiltration was demonstrated (*). (**C**) Color Doppler ultrasound of 2D-TEE showing a blood shunt from the left atrium to the right atrium (arrow) from 0° view. (**D**) Color Doppler ultrasound of 2D-TEE showing left-to-right shunt through ASD (arrow) from 119° view. (**E**) RT4D-TEE imaging reflected the whole ASD was surrounded by lipomatous hypertrophy of atrial septum (arrow) from 86° view. (**F**) Color Doppler ultrasound of RT4D-TEE showing blood flow of the ASD from the left to the right atrium (arrow). LA, left atrium; RA, right atrium.

and ASD with rim deficiency. In our case, 2D-TEE imaging indicated that LASH was associated with ASD, as evidenced by a left-to-right shunt flow signal on TEE. Finally, using 4D imaging, we confirmed the diagnosis of LASH combined with ASD, an uncommon condition illustrated as the deposition of unencapsulated fat cells in the atrial septum and oval hole.

In addition, the images could be misinterpreted as a tumor or other structural abnormalities (21–23). Masses in and near the interatrial septum may be either benign or malignant tumors. Kleiman et al. (22) reported a left atrial myxoma attached to the interatrial septum, increasing its thickness, a condition known as LASH. They then made an accurate diagnosis through TEE imaging. The interatrial septum was well visualized by echocardiography, although the image quality with TTE imaging is suboptimal compared with that of TEE imaging. If diagnosing a mass in or near the atrial septum is difficult, other available

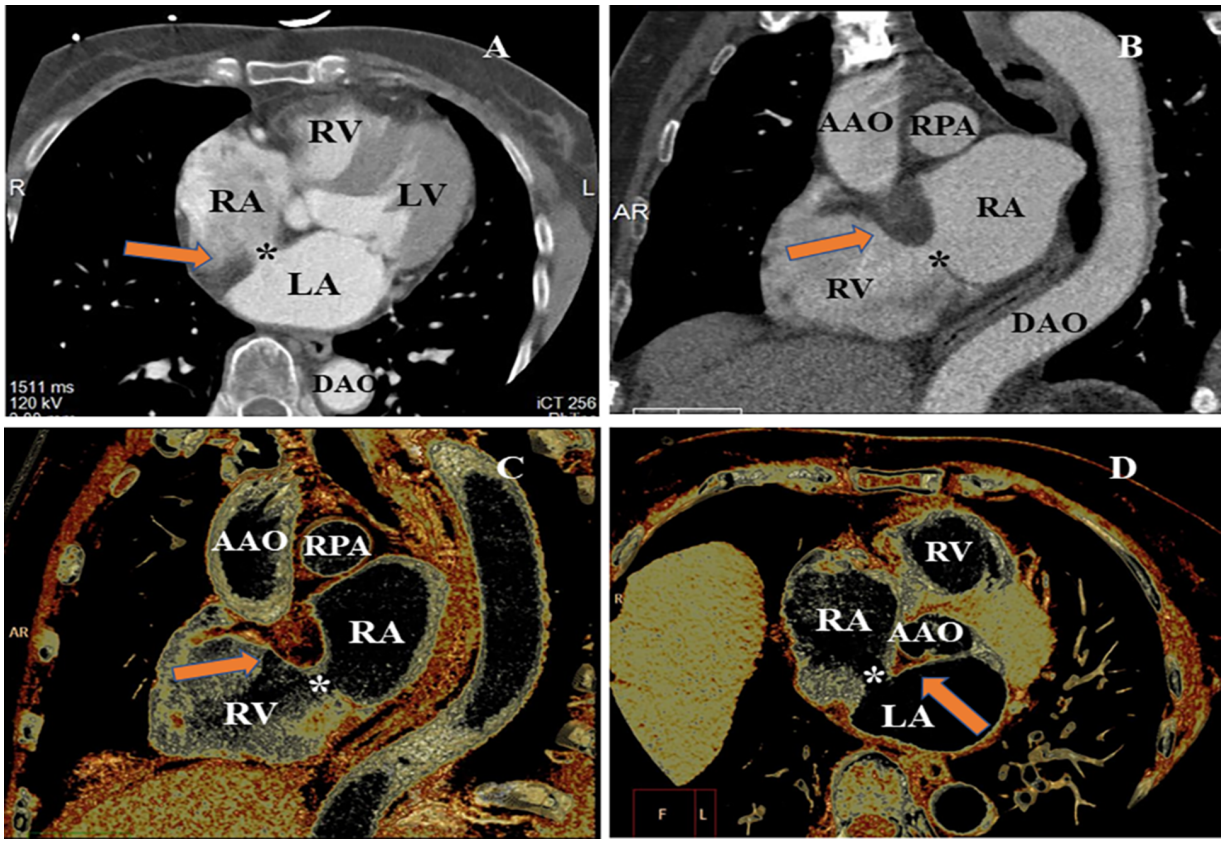

FIGURE 2
CCTA evaluating the LASH with ASD from different perspectives. (**A**) MPR image of CCTA found the loss of echogenicity between the left atrium and the right atrium (*). (**B**) MPR showed significant hypertrophy of the atrial septum (arrow), producing a dumbbell shape. (**C**) VR image indicated the thickened interatrial septum (arrow). (**D**) VR image of CCTA demonstrating the ASD and significant hypertrophy of atrial septum (arrow and *). MPR, multiplanar reconstruction; VR, volume rendering; LV, left ventricle; RV, right ventricle; RPA, right pulmonary artery; AAO, ascending aorta; DAO, descending aorta.

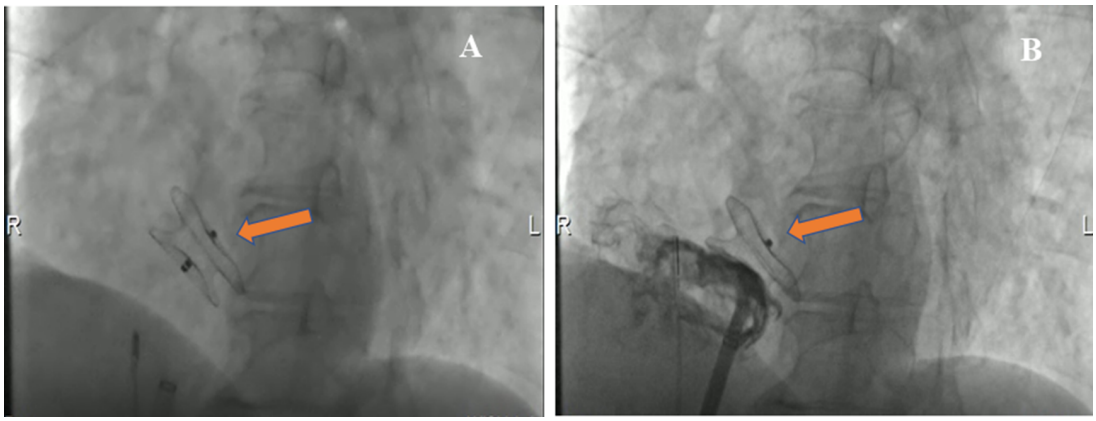

FIGURE 3
Cardioangiography (CAG) images demonstrating the closure with a Pushi septal occluder device. (**A**) CAG image visualized the position of a Pushi septal occluder device during the operation (arrow). (**B**) CAG image revealed the position of the septal occluder device was good, and there was no shunt between the left atrium and the right atrium after occlusion (arrow).

imaging modalities include cardiac magnetic resonance (CMR) imaging, myocardial perfusion imaging, and PET-CT. CMR imaging is useful in elaborating on imaging features, such as the location, shape, and signal intensity of LASH. It can reveal the presence of fatty tissues in the interatrial septum with the characteristic "dumbbell" shape and confirm the diagnosis. CMR

can evaluate potential obstructions in the inflow of the right atrium and outflow of the right ventricle and accurately diagnose benign and malignant tumors (3, 24).

In this case, TEE played an important role in diagnosing LASH with ASD. Multiple sectional views at 0°–180° could be presented during TEE examinations (25), which help visualize LASH with ASD and exclude cardiac tumors. However, in patients with significant hypertrophy of the interatrial septum, diagnosing LASH with ASD by 2D-TEE may be technically challenging. Thus, it is crucial to further evaluate LASH with ASD in one cardiac cycle using RT4D-TEE imaging, which could provide some additional valuable information. By imaging in >1 RT4D-TEE planes, LASH can be seen and confirmed with an oval hole in the center of the atrial septum. In addition, RT4D-TEE offers a thorough evaluation of the interatrial septum. Thus, it can visualize the entire significant hypertrophy of the interatrial septum and ASD in the center of the septum. Meanwhile, the diagnosis of LASH should exclude atrial septal tumors. LASH has identified a uniform internal echo of the atrial septal tissue, distinct from the appearance of the neoplasm. Next, the high spatial resolution of CCTA has the advantage of visualizing significant hypertrophy of the atrial septum. ICE may provide additional information to aid a successful operation. It used to believe that catheter-based closure of ASD was contraindicated in patients with LASH (14). Lin et al. (12) reported a successful closure of ASDs in two patients with LASH using the Amplatzer muscular ventricular septal defect closure device. This device fitted well to the atrial septum and had no residual shunts at the 1-month follow-up. In our case, intraoperative ICE guidance combined with preoperative imaging examination results is safer, and the ASD occluder can be selected more accurately. To the best of our knowledge, this study is the first report of a successful percutaneous transcatheter closure using a Pushi septal occluder device for ASD combined with LASH.

In conclusion, in this case, the multimodality imaging techniques, especially for RT4D-TEE imaging, are pivotal for diagnosing a rare LASH with ASD and for deciding to perform the occlusion of ASD guided by ICE.

Data availability statement

The original contributions presented in the study are included in the article/**Supplementary Material**, further inquiries can be directed to the corresponding authors.

Ethics statement

The Ethics Committee of Xinhua Hospital Affiliated to Shanghai Jiao Tong University School of Medicine approved the studies involving humans. The studies were conducted in accordance with local legislation and institutional requirements. The participants provided their written informed consent to participate in this study. Written informed consent for the publication of any potentially identifiable images or data included in this article was obtained from the individual(s).

Author contributions

YY participated in conception and design. Y-GL and Y-PW provided administrative support. S-YC and J-LC provided materials or patients. MD and TW performed collection and assembly of data. X-MY and Y-HC performed data analysis and interpretation. All authors contributed to the article and approved the submitted version.

Funding

Funding for this study was provided in part by grant number 17411954800 from Shanghai Science and Technology Committee Clinical Field Project Fund (YY), grant number 202240110 from the Shanghai Health and Family Planning Commission (YY), and grant number XHKC2021-07 from Xinhua Hospital Affiliated with the School of Medicine (YY).

Acknowledgments

We appreciate the doctors in the Department of Cardiology, Xinhua Hospital of Jiaotong University, for treating these patients.

Conflict of interest

The authors declare that the research was conducted in the absence of any commercial or financial relationships that could be construed as a potential conflict of interest.

Publisher's note

Supplementary material

The Supplementary Material for this article can be found online at: https://www.frontiersin.org/articles/10.3389/fcvm.2023.1245213/full#supplementary-material

References

1. Laura DM, Donnino R, Kim EE, Benenstein R, Freedberg RS, Saric M. Lipomatous atrial septal hypertrophy: a review of its anatomy, pathophysiology, multimodality imaging, and relevance to percutaneous interventions. *J Am Soc Echocardiogr*. (2016) 29:717–23. doi: 10.1016/j.echo.2016.04.014

2. Xanthos T, Giannakopoulos N, Papadimitriou L. Lipomatous hypertrophy of the interatrial septum: a pathological and clinical approach. *Int J Cardiol*. (2007) 121:4–8. doi: 10.1016/j.ijcard.2006.11.150

3. Xanthopoulos A, Giamouzis G, Alexopoulos N, Kitai T, Triposkiadis F, Skoularigis J. Lipomatous hypertrophy of the interatrial septum: a case report and review of the literature. *CASE*. (2017) 1:182–9. doi: 10.1016/j.case.2017.06.005

4. Takayama S, Sukekawa H, Arimoto T, Ikeno E, Komatu T, Rikimaru H, et al. Lipomatous hypertrophy of the interatrial septum with cutaneous lipomatosis. *Circ J*. (2007) 71:986–9. doi: 10.1253/circj.71.986

5. Bielicki G, Lukaszewski M, Kosiorowska K, Jakubaszko J, Nowicki R, Jasinski M. Lipomatous hypertrophy of the atrial septum—a benign heart anomaly causing unexpected surgical problems: a case report. *BMC Cardiovasc Disord*. (2018) 18:152. doi: 10.1186/s12872-018-0892-3

6. Breuer M, Wippermann J, Franke U, Wahlers T. Lipomatous hypertrophy of the interatrial septum and upper right atrial inflow obstruction. *Eur J Cardiothorac Surg*. (2002) 22:1023–5. doi: 10.1016/S1010-7940(02)00619-X

7. Tugcu A, Yildirimturk O, Rizaoglu E, Sagbas E, Akpinar B, Aytekin S. Lipomatous hypertrophy of the interatrial septum presenting as an obstructive right atrial mass in a patient with exertional dyspnea. *J Am Soc Echocardiogr*. (2007) 20:1319.e3–5. doi: 10.1016/j.echo.2007.04.012

8. Søholm H, Iversen K, Olsen PS, Andersen CB, Hassager C. Superior vena cava syndrome as a rare complication to lipomatous atrial septal hypertrophy (LASH). *Eur Heart J Cardiovasc Imaging*. (2013) 14:717. doi: 10.1093/ehjci/jes324

9. Takafuji H, Obunai K, Kato N, Honda M, Watanabe H. Lipomatous atrial septal hypertrophy and atrial septal defect with rim deficiency. *JACC Cardiovasc Interv*. (2022) 15:e31–3. doi: 10.1016/j.jcin.2021.09.040

10. Brienesse SC, Sugito S, Mejia R, Leitch J, Wilsmore B. An electrophysiological and anatomical space-occupying lesion: lipomatous hypertrophy of the interatrial septum in a patient presenting with atrial tachycardia. *Heart Rhythm Case Reports*. (2021) 7:542–5. doi: 10.1016/j.hrcr.2021.05.003

11. Sato Y, Matsuo S, Kusama J, Kunimasa T, Yoda S, Matsumoto N, et al. Lipomatous hypertrophy of the interatrial septum presenting as sick sinus syndrome. *Int J Cardiol*. (2007) 119:280–1. doi: 10.1016/j.ijcard.2006.07.161

12. Lin CH, Balzer DT, Lasala JM. Defect closure in the lipomatous hypertrophied atrial septum with the Amplatzer muscular ventricular septal defect closure device: a case series. *Catheter Cardiovasc Interv*. (2011) 78:102–7. doi: 10.1002/ccd.22858

13. Czekajska-Chehab E, Tomaszewska M, Olchowik G, Tomaszewski M, Adamczyk P, Drop A. Lipomatous hypertrophy of the interatrial septum in ECG-gated multislice computed tomography of the heart. *Med Sci Monit*. (2012) 18: MT54–9. doi: 10.12659/MSM.883197

14. Zanchetta M, Rigatelli G, Pedon L, Zennaro M, Maiolino P, Onorato E. Role of intracardiac echocardiography in atrial septal abnormalities. *J Intervent Cardiol*. (2003) 16:63–77. doi: 10.1046/j.1540-8183.2003.08004.x

15. Laura DM, Donnino R, Kim EE, Benenstein R, Freedberg RS, Saric M. Lipomatous atrial septal hypertrophy: a review of its anatomy, pathophysiology, multimodality imaging, and relevance to percutaneous interventions. *J Am Soc Echocardiogr*. (2016) 8:717–23. doi: 10.1016/j.echo.2016.04.014

16. Augoustides JG, Weiss SJ, Ochroch AE, Weiner J, Mancini J, Savino JS, et al. Analysis of the interatrial septum by transesophageal echocardiography in adult cardiac surgical patients: anatomic variants and correlation with patent foramen ovale. *J Cardiothorac Vasc Anesth*. (2005) 19:146–9. doi: 10.1053/j.jvca.2005.01.021

17. López-Candales A. Is the presence of interatrial septal hypertrophy a marker for atrial fibrillation in the elderly? *Am J Geriatr Cardiol*. (2002) 11:399–403. doi: 10.1111/j.1076-7460.2002.01629.x

18. Abboud H, Brochet E, Amarenco P. Lipomatous hypertrophy of the inter-atrial septum and stroke. *Cerebrovasc Dis*. (2004) 18:178. doi: 10.1159/000079740

19. Heyer CM, Kagel T, Lemburg SP, Bauer TT, Nicolas V. Lipomatous hypertrophy of the interatrial septum. *Chest*. (2003) 124:2068–73. doi: 10.1378/chest.124.6.2068

20. Moir WS, McGaw DJ, Harper RW, Gelman J. Atrial septal defect device closure in a patient with lipomatous hypertrophy of the atrial septum. *Circulation*. (2003) 107:e217. doi: 10.1161/01.CIR.0000069908.63932.0A

21. Agmon Y, Meissner I, Tajik AJ, Seward JB, Petterson TM, Christianson TJH, et al. Clinical, laboratory, and transesophageal echocardiographic correlates of interatrial septal thickness: a population-based transesophageal echocardiographic study. *J Am Soc Echocardiogr*. (2005) 18:175–82. doi: 10.1016/j.echo.2004.09.002

22. Kleiman AM, Harding LM, Bechtel AJ. Concomitant lipomatous hypertrophy and left atrial mass: distinguishing benign from malignant. *Echocardiography*. (2018) 35:534–6. doi: 10.1111/echo.13834

23. Bassareo PP, Tumbarello R, Mercuro G. Cor triatriatum and lipomatous hypertrophy of the interatrial septum in the elderly: a case report. *Cardiovasc Ultrasound*. (2010) 8:4. doi: 10.1186/1476-7120-8-4

24. Hudzik B, Filipiak K, Zembala M, Szkodzinski J, Miszalski-Jamka K, Niklewski T, et al. Lipomatous hypertrophy of the interatrial septum: a rare cause of right ventricular impairment. *J Card Surg*. (2010) 25:171–4. doi: 10.1111/j.1540-8191.2009.00961.x

25. Silvestry FE, Cohen MS, Armsby LB, Burkule NJ, Fleishman CE, Hijazi ZM, et al. Guidelines for the echocardiographic assessment of atrial septal defect and patent foramen ovale: from the American Society of Echocardiography and Society for Cardiac Angiography and Interventions. *J Am Soc Echocardiogr*. (2015) 28:910–58. doi: 10.1016/j.echo.2015.05.015

frontiers | Frontiers in Cardiovascular Medicine

TYPE Case Report
PUBLISHED 01 November 2023
DOI 10.3389/fcvm.2023.1278457

OPEN ACCESS

EDITED BY
Riccardo Liga,
Pisana University Hospital, Italy

REVIEWED BY
Mitra Chitsazan,
Iran University of Medical Sciences, Iran
Constantina Aggeli,
National and Kapodistrian University of Athens, Greece

*CORRESPONDENCE
Ai-Ai Chu
✉ aiaichu@126.com

RECEIVED 16 August 2023
ACCEPTED 13 October 2023
PUBLISHED 01 November 2023

CITATION
Zhang R, Zhao F, Wang J, Qin Y, Wang T and Chu A-A (2023) Case Report: Integrated echocardiographic assessment guided Liwen procedure for treating obstructive hypertrophic cardiomyopathy with ventricular aneurysm. Front. Cardiovasc. Med. 10:1278457. doi: 10.3389/fcvm.2023.1278457

Case Report: Integrated echocardiographic assessment guided Liwen procedure for treating obstructive hypertrophic cardiomyopathy with ventricular aneurysm

Rui Zhang, Fan Zhao, Jing Wang, Yahong Qin, Tingting Wang and Ai-Ai Chu*

Department of Echocardiography, First Clinical Medicine School, Gansu Province Hospital, Gansu University of Chinese Medicine, Lanzhou, China

Hypertrophic cardiomyopathy (HCM) is a genetic myocardial disease, with an estimated incidence of 0.2%–6%, and is the main cause of sudden cardiac death (SCD) in young athletes. Left ventricular apical aneurysm (LVAA) is a rare subtype of HCM, accounting for about 5% of HCM patients, and has a higher incidence of cardiovascular adverse events. In cases of hypertrophic obstructive cardiomyopathy with LVAA (HOCM-LVAA) that do not respond adequately to optimized medical therapy, the echocardiography-guided percutaneous intra-myocardial septal radiofrequency ablation (PIMSRA, Liwen procedure) emerges as a promising and effective novel therapeutic approach. In this case report, we present for the first time a comprehensive application of echocardiographic techniques, including TTE, 2-D STE, and contrast enhancement, in the diagnosis, treatment, surgical guidance, and assessment of therapeutic outcomes in a case of HOCM-LVAA.

KEYWORDS

hypertrophic obstructive cardiomyopathy, hypertrophic cardiomyopathy, transthoracic echocardiography, contrast-enhanced echocardiography, speckle tracking echocardiography

Introduction

Hypertrophic cardiomyopathy (HCM) is a genetic myocardial disease, with an estimated incidence of 0.2%–0.6%, and is the main cause of sudden cardiac death (SCD) in young athletes (1–3). Left ventricular apical aneurysm (LVAA) is a rare subtype of HCM, accounting for about 5% of HCM patients, and has a higher incidence of cardiovascular adverse events (4, 5). In cases of hypertrophic obstructive cardiomyopathy with LVAA (HOCM-LVAA) that do not respond adequately to optimized medical therapy, the echocardiography-guided percutaneous intra-myocardial septal radiofrequency ablation (PIMSRA, Liwen procedure) emerges as a promising and effective novel therapeutic approach (6, 7). During the procedure, various echocardiographic images play essential roles in diagnosis, treatment, and outcome evaluation. Transthoracic echocardiography (TTE) enables real-time visualization of cardiac structures, furnishing valuable insights into cardiac chamber dimensions and guiding the procedure (6). Contrast-enhanced echocardiography enables precise assessment structural changes within the left ventricle,

crucial for the diagnosis of HOCM-LVAA (7). Strain imaging, 2-D speckle tracking echocardiography (2-D STE) offers valuable insights into alterations in myocardial contractility following the procedure, thereby evaluating the effects of Liwen procedure on HOCM. In this case report, we present for the first time a comprehensive application of echocardiographic techniques, including TTE, 2-D STE, and contrast enhancement, in the diagnosis, treatment, surgical guidance, and assessment of therapeutic outcomes in a case of HOCM-LVAA.

A 57-year-old woman presented with worsen dyspnea after exercise for 5 years. TTE revealed thickening of the interventricular septum (up to 20 mm) and increased flow velocity in the left ventricular outflow tract (LVOT) with a peak velocity of 4.52 m/s and evaluated peak pressure gradient of 85 mmHg. Localized thinning of the ventricular wall at the apex, approximately 5 mm in thickness, was noted, with mild paradoxical motion, covering an area of approximately 19 mm × 30 mm. M-mode echocardiography revealed positive systolic anterior motion of the mitral valve (SAM) and moderate mitral regurgitation. 2-D STE examination were applied for the strain evaluation pre- and post-operation. Pre-operative STE demonstrated the lowest strain value in the basal interventricular septum, decreasing to −5.9%, and the lowest strain value in the left ventricular apex, decreasing to −11.9% (Figure 1A). The patient reported experiencing chest discomfort, shortness of breath, occasional precordial pain, along with fatigue and palpitations, particularly after physical activity. These symptoms would alleviate with rest. Coronary angiography indicated normal origins and courses of the left and right coronary arteries without significant stenosis. Cardiac magnetic resonance imaging (MRI) findings

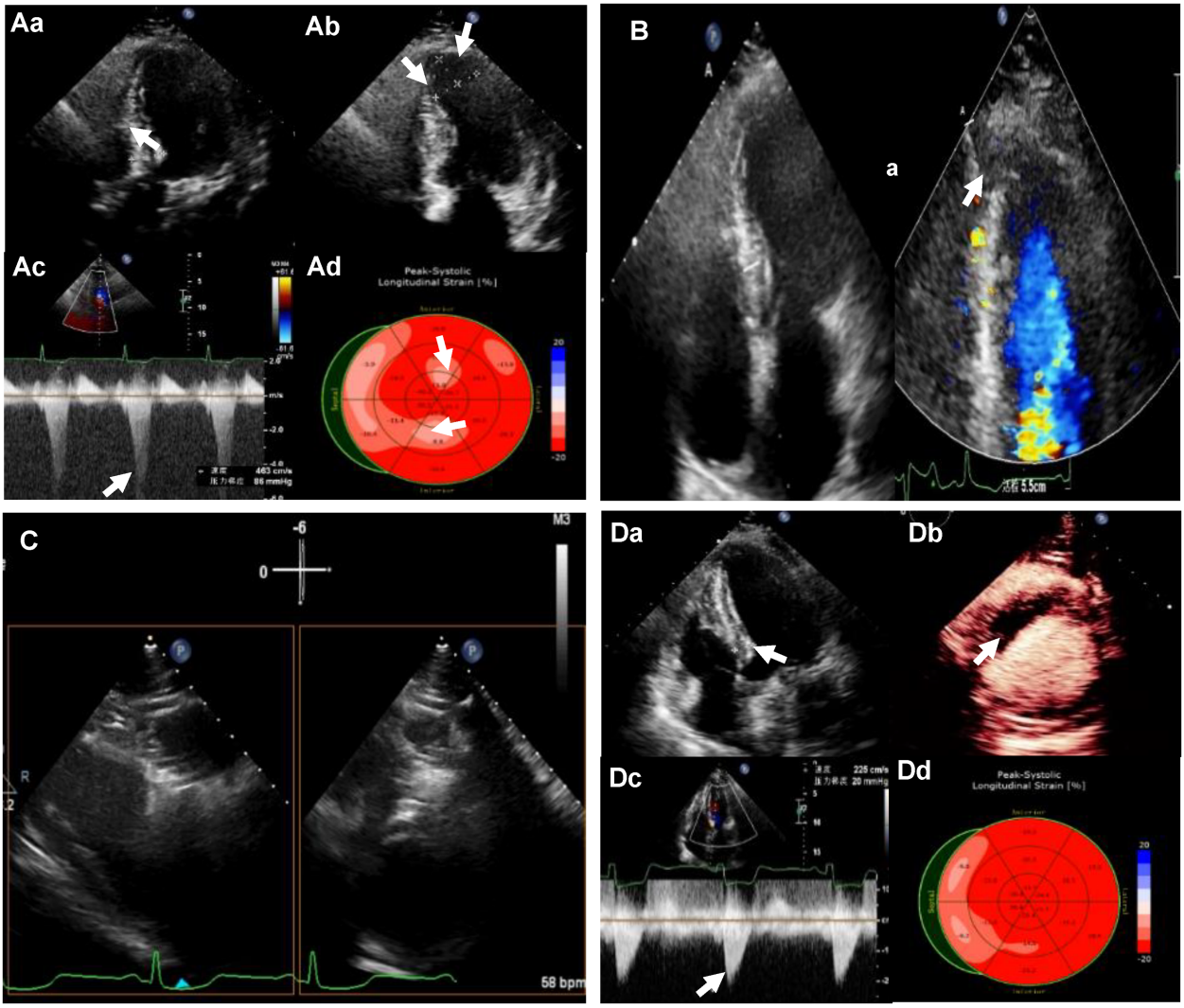

FIGURE 1
(**Aa**) Preoperative transthoracic echocardiography (TTE): left ventricular (LV) septal thickness of 20mm; (**Ab**) the extent of ventricular aneurysm; (**Ac**) left ventricular outflow tract (LVOT) obstruction at rest; (**Ad**) reduced strain value of local LV apex by strain echocardiography (SE). (**B**) LV apical entrance of the ablation needle guided by TTE. (**C**) Bi-plane showing ablation needle position. (**Da**) LV septal thickness of 12 mm after ablation; (**Db**) myocardial contrast-enhanced echocardiography (MCE) showing a contrast filling defect in the ablation zone; (**Dc**) LVOT gradient of 20 mm Hg after the ablation; (**Dd**) LV apical systolic synchrony detected by SE.

suggested a diagnosis of hypertrophic cardiomyopathy with asymmetrical myocardial hypertrophy, interstitial fibrosis, and left ventricular outflow tract (LVOT) obstruction (**Figure 2A**). Initial laboratory investigations revealed elevated NT-proBNP levels at 854 pg/ml and cTNT levels at 12.19 ng/L. The electrocardiogram showed sinus rhythm with abnormal Q waves in leads I, II, avL, and V3–V6, as well as horizontal ST-segment depression of 0.05–0.2 mv in leads I, II, III, avF, and V3–V6, accompanied by bidirectional T-wave changes in the same leads. The patient was classified as NYHA III in terms of functional capacity (**Figure 2E**). Despite undergoing optimal medical therapy, the patient continues to experience symptoms of heart failure, including chest pain, chest tightness, and shortness of breath, classified as NYHA Class III. According to a multidisciplinary consultation, it was recommended that the patient undergo surgical resection and alcohol septal ablation. However, the patient was unwilling to undergo cardiac surgery. Although coronary alcohol septal ablation presents itself as a viable alternative, the ventricular septal branch and location of myocardial hypertrophy is incongruent in this patient. This inconsistency renders it less effective and potentially raises the risk of pacemaker reliance, making it unsuitable for targeted alcohol injection. As a result, we proposed a novel treatment approach in our center, employing radiofrequency ablation for HOCM-LVAA, Liwen procedure.

The patient undergone Liwen procedure under general anesthesia in the supine position. Considering the ventricular aneurysm, we attempted the modified needle technique guided by TTE, in which the approach was reverse insertion to avoid pericardial tamponade caused by insertion into the left ventricle (**Figure 1B**). The location and characteristics of the aneurysm necessitated a specific approach when choosing the Liwen procedure. Due to the aneurysm's location and features, we opted for a modified insertion approach, transitioning from the conventional B-line approach to the A-line approach. We also rotated the ultrasound probe by 180° and carefully positioned the needle tip along the aneurysmal wall to target the basal interventricular septum for ablation. The presence of the ventricular aneurysm compelled us to pay special attention to the insertion direction and needle tip placement within the aneurysmal myocardium during the Liwen procedure to avoid inadvertent entry into the cardiac chamber and the risk of pericardial tamponade (**Figure 1C**). The ACT-1530 radiofrequency needle was advanced along the ventricular wall to the hypertrophic portion of the anterior septum under ultrasound guidance. We employed the Philips X5-1 probe with X-plane dual-plane functionality to guide the needle tip's positioning, ensuring it was located in the basal portions of the anterior septum (Zone I, Zone II, Zone III). Radiofrequency energy was then applied, with a maximum power of 80 W, 80 W, and 105 W for each respective zone, and treatment durations of 7 min, 8 min, and 3 min. After ablation, myocardial contrast echocardiography revealed a contrast filling defect in the ablation zone of the interventricular septum. One week later, the thickness of the myocardium in the interventricular septum decreased from 20 mm to 12 mm, and LVOT obstruction was significantly relieved (peak gradient of 20 mmHg). STE showed

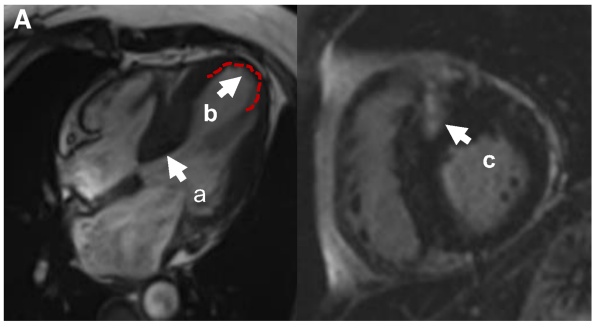

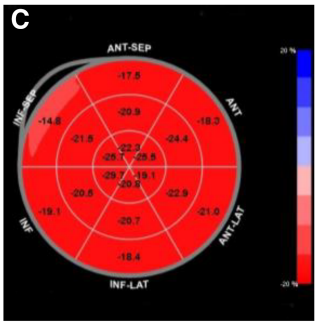

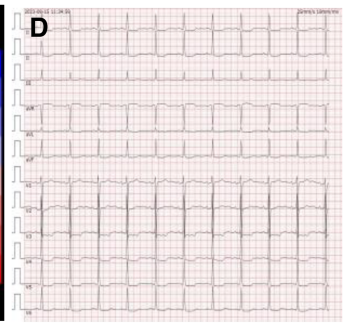

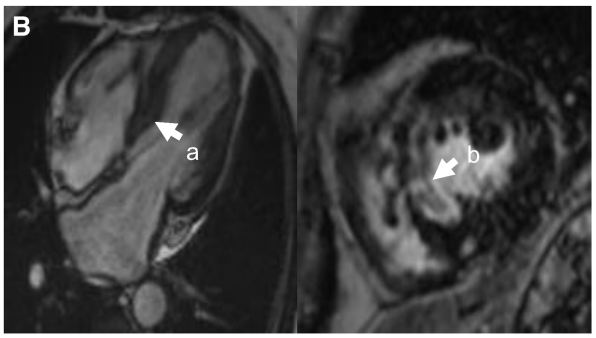

E

	LA' size (mm)	LVOT gradient (mmHg)	Maximal VWT (mm)	Nonsustained ventricular velocity	Unexplained syncope	Family history	Age	SCD rate
Pre-operation	45	Provocation: 121	22	No	No	No	59	3.01%
Post-operation	45	Provocation: 25	12	No	No	No	61	1.06%

F

Echocardiographic Parameters	Pre-operation		Post-operation	
	Resting	Stress	Resting	Stress
Interventricular septum (mm)	22	-	12	-
Left ventricular outflow peak gradient (mmHg)	85	121	20	25
ST segment depression (mv)	-0.22	-0.29	-0.20	-0.25
Heart rate (beats/min)	50	113	59	103
Systolic blood pressure (mmHg)	131	156	117	183
Diastolic blood pressure (mmHg)	77	95	82	104
Chest pain (+/-)	-	+	-	-

FIGURE 2
(A) Preoperational cardiac magnetic resonance imaging (MRI). (a) Thickened interventricular septum, (b) the extent of ventricular aneurysm, (c) myocardial interstitial fibrosis; (B) post-operational cardiac MRI. (a) Interventricular septal thickness, (b) hypoperfusion area of myocardium at the base of ventricular septum; (C) recovered strain values of local LV apex post-operation; (D) electrocardiogram post-operation; (E) sudden cardiac death score pre- and post-operation; (F) stress echocardiographic parameters of pre- and post-operation.

LV systolic synchrony was achieved, and the apical aneurysm returned to normal appearance of morphology (Figure 1D). One year post the procedure, STE showed an increase in strain values in the basal interventricular septum, reaching −17.5%, and a significant recovery in strain value in the left ventricular apex, returning −22.3%" (with the anterior wall as a reference) (Figure 2B). Through the stress echocardiographic examination, we detected an increased LVOT with a peak velocity of 5.5 m/s and a peak pressure gradient of 121 mmHg in this case. However, 1 year after the procedure, stress echocardiography showed a reduced flow velocity in the LVOT, with a peak velocity of 2.5 m/s and a peak pressure gradient of 25 mmHg (Figure 2F). One-week postoperative assessment, laboratory results indicated NT-proBNP levels at 907 pg/ml and cTNT levels at 5,335 ng/L. Subsequent follow-up examinations at 1 year and 2 years post-procedure showed a reassuring trend with NT-proBNP levels at 801 pg/ml and 657 pg/ml, respectively, and cTNT levels at 13.7 ng/L and 14.8 ng/L, respectively. Postoperative electrocardiography revealed sinus rhythm with horizontal ST-segment depression of 0.05–0.20 mv in leads I, II, III, avF, and V4–V6, with a P-wave duration of 122 ms. Follow-up electrocardiograms at 1 year and 2 years post-procedure continued to show sinus rhythm with horizontal ST-segment depression of 0.05–0.15 mv in leads I, II, avF, and V3–V6, with a P-wave duration of 122 ms (Figure 2C).

Discussion

We successfully treated a patient with HOCM-LVAA through PIMSRA, Liwen's surgery under various echocardiographic guidance, demonstrating gradient descent, functional recovery, and no post-operative complications. The pathogenesis of HOCM-LVAA includes chronic overload and high pressure in the apex of the heart, ventricular remodeling, and gradual exacerbation of myocardial hypertrophy, leading to local damage and dilation of the ventricle, and irreversible changes in the structure and function of the ventricle, eventually resulting in the formation of a ventricular aneurysm (8). Liwen's Procedure is a novel interventional surgery that uses percutaneous access to puncture the ventricular wall and deliver a certain amount of radiofrequency energy to ablate the obstructive myocardial tissue, thus reducing outflow tract obstruction and improving heart function (7, 9). The indications for Liwen procedure primarily include patients who, despite receiving maximum tolerated doses of optimized medication, continue to experience severe symptoms such as breathlessness, chest pain, or exercise-induced syncope, with their cardiac function classified as NYHA Grade III/IV or CCS Grade III/IV. After a comprehensive evaluation of the patient's clinical condition, which suggested a low risk of arrhythmias and a lower likelihood of sudden cardiac death (SCD), implantable cardioverter-defibrillator (ICD) implantation was not deemed necessary as a part of the overall therapeutic approach in this case. In addition, Liwen procedure indications also include a left ventricular outflow tract gradient (LVOTG) or left ventricular intracavitary pressure difference of ≥50 mmHg at rest and during provocation, as determined through echocardiographic assessment. Patients who do not meet the above criteria but exhibit other high-risk factors or severe symptoms may also be considered for Liwen surgery. In comparison, alcohol septal ablation (ASA) has more stringent indications. ASA is recommended for patients who meet criteria including clinical, hemodynamic, and morphological indications (10). Clinical indications involve persistent symptoms despite standard medication treatment, a baseline heart rate around 60 beats per minute, and classification as NYHA Grade III/IV or CCS Grade III for chest pain. High-risk factors or exercise-induced syncope may also qualify. Hemodynamic indication requires specific LVOTG values at rest or after provocation. Morphological indications encompass septal thickness, obstruction location, and various anatomical considerations, including the absence of papillary muscle involvement. Coronary angiography and myocardial acoustic imaging are used to identify suitable septal branches for ablation. Therefore, both Liwen surgery and alcohol septal ablation are viable treatment options for HOCM patients with ventricular septal hypertrophy. However, Liwen surgery is generally associated with less trauma and offers greater precision in interventional treatment. Guided by echocardiography, Liwen surgery enables physicians to control the treatment area more accurately, reducing the associated risks. Different areas can be treated during Liwen procedure as needed to alleviate myocardial hypertrophy and achieve better outcomes. Alcohol septal ablation, on the other hand, uses coronary artery catheterization techniques, which, while more convenient in some situations, can lead to discomfort due to the injected alcohol causing coronary artery spasm or damage, potentially resulting in coronary artery stenosis or other complications (11–13). For HOCM patients with ventricular septal hypertrophy, Liwen surgery may be an effective treatment option, while alcohol septal ablation may be more suitable for specific patients, especially those who are not suitable for Liwen surgery or require rapid symptom relief. Wang et al. reported 68 patients with drug resistant HOCM who underwent PIMSRA with Liwen procedure (14). All procedures were technically successful, and the ablation functioned without errors. The research demonstrates that the Liwen procedure effectively reduces LVOT gradients over a 12-month follow-up period, indicating its potential as an alternative treatment for HOCM patients with promising safety and efficacy (14).

Although electrocardiography, cardiac magnetic resonance imaging, and cardiac catheterization serve as auxiliary diagnostic methods for HOCM-LVAA, the primary diagnosis counts on echocardiography. TTE can be used to evaluate myocardium hypertrophy and the morphological characteristics of the ventricular aneurysm, enabling accurate early diagnosis. In this case, we utilized TTE and left ventricular opacification (LVO) to provide high-resolution cardiac images, clearly showing the structure and thickness of the ventricular myocardium, thus confirming the diagnosis of HOCM-LVAA. TTE accurately evaluates the morphological features, location, and size of the apical aneurysm, which provides essential information for surgical intervention. Due to the aneurysm's

location and features, we modified the insertion approach, transitioning from the conventional B-line to the A-line. We also rotated the ultrasound probe by 180° and precisely positioned the needle tip along the aneurysmal wall to target the basal interventricular septum for ablation, guided by echocardiography. This adjustment was crucial in preventing inadvertent entry into the cardiac chamber and minimize the risk of pericardial tamponade.

For patients with HOCM-LVAA, early intervention is especially crucial. The treatments include medical therapy, surgical septal myectomy, and percutaneous septal ablation to alleviate left ventricular outflow tract obstruction, improve heart function, relieve symptoms, and prevent adverse cardiovascular events. Considering the specific conditions of patients with ventricular aneurysms, individualized treatment is required, considering factors such as age, severity of the condition, and coexisting complications. STE is an emerging ultrasound technique that measures myocardial strain, reflecting myocardial contractile function. In this case, we used strain echocardiography to not only detect reduced strain in the basal segment of the septum but also to identify decreased strain values in the left ventricular apical myocardium, indicating the presence of myocardial dysfunction in the apical region. As the patient still experienced symptoms of heart failure despite optimized medical therapy, we suggested this patient undergo percutaneous septal ablation, Liwen's Procedure. In this case, the patient was diagnosed with hypertrophic cardiomyopathy, which met the indications for Liwen's Procedure. During surgery, we adopted an improved needle technique guided by TTE, accurately locating the ventricular aneurysm, and determining the position and depth of radiofrequency energy delivery to maximize the relief of outflow tract obstruction. Immediate myocardial opacification after surgery revealed a local filling defect in the region of septal ablation, providing an accurate assessment of the surgical outcome. One-week post-operation left ventricular opacification showed that the myocardial thickness of the septum decreased from 20 mm to 12 mm, with a significant alleviation of LVOT obstruction (peak gradient of 20 mmHg), indicating the disappearance of the ventricular aneurysm and restoration of a normal appearance. STE showed synchronous contraction of the left ventricle, suggesting a significant improvement in apical myocardial contractility.

In conclusion, the Liwen Procedure introduces novel avenues for treating HOCM-LVAA, with echocardiographic approaches playing a pivotal role in diagnosis, surgical guidance, and outcome assessment (15). For patients with HOCM-LVAA, Liwen's Procedure alleviates left ventricular outflow tract obstruction and significantly improves cardiac function. The combined application of novel echocardiographic techniques refines disease diagnosis and treatment, enhancing the precision and efficacy of Liwen's Procedure. We propose that the integration of novel echocardiographic approaches to guide Liwen's Procedure not only facilitates the diagnosis and management of HOCM-LVAA but also substantially enhances patients' quality of life and long-term prognosis.

Data availability statement

The raw data supporting the conclusions of this article will be made available by the authors, without undue reservation.

Ethics statement

The studies involving humans were approved by Gansu Provincial Hospital Ethics Committee. The studies were conducted in accordance with the local legislation and institutional requirements. Written informed consent for participation in this study was provided by the participants' legal guardians/next of kin. Written informed consent was obtained from the individual(s) for the publication of any potentially identifiable images or data included in this article.

Author contributions

AC: Conceptualization, Data curation, Funding acquisition, Investigation, Resources, Supervision, Visualization, Writing – original draft, Writing – review & editing. RZ: Methodology, Data curation, Validation, Investigation, Software, Visualization, Writing – original draft, Writing – review & editing. FZ: Data curation, Writing – review & editing. JW: Data curation, Writing – review & editing. YQ: Data curation, Writing – review & editing. TW: Data curation, Writing – review & editing.

Funding

The authors declare financial support was received for the research, authorship, and/or publication of this article.

This work was supported by a grant from Natural Science Foundation of Gansu Province (project number 21JR7RA604), In-Hospital Cultivation Fund of Gansu Provincial Hospital (project number 19SYPYB-2) and the State Key Laboratory of Respiratory Disease-Open Project (project number SKLRD-OP-202301).

Conflict of interest

The authors declare that the research was conducted in the absence of any commercial or financial relationships that could be construed as a potential conflict of interest.

Publisher's note

References

1. Maron BJ, Gardin JM, Flack JM, Gidding SS, Kurosaki TT, Bild DE. Prevalence of hypertrophic cardiomyopathy in a general population of young adults. Echocardiographic analysis of 4111 subjects in the CARDIA study. Coronary artery risk development in (young) adults. *Circulation*. (1995) 92:785–9. doi: 10.1161/01.CIR.92.4.785

2. Semsarian C, Ingles J, Maron MS, Maron BJ. New perspectives on the prevalence of hypertrophic cardiomyopathy. *J Am Coll Cardiol*. (2015) 65:1249–54. doi: 10.1016/j.jacc.2015.01.019

3. Vasile VC, Will ML, Ommen SR, Edwards WD, Olson TM, Ackerman MJ. Identification of a metavinculin missense mutation, R975W, associated with both hypertrophic and dilated cardiomyopathy. *Mol Genet Metab*. (2006) 87:169–74. doi: 10.1016/j.ymgme.2005.08.006

4. Ando G, Saporito F, Arrigo F. Letter by Ando, et al. Regarding article, "prevalence, clinical significance, and natural history of left ventricular apical aneurysms in hypertrophic cardiomyopathy". *Circulation*. (2009) 119:e557; author reply e558. doi: 10.1161/CIRCULATIONAHA.108.828293

5. Rowin EJ, Maron BJ, Haas TS, Garberich RF, Wang W, Link MS, et al. Hypertrophic cardiomyopathy with left ventricular apical aneurysm: implications for risk stratification and management. *J Am Coll Cardiol*. (2017) 69:761–73. doi: 10.1016/j.jacc.2016.11.063

6. Liu L, Li J, Zuo L, Zhang J, Zhou M, Xu B, et al. Percutaneous intramyocardial septal radiofrequency ablation for hypertrophic obstructive cardiomyopathy. *J Am Coll Cardiol*. (2018) 72:1898–909. doi: 10.1016/j.jacc.2018.07.080

7. Li J, Zhang J, Shi Y, Sievert H, Taub CC, Bertog S, et al. Myocardial mechanics of percutaneous intramyocardial septal radiofrequency ablation. *Heart*. (2023) 109:289–96. doi: 10.1136/heartjnl-2022-321597

8. Ommen SR, Mital S, Burke MA, Day SM, Deswal A, Elliott P, et al. 2020 AHA/ACC guideline for the diagnosis and treatment of patients with hypertrophic cardiomyopathy: executive summary: a report of the American college of cardiology/American heart association joint committee on clinical practice guidelines. *Circulation*. (2020) 142:e533–57. doi: 10.1161/CIR.0000000000000938

9. Han C, Zhou M, Hu R, Wang B, Zuo L, Li J, et al. Trans-septal myocardial biopsy in hypertrophic cardiomyopathy using the Liwen procedure: an introduction of a novel technique. *J Interv Cardiol*. (2021) 2021:1905184. doi: 10.1155/2021/1905184

10. Achim A, Serban AM, Mot SDC, Leibundgut G, Marc M, Sigwart U. Alcohol septal ablation in hypertrophic cardiomyopathy: for which patients? *ESC Heart Fail*. (2023) 10:1570–9. doi: 10.1002/ehf2.14272

11. Rigopoulos AG, Ali M, Abate E, Matiakis M, Melnyk H, Mavrogeni S, et al. Review on sudden death risk reduction after septal reduction therapies in hypertrophic obstructive cardiomyopathy. *Heart Fail Rev*. (2019) 24:359–66. doi: 10.1007/s10741-018-09767-w

12. Veselka J. Ten tips and tricks for performing alcohol septal ablation in patients with hypertrophic obstructive cardiomyopathy. *Int J Angiol*. (2020) 29:180–2. doi: 10.1055/s-0040-1709463

13. Gragnano F, Pelliccia F, Guarnaccia N, Niccoli G, De Rosa S, Piccolo R, et al. Working group of interventional cardiology of the Italian society of C. alcohol septal ablation in patients with hypertrophic obstructive cardiomyopathy: a contemporary perspective. *J Clin Med*. (2023) 12(8):2810. doi: 10.3390/jcm12082810

14. Wang Z, Zhao R, Sievert H, Ta S, Li J, Bertog S, et al. First-in-man application of Liwen RF ablation system in the treatment of drug-resistant hypertrophic obstructive cardiomyopathy. *Front Cardiovasc Med*. (2022) 9:1028763. doi: 10.3389/fcvm.2022.1028763

15. Liu L, Zhou M, Zuo L, Li J, Chen W, Xu B, et al. Echocardiography guided Liwen procedure() for the treatment of obstructive hypertrophic cardiomyopathy in a patient with prior aortic valve replacement surgery: Liwen procedure for intra-myocardial radiofrequency ablation. *Echocardiography*. (2018) 35:1230–2. doi: 10.1111/echo.14040

frontiers | Frontiers in Cardiovascular Medicine

TYPE Case Report
PUBLISHED 23 November 2023
DOI 10.3389/fcvm.2023.1287907

OPEN ACCESS

EDITED BY
Grigorios Korosoglou,
GRN Klinik Weinheim, Germany

REVIEWED BY
Haitham Abu Sharar,
Heidelberg University, Germany
Christian Tesche,
Augustinum Klinik München, Germany

*CORRESPONDENCE
Cheng-Yu Ko
✉ iznay0908@gmail.com

RECEIVED 03 September 2023
ACCEPTED 08 November 2023
PUBLISHED 23 November 2023

CITATION
Su P-H, Ko C-Y and Lee C-H (2023) Case Report: Rare percutaneous coronary intervention for "right" main bifurcation. Front. Cardiovasc. Med. 10:1287907. doi: 10.3389/fcvm.2023.1287907

Case Report: Rare percutaneous coronary intervention for "right" main bifurcation

Po-Hsueh Su[1,2], Cheng-Yu Ko[1]* and Cheng-Han Lee[1]

[1]Division of Cardiology, Department of Internal Medicine, National Cheng Kung University Hospital, College of Medicine, National Cheng-Kung University, Tainan, Taiwan, [2]Division of Cardiology, Department of Internal Medicine, Madou Sin-Lau Hospital, Tainan, Taiwan

We presented the case of a patient with non-ST-elevation myocardial infarction with coronary arteries of an anomalous origin, an interarterial course of the LMCA, a unique wide-angle "right" main bifurcation lesion, and a high SYNTAX score. Management with contemporary PCI and imaging may be an alternative to surgery.

KEYWORDS

congenital coronary anomalies, coronaries of anomalous origin, percutaneous coronary intervention, "right" main bifurcation, IVUS guided PCI

Introduction

This was a rare case of patient with anomalous aortic origin of a coronary artery (AAOCA), an interarterial course of the LMCA, and a unique wide-angle "right" main bifurcation lesion (bifurcation of the RCA and LMCA) who presented with acute myocardial infarction. The patient was successfully managed using double guide catheters under the guidance of CCTA and IVUS.

Case description

An 83-year-old man with diabetes mellitus and hypertension, without the history of coronary artery disease before, presented with chest tightness for several hours and received a diagnosis of non-ST-elevation myocardial infarction on the basis of troponin elevation and electrocardiography indicating ST depression in the lateral leads. Invasive coronary angiography showed a common origin of the right and left coronary arteries at the right coronary cusp with diffuse atherosclerosis and multiple stenotic lesions (**Figure 1**; **Supplementary Video S1**). For detailed anatomy, we performed coronary computed tomography angiography (CCTA), which revealed an anomalous origin of the left main coronary artery (LMCA) from the right sinus of Valsalva and an interarterial course between the aorta and the pulmonary artery; the "right" main bifurcation angle was close to 180° (**Figure 2**). This patient was diagnosed coronary artery disease at first time.

Diagnostic assessment

On the basis of the anomalous origin of the LMCA with an interarterial course and a high SYNTAX score of 47, surgical intervention was recommended consistently with

Abbreviations
RCA, right coronary artery; LMCA, left main coronary artery; PCI, percutaneous coronary intervention; IVUS, intravascular ultrasound; CCTA, coronary computed tomography angiography; AAOCA, anomalous aortic origin of a coronary artery.

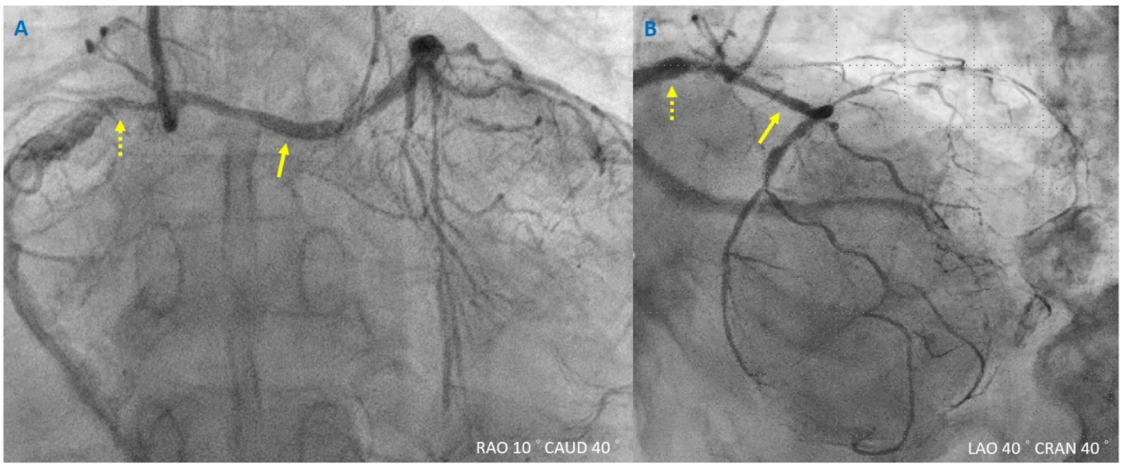

FIGURE 1
Coronary angiography for non-ST-elevation myocardial infarction. (A,B) Yellowish dashed arrow indicates the right coronary artery, and yellowish arrow indicates the left main coronary artery. Different views of anomalous aortic origin of a coronary artery with a common ostium.

current guidelines (1). However, the patient refused surgery and chose percutaneous coronary intervention (PCI) because of his older age and frailty.

Our strategy was to perform stenting with little protrusion of the stents into the common ostium. We would not like excessive stent protrusion because the common ostium was large, more than 6 mm, without significant stenosis. Due to the wide angle of the "right" main bifurcation and for more precise stent deployment, two guide catheters were used to engage the common ostium: a JR4 guide catheter and a SAL1 guide catheter (6 Fr; Medtronic, Minneapolis, MN, USA; **Supplementary Video S2**). After the insertion of coronary guidewires (Runthrough NS Hypercoat, Terumo, Tokyo, Japan; Fielder FC, Asahi Intecc, Seto, Japan) into the left anterior descending artery and the right coronary artery (RCA), we noted diffuse stenosis and calcification on intravascular ultrasound (IVUS) (**Supplementary Video S3A** and **Video S3B**). Under the guidance of IVUS and CCTA, a SYNERGY stent (3.5 mm × 38 mm; Boston Scientific, Marlborough, MA, USA) was deployed within the LMCA from LMCA orifice to distal part, before the bifurcation of LAD and LCX to cover diffuse LMCA lesions and the inter-arterial course. Two SYNERGY stents (4.5 mm × 24 mm and 5.0 mm × 12 mm) were deployed within the RCA from the orifice to middle part. (**Figure 3**; **Supplementary Video S4**). The LMCA was stented to cover the inter-arterial course of an anomalous coronary artery. The stents were used in both orifices with little protrusion to the common ostium. Afterward, the kissing balloon technique was used to ensure complete stent apposition in both orifices; to accomplish this, a noncompliance balloon catheter (4.0 mm × 15 mm; Conqueror, APT Medical, Shenzhen, China) was used for the LMCA and a noncompliance balloon catheter (5.0 mm × 12 mm; Emerge, Boston Scientific, Marlborough, MA, USA) was used for the RCA (**Figure 3**). The IVUS showed that the stents were well apposed without external compression on images, and the final angiography revealed improved flow (**Figure 4**; **Supplementary Video S5**). The interarterial course of an anomalous coronary

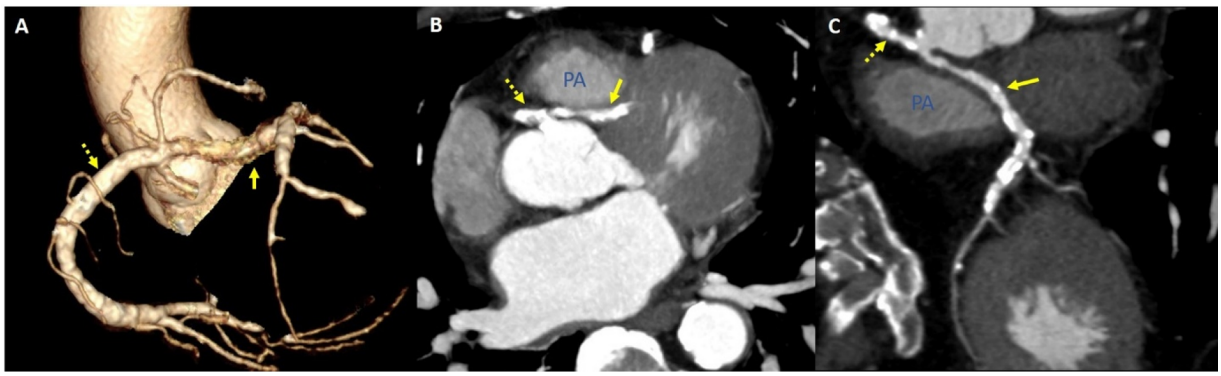

FIGURE 2
Coronary computed tomography angiography assessment for anomalous aortic origin of a coronary artery. (A) Reconstructive image revealed "right" main bifurcation. (B,C) Coronary computed tomography angiography showed a common ostium for the left main coronary artery and the right coronary artery, characterized by an interarterial course.

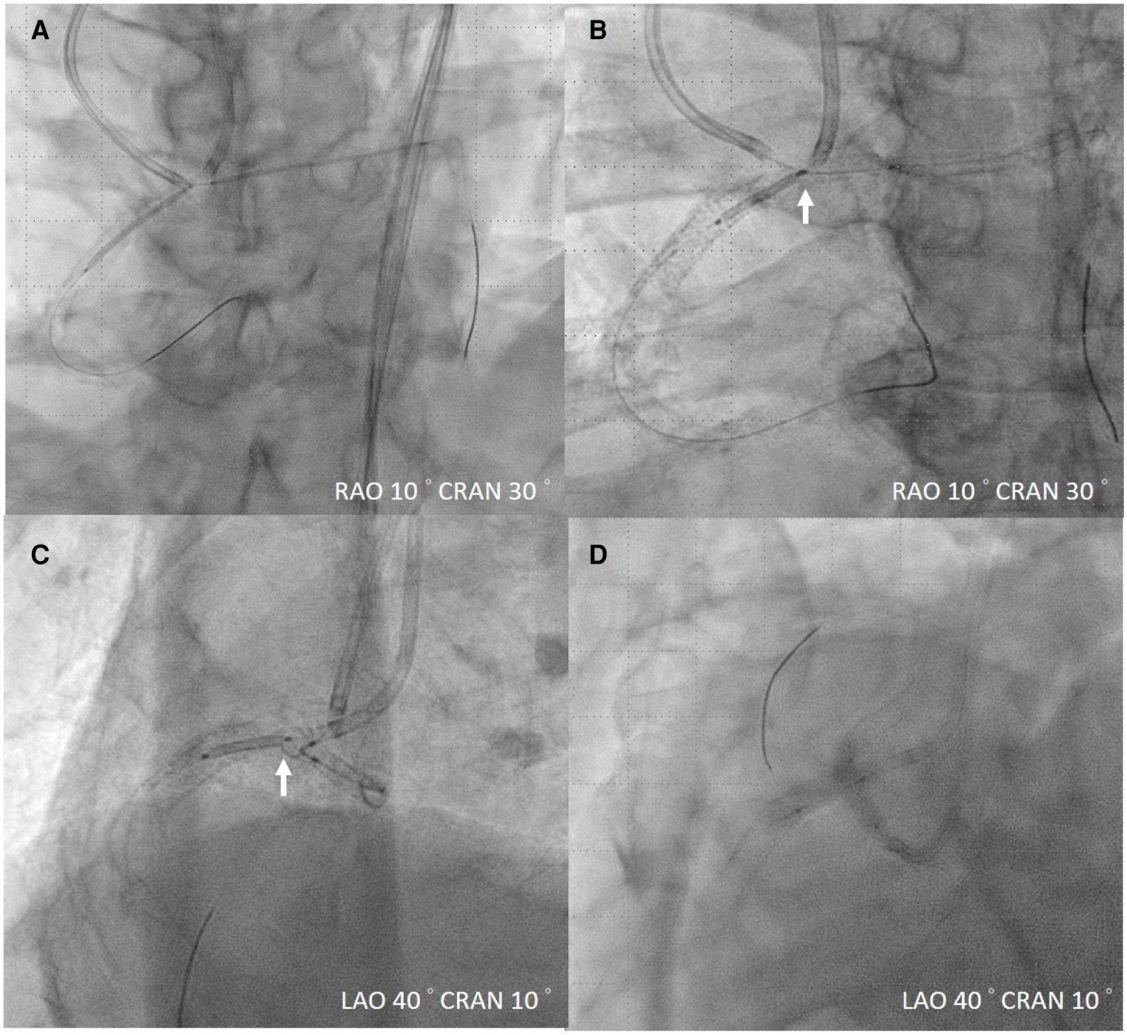

FIGURE 3
Management of AAOCA stenosis. (**A**) Intravascular ultrasound (IVUS)-guided stent deployment. (**B**,**C**) White arrow indicates the proximal mark of the right coronary artery stent, positioned close to the center of the proximal left main coronary artery stent, in accordance with IVUS guidance. (**D**) Kissing balloon technique for ostium bifurcation. AAPCA, anomalous aortic origin of a coronary artery.

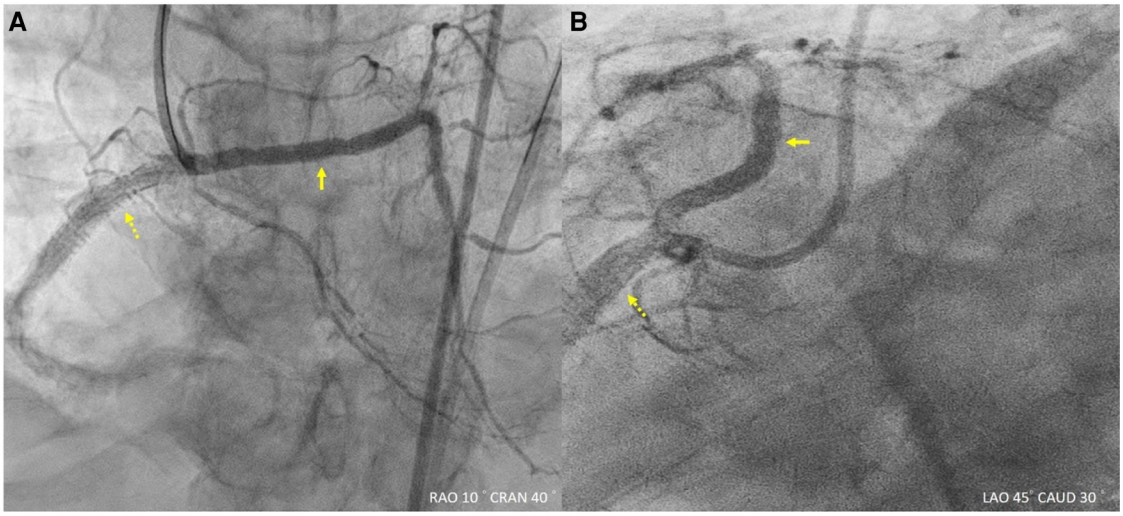

FIGURE 4
Final angiography. (**A**,**B**) Final angiography revealed improved flow.

artery was stented according to correspond coronary CTA. The patient was discharged several days after the procedure, without any recurrent symptoms. The patient was discharged smoothly several days after the procedure, and had no recurrent angina. The follow-up echocardiography one year later revealed preserved left ventricular ejection fraction and the patient still could walk with canes.

Discussion

Although AAOCA affects at least 1 in 1,000 individuals, it is difficult to extrapolate the accurate estimate of its burden due to heterogeneous observational studies. One review article suggested that interarterial anomalous left coronary artery is even rare with a weighted prevalence of 0.03% from the observational data (2, 3). Most patients with AAOCA are asymptomatic (4). Natural history studies focusing on patients with untreated AAOCA are scarce (5). The optimal management of this condition remains controversial, particularly in patients with an interarterial course of an anomalous coronary artery, which is thought to increase the risk of serious complications such as angina pectoris, myocardial infarction, syncope, and ventricular tachycardia. A previously proposed pathophysiological mechanism suggests that the LMCA located between the aortic root and the pulmonary trunk can worsen the preexisting angulation of the coronary artery and reduce the diameter of the lumen in the proximal portion of the coronary artery during exercise (6). Surgery is recommended for AAOCA in patients with typical angina symptoms presenting with the symptoms of stress-induced myocardial ischemia in a relevant high-risk anatomical area (5).

Very few cases of patients with AAOCA and concomitant acute myocardial infarction have been reported, and no case report indicated an interarterial course with complex bifurcation lesions. Surgical intervention was recommended for our patient on the basis of current guidelines. One case was reported involving similar coronary anatomy with a common ostium arising from the right sinus of Valsalva (7); emergent PCI was performed for the RCA, but the procedure failed because of the complex anatomy involved.

Our patient had a high SYNTAX score but chose to receive PCI because of his older age and frailty. Surgical intervention was recommended on the basis of the current guidelines. Nonetheless, PCI using contemporary techniques, such as double guide catheters, and imaging techniques, such as IVUS and CCTA, may be alternatives to surgery.

Conclusion

We presented the case of a patient with non-ST-elevation myocardial infarction with coronary arteries of an anomalous origin, an interarterial course of the LMCA, a unique wide-angle "right" main bifurcation lesion, and a high SYNTAX score. Management with contemporary PCI and imaging may be an alternative to surgery.

Data availability statement

The raw data supporting the conclusions of this article will be made available by the authors, without undue reservation.

Ethics statement

Written informed consent was obtained from the individual(s) for the publication of any potentially identifiable images or data included in this article. Written informed consent was obtained from the participant/patient(s) for the publication of this case report.

Author contributions

P-HS: Writing – original draft, Writing – review & editing. C-YK: Writing – review & editing. C-HL: Writing – review & editing.

Funding

The author(s) declare financial support was received for the research, authorship, and/or publication of this article.

This study was supported by National Cheng Kung University Hospital, Tainan, Taiwan (grant no. NCKUH- 11205002).

Conflict of interest

The authors declare that the research was conducted in the absence of any commercial or financial relationships that could be construed as a potential conflict of interest.

Publisher's note

Supplementary material

The Supplementary Material for this article can be found online at: https://www.frontiersin.org/articles/10.3389/fcvm.2023.1287907/full#supplementary-material

SUPPLEMENTARY VIDEO S1
Diagnostic coronary angiography. During the diagnostic angiography performed for the right coronary artery by using a JR4 catheter, we discovered that the left main coronary artery originates from the right coronary cusp, sharing an ostium.

SUPPLEMENTARY VIDEO S2
Percutaneous coronary intervention for coronary artery stenosis. We used a JR4 guide catheter with a Fielder FC guidewire for the right common artery and a SAL1 guide catheter with a Runthrough NS Hypercoat guidewire for the left anterior descending artery.

SUPPLEMENTARY VIDEO S3
(**A**) Pre-IVUS image for RCA; (**B**) Pre-IVUS image for LMCA. After placing coronary guidewire to RCA and LMCA, diffuse stenosis and calcification were noted on intravascular ultrasound.

SUPPLEMENTARY VIDEO S4
Intravascular ultrasound–guided deployment of second RCA stent. The second RCA stent should be deployed such that the proximal mark of the RCA stent is near the center of the proximal left main coronary artery stent, as per intravascular ultrasound guidance. RCA, right coronary artery.

SUPPLEMENTARY VIDEO S5
Final coronary angiography. (**A**,**B**) Right and left anterior oblique angiographic views indicating favorable results.

References

1. Stout KK, Daniels CJ, Aboulhosn JA, Bozkurt B, Borberg CS, Colman JM, et al. 2018 AHA/ACC guideline for the management of adults with congenital heart disease: a report of the American college of cardiology/American heart association task force on clinical practice guidelines. *Circulation*. (2019) 139(14):e698–800. doi: 10.1016/j.jacc.2018.08.1028

2. Cheezum MK, Liberthson RR, Shah NR, Villines TC, O'Gara PT, Landzberg MJ, et al. Anomalous aortic origin of a coronary artery from the inappropriate sinus of valsalva. *J Am Coll Cardiol*. (2017) 69(12):1592–608. doi: 10.1016/j.jacc.2017.01.031

3. Gentile F, Castiglione V, Caterina RD. Coronary artery anomalies. *Circulation*. (2021) 144:983–96. doi: 10.1161/CIRCULATIONAHA.121.055347

4. Khalighi K, Sharma M, Toor A, Toor RS, Costacurta G. Anomalous left main coronary artery arising from the right sinus of valsalva in a young man presenting with recurrent syncope and myocardial infarction. *Case Rep Cardiol*. (2018) 2018:9805061. doi: 10.1155/2018/9805061

5. Baumgartner H, De Backer J, Babu-Narayan SV, Budts W, Chessa M, Diller G, et al. 2020 ESC guidelines for the management of adult congenital heart disease: the task force for the management of adult congenital heart disease of the European society of cardiology (ESC). Endorsed by: association for European paediatric and congenital cardiology (AEPC), international society for adult congenital heart disease (ISACHD). *Eur Heart J*. (2020) 42(6):563–645. doi: 10.1093/eurheartj/ehaa554

6. Peñalver JM, Mosca RS, Weitz D, Phoon CKL. Anomalous aortic origin of coronary arteries from the opposite sinus: a critical appraisal of risk. *BMC Cardiovasc Disord*. (2012) 12(1):83. doi: 10.1186/1471-2261-12-83

7. Shtembari J, Shrestha DB, Oli PR, Munagala A, Mullaj E, Shehata K, et al. Anomalous origin of the left coronary artery from the right coronary cusp: a case report. *Cureus*. (2023) 15(3):e35711. doi: 10.7759/cureus.35711

frontiers | Frontiers in Cardiovascular Medicine

TYPE Case Report
PUBLISHED 08 January 2024
DOI 10.3389/fcvm.2023.1295602

OPEN ACCESS

EDITED BY
Riccardo Liga,
Pisana University Hospital, Italy

REVIEWED BY
Rodrigo Salgado,
Antwerp University Hospital & Holy Heart Lier, Belgium
Valeria Pergola,
University Hospital of Padua, Italy

*CORRESPONDENCE
Patrick McAlpin
✉ pmca0001@radiology.ufl.edu

RECEIVED 16 September 2023
ACCEPTED 03 November 2023
PUBLISHED 08 January 2024

CITATION
McAlpin P, Purlee M, Dickey A, Chandran A and Al-Ani MAZ (2024) Case Report: Multimodality evaluation and clinical management of a single coronary artery.
Front. Cardiovasc. Med. 10:1295602.
doi: 10.3389/fcvm.2023.1295602

Case Report: Multimodality evaluation and clinical management of a single coronary artery

Patrick McAlpin[1]*, Matthew Purlee[1], Ann Dickey[2], Arun Chandran[1] and Mohammad Ahmad Zaki Al-Ani[1]

[1]Division of Cardiovascular Imaging, Department of Radiology, University of Florida, Gainesville, FL, United States, [2]Lake Erie College of Osteopathic Medicine-Bradenton, Bradenton, FL, United States

A 14-year-old male with no significant medical history presented with intermittent palpitations for 2–3 months that occurred at rest and were associated with light-headedness. Electrocardiogram in clinic showed sinus arrhythmia with early repolarization and no ischemic changes. The echocardiogram showed normal cardiac structure and function, however, there was a concern for possible anomalous origin of the left coronary artery. Contrast-enhanced CT coronary artery angiogram confirmed a single coronary origin from the right coronary sinus. The single main coronary artery gave rise to the right coronary artery (RCA) and the left coronary artery (LCA). The LCA demonstrated a trans-septal course before it gave rise to the left anterior descending and left circumflex artery. There were intraarterial and intramural portions of the LCA, and the sinoatrial node artery arose from the LCA. The RCA demonstrated a normal course to the right atrioventricular groove, and the posterior descending artery arose from the RCA. Treadmill exercise stress test showed excellent functional capacity without exercise-induced chest pain or ischemic ECG changes. Invasive coronary angiography ruled out luminal narrowing or dynamic compression. Given the absence of physiologic or anatomic evidence of coronary flow restriction, no intervention was pursued and the palpitations were deemed to be likely unrelated to the coronary anomaly and eventually subsided spontaneously on 6 month follow-up.

KEYWORDS
coronary artery anomaly (CAA), single coronary artery, interarterial, intramural, pediatric

Introduction

A coronary artery anomaly is a rare anatomic variant of the coronary system with a range of clinical significance from those patients who remain asymptomatic to others predisposed to major cardiac events, especially sudden cardiac death when in the presence of certain, high-risk morphological features. Therefore, when coronary artery anomalies are suspected, a thorough clinical evaluation with the concomitant use of multi-modality imaging is essential to guide clinical management. In this report, we detail the case of a 14-year-old male who presented with palpitations and was later diagnosed with a single coronary artery arising from the right coronary sinus with certain unusual features.

Presentation

A 14-year-old male with no significant medical history presented with intermittent palpitations for 2–3 months that occurred at rest and were associated with light-headedness. Electrocardiogram in clinic showed sinus arrhythmia with early repolarization and no ischemic changes. The echocardiogram showed normal cardiac structure and function, however, there was a concern for possible anomalous origin of the left coronary artery (Figure 1).

Contrast-enhanced CT coronary artery angiogram confirmed a single coronary origin from the right coronary sinus. The single main coronary artery gave rise to the right coronary artery (RCA) and the left coronary artery (LCA). The LCA demonstrated a trans-septal course before it gave rise to the left anterior descending and left circumflex artery (Figures 2, 3). There were interarterial and intramural portions of the LCA, and the sinoatrial node artery arose from the LCA (Figure 4). The RCA demonstrated a normal course to the right atrioventricular groove, and the posterior descending artery arose from the RCA. Treadmill exercise stress test showed excellent functional capacity without exercise-induced chest pain or ischemic ECG changes. Invasive coronary angiography ruled out luminal narrowing or dynamic compression. Given the absence of physiologic or anatomic evidence of coronary flow restriction, no intervention was pursued and the palpitations were deemed to be likely unrelated to the coronary anomaly and eventually subsided spontaneously on 6 month follow-up.

Discussion

The term "coronary artery anomaly" refers to a broad spectrum of various configurations of the typical coronary artery system. An anomaly is defined as any coronary pattern with a feature that is not commonly encountered, whether it refers to the ostium, course, branching pattern, etc (1). Coronary artery anomalies occur in <1% of the general population (1). The coronary artery anomaly may be clinically silent, however there is a spectrum of clinical sequelae attributed to coronary artery anomalies that includes chest pain, sudden death, cardiomyopathy, syncope, dyspnea, ventricular fibrillation, and myocardial infarction (2). There are multiple classification schemes in the literature that stratify the rarity and clinical significance of each anomaly (3). Generally, coronary artery anomalies can be classified into three groups that include anomaly of origination and course, anomaly of intrinsic coronary arterial anatomy, and anomaly of coronary termination (4, 5). A single coronary artery, as seen in this case, is exceedingly rare as it occurs in 0.0024%–0.044% of the population and carries a high risk for sudden death (5). A single coronary artery may arise from either the left or right coronary sinus, and its course may demonstrate features that are risk

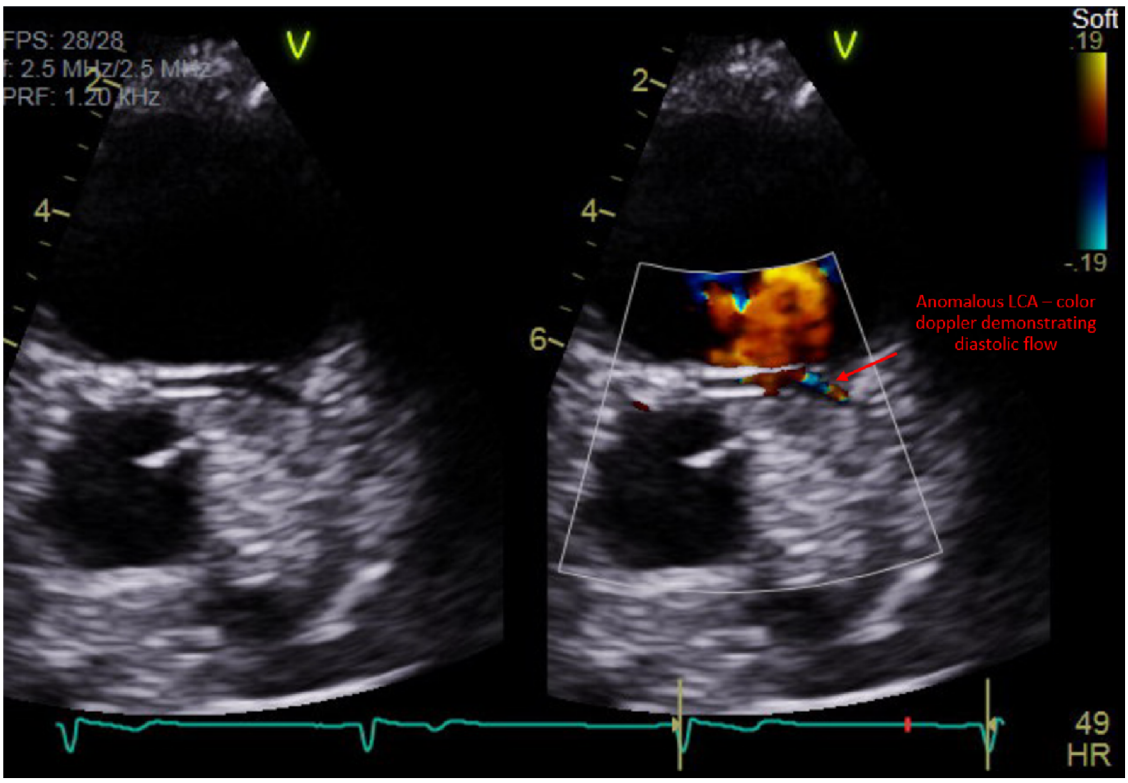

FIGURE 1
Transthoracic echocardiogram demonstrating diastolic flow via color Doppler within a vessel that was concerning for a left coronary artery with an anomalous origin.

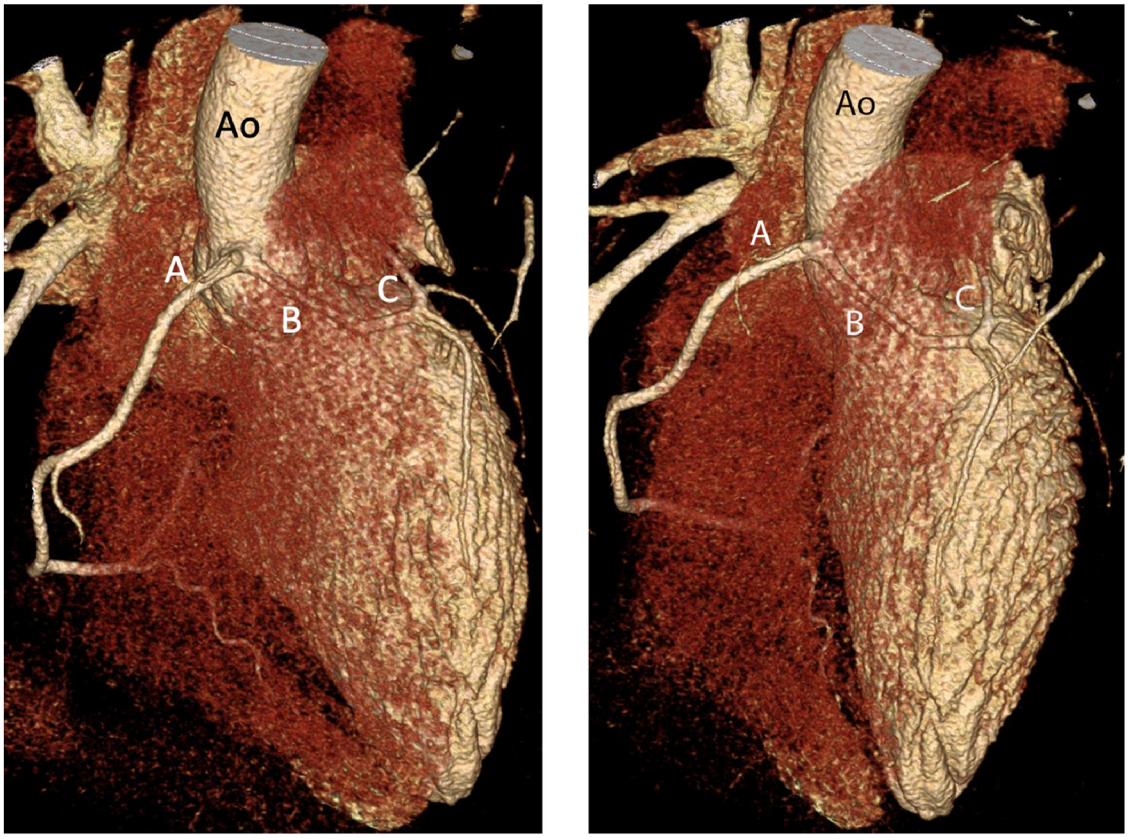

FIGURE 2
An oblique (left) and anteroposterior (right) projection of a volume-rendered 3D reconstruction of the heart demonstrating a single CA dividing into the RCA (**A**) and LCA (**B**) with subsequent trans-septal course of the LCA (**C**) Ao, aorta.

factors for clinically significant symptoms, such as a course with interarterial and/or intramural portions (1). The most frequent type of clinically significant variant anatomy is the interarterial course of the anomalous coronary artery with abnormal origin from the opposite sinus of Valsalva (5). An interarterial course means the coronary artery courses between the pulmonary arterial trunk and the aorta, which when present there may be constriction of the anomalous coronary artery during intense physical activity, leading to decreased blood flow (3, 6). Therefore, this anatomic feature carries a higher risk of sudden cardiac death among the previously mentioned complications (7). Additional risk factors of a sudden cardiac death include an acute angle of take-off, an intramural course of the anomalous coronary artery, and a crevice-like ostium (6, 8).

There are multiple studies in the literature that support the risk of sudden cardiac death with coronary artery anomalies, with a reported range of 11.8%–19% of deaths in young athletes in the US being related to coronary artery anomalies (9, 10). Screening efforts have been proposed given the risk of sudden cardiac death in this population, in addition to military personnel who undergo strenuous activity, each with their respective limitations. Such screening methods include echocardiography, contrast-enhanced electron-beam tomography, magnetic resonance imaging, and coronary angiography (1). Echocardiography, transthoracic or transesophageal, with Doppler interrogation is the initial modality choice for evaluating an anomalous coronary artery when clinically suspected. If at least two normally located coronary ostia are identified with echocardiography, no further workup is likely required (11). If further imaging is required, contrast-enhanced CT or MRI may be performed. Contrast-enhanced CT offers excellent spatial resolution and identifies most anomalies of coronary course with drawbacks including the use of ionizing radiation and contrast agents that may be potentially nephrotoxic or allergenic (12). MRI offers the advantage of no ionizing radiation or potentially harmful contrast agents with the added benefits of great visualization of the coronary artery origins, especially in patients with congenital defects (13). The main limitation of MRI is the poor visualization of the distal coronary artery course (13). Finally, coronary angiography is a strong modality for diagnosis of an anomalous coronary artery, especially when compared to echocardiography. One study demonstrated a 0.17% incidence of an anomalous coronary artery arising from the opposite sinus, while coronary angiography demonstrated a 1.07% incidence (11). The drawback of coronary angiography is that it is a more invasive exam, though (11).

There is a range of opinions regarding a trans-septal course of a LCA from a single RCA with a recent study pointing to a benign

10.3389/fcvm.2023.1295602

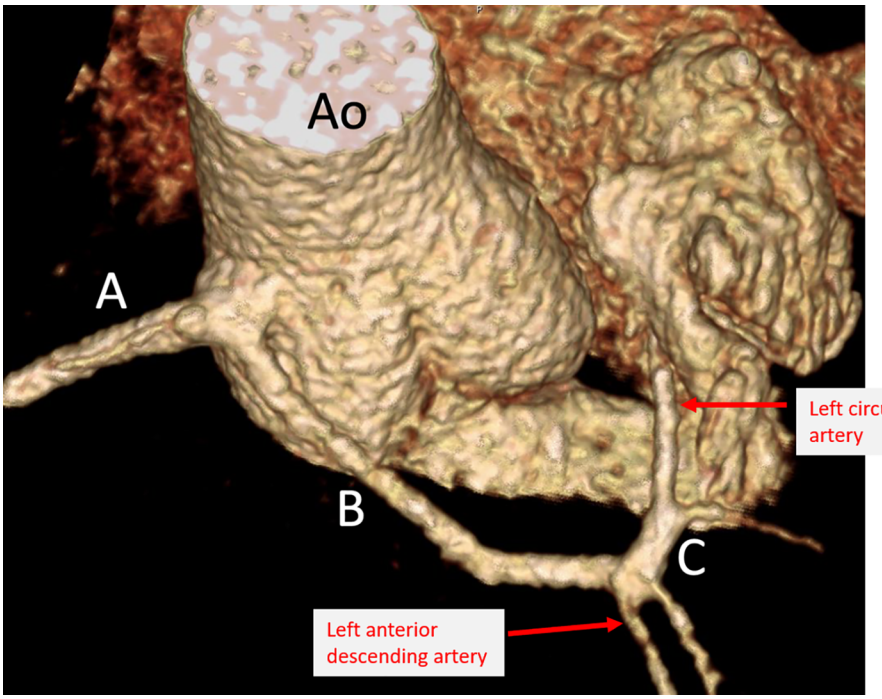

FIGURE 3
Selective view of a volume-rendered 3D reconstruction demonstrating single coronary artery dividing into RCA (**A**) and LCA (**B**) with subsequent transseptal course of the LCA (**C**). Ao, aorta.

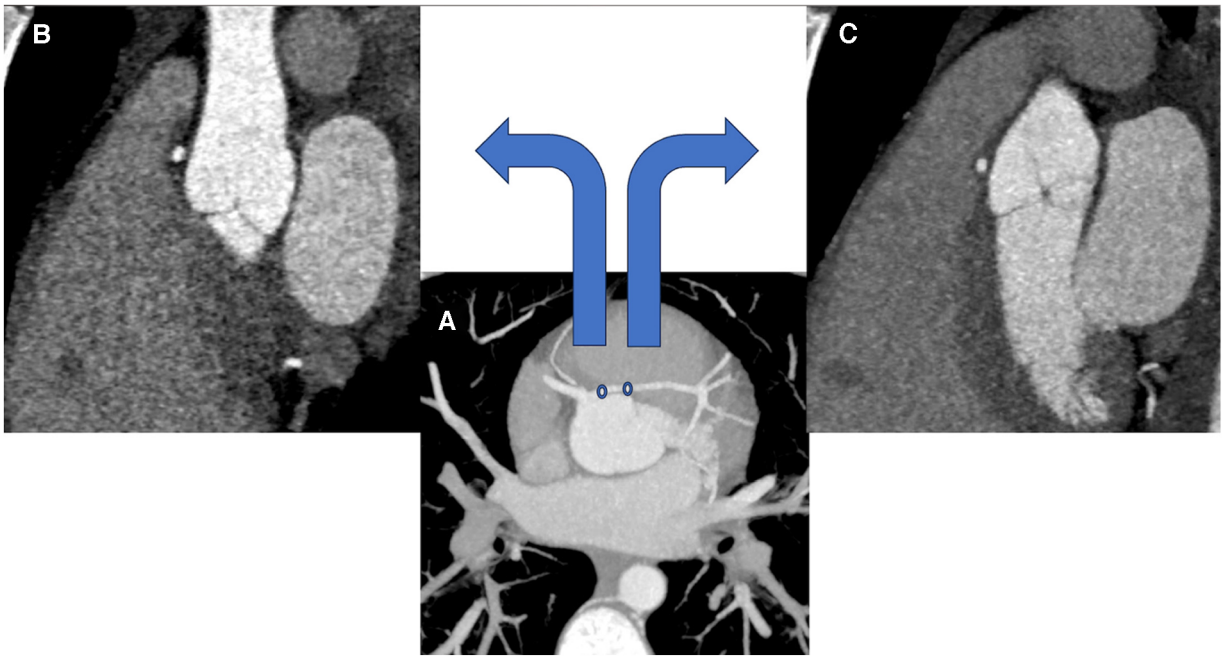

FIGURE 4
(**A**) is a coronary CTA displaying the course of the single coronary artery as it arises from the right coronary sinus in an axial plane with maximal image projection. (**B**) corresponds to the first circle of the proximal LCA seen on (**A**) and displays its interarterial course – note the presence of mediastinal fat surrounding the LCA. (**C**) corresponds to the second circle of the LCA seen on (**A**) and displays its intramural course. Images were obtained at early diastole.

course while a paper from 2018 revealed that these patients could pose a high-risk variant (14, 15). The difficulty however lies in the surgical approach to the trans-septal course since potentially approaching it with an un-roofing procedure would involve exposure of a long trans-septal course, which carries a higher incidence potential for post-operative stenotic complications. Coronary un-roofing is performed for CAAs with an intramural segment, where the wall between the intramural segment and the aorta is unroofed creating a wide neo-ostium (14). Un-roofing carries an additional risk of aortic insufficiency given the risk of damaging the intercoronary commissure. Accordingly, the threshold for surgical indication in this particular variant is high, and since this patient had no specific ischemic symptoms or signs on imaging, a more conservative approach to management was taken.

Demonstration of the clinical significance of an anomalous coronary artery, i.e., myocardial ischemia, is challenging as standard clinical submaximal stress-test protocols are often inadequate to provide definitive information (1). Stress-perfusion tests (CT or MR) can delineate any myocardial ischemia associated with CAAs, which can be nuanced in certain cases and difficult to link to clinical significance. However, the presence of large perfusion defects certainly helps guide management toward a more invasive route, such as in cases of pulmonary origin of coronary arteries and coronary atresia (1). Long-term Holter monitoring is considered to rule out ventricular tachycardia that may be induced by ischemia (1). Most individuals are asymptomatic for long periods of time with the discovery of an anomaly as a result of a diagnostic work-up prompted by an atypical chest-pain syndrome (14). This clinical course contrasts with the individuals who die suddenly, commonly at a young age and after strenuous activity (14). Conservative treatment that includes observation and use of pharmaceutical therapy is often employed in cases of asymptomatic individuals (14). For those who are at high risk of sudden cardiac death, surgical treatment, such as coronary reimplantation or CABG, should be considered (3). Should be noted, however, CABG is of limited utility in pediatric patients who will likely outlast their bypass grafts, while reimplantation is a technically challenging surgery requiring an appropriate take-off angle when transferring the CAA ostium to its correct sinus (14).

Coronary artery anomalies exist across a broad spectrum of both anatomic configuration and clinical presentation, often appearing incidentally on imaging obtained for other indications. Providers need to be able to recognize the differences between clinically significant and benign CAAs, which requires the use of multimodality imaging ranging from echocardiography to invasive angiography. Examples of major features of CAAs that are associated with clinical significance include intramural and interarterial segments of the anomalous coronary artery. Once the underlying anatomy is defined, stress tests can be performed among other options to help delineate prognostic information. Depending on the information acquired during the clinical investigation, management may require simple observation vs. surgical intervention. Proper recognition and risk stratification of CAAs will ultimately lead to improved outcomes in this patient population and continued research into this ever-growing subject.

Data availability statement

The original contributions presented in the study are included in the article/Supplementary Material, further inquiries can be directed to the corresponding author.

Ethics statement

Written informed consent was obtained from the minor(s)' legal guardian/next of kin for the publication of any potentially identifiable images or data included in this article.

Author contributions

PM: Writing – review & editing. MP: Writing – review & editing. AD: Writing – review & editing. AC: Conceptualization, Supervision, Writing – review & editing. MA-A: Conceptualization, Supervision, Writing – review & editing.

Funding

The author(s) declare that no financial support was received for the research, authorship, and/or publication of this article.

Conflict of interest

The authors declare that the research was conducted in the absence of any commercial or financial relationships that could be construed as a potential conflict of interest.

Publisher's note

References

1. Angelini P, Velasco JA, Flamm S. Coronary anomalies. *Circulation*. (2002) 105 (20):2449–54. doi: 10.1161/01.cir.0000016175.49835.57

2. Angelini P, Villason S, Chan AV, Diez JG. Normal and anomalous coronary arteries in humans. In: Angelini P, editors. *Coronary artery anomalies: A comprehensive approach*. Philadelphia: Lippincott Williams & Wilkins (1999). p. 27–150.

3. Gać P, Żórawik A, Poręba R. *A single coronary artery originating from the right coronary sinus with a typical course of the right coronary artery and the interarterial course of the left main, left anterior descending, and left circumflex as an example of a rare case of high-risk coronary anomaly, Diagnostics (Basel, Switzerland)*. Available at: https://www.ncbi.nlm.nih.gov/pmc/articles/PMC8774391/ (Accessed June 4, 2023) (2022).

4. Ropers D, Gehling G, Pohle K, Maeffert R, Regenfus M, Moshage W, et al. Images in cardiovascular medicine. Anomalous course of the left main or left anterior descending coronary artery originating from the right sinus of valsalva: identification of four common variations by electron beam tomography. *Circulation*. (2002) 105:e42–3. doi: 10.1161/hc0602.102020

5. Neves PO, Andrade J, Monção H. Artérias coronárias anômalas: O que o radiologista precisa saber. *Radiol Bras*. (2015) 48:233–41. doi: 10.1590/0100-3984.2014.0004

6. Gräni C, Kaufmann PA, Windecker S, Buechel RR. Diagnosis and management of anomalous coronary arteries with a malignant course. *Interv Cardiol*. (2019) 14:83–8. doi: 10.15420/icr.2019.1.1

7. Shriki JE, Shinbane JS, Rashid MA, Hindoyan A, Withey JG, DeFrance A, et al. Identifying, characterizing, and classifying congenital anomalies of the coronary arteries. *Radiographics*. (2012) 32:453–68. doi: 10.1148/rg.322115097

8. Frommelt PC, Frommelt MA. Congenital coronary artery anomalies. *Pediatr Clin N Am*. (2004) 51:1273–88. doi: 10.1016/j.pcl.2004.04.014

9. Van Camp SP, Bloor CM, Mueller FO, Cantu RC, Olson HG. Nontraumatic sports death in high school and college athletes. *Med Sci Sports Exerc*. (1995) 27:641–7. doi: 10.1249/00005768-199505000-00005

10. Maron BJ, Thompson PD, Puffer JC, McGrew CA, Strong WB, Douglas PS, et al. Cardiovascular preparticipation screening of competitive athletes: a statement for health professionals from the sudden death committee (clinical cardiology) and congenital cardiac defects committee (cardiovascular disease in the young), American heart association. *Circulation*. (1996) 94:850–6. doi: 10.1161/01.CIR.94.4.850

11. Angelini P. Coronary artery anomalies: an entity in search of an identity. *Circulation*. (2007) 115:1296–305. doi: 10.1161/CIRCULATIONAHA.106.618082

12. Ropers D, Moshage W, David WG, Jessl J, Gottwik M, Achenbach S. Visualization of coronary artery anomalies and their anatomic course by contrast-enhanced electron beam tomography and three-dimensional reconstruction. *Am J Cardiol*. (2001) 87:193–7. doi: 10.1016/S0002-9149(00)01315-1

13. Taylor AM, Thorne SA, Rubens MB, Jhooti P, Keegan J, Gatehouse PD, et al. Coronary artery imaging in grown up congenital heart disease: complementary role of magnetic resonance and x-ray coronary angiography. *Circulation*. (2000) 101:1670–167. doi: 10.1161/01.CIR.101.14.1670

14. Agarwal PP, Dennie C, Pena E, Nguyen E, LaBounty T, Yang B, et al. Anomalous coronary arteries that need intervention: review of pre- and postoperative imaging appearances. *RadioGraphics*. (2017) 37(3):740–57. doi: 10.1148/rg.2017160124

15. Glushko T, Seifert R, Brown F, Vigilance D, Iriarte B, Teytelboym OM. Transseptal course of anomalous left main coronary artery originating from single right coronary orifice presenting as unstable angina. *Radiol Case Rep*. (2018) 13 (3):549–54. doi: 10.1016/j.radcr.2018.02.009

frontiers | Frontiers in Cardiovascular Medicine

TYPE Case Report
PUBLISHED 23 January 2024
DOI 10.3389/fcvm.2024.1332307

OPEN ACCESS

EDITED BY
Riccardo Liga,
Pisana University Hospital, Italy

REVIEWED BY
Elias Ylä-Herttuala,
University of Eastern Finland, Finland
Guang-Yuan Song,
Capital Medical University, China

*CORRESPONDENCE
Xing Liu
liuxingcardio@swmu.edu.cn

†These authors share first authorship

RECEIVED 02 November 2023
ACCEPTED 09 January 2024
PUBLISHED 23 January 2024

CITATION
Jiang M, Zhang G, Li L, He Y, Li G, Yu J, Feng J and Liu X (2024) Case Report: A case report of myocardial fibrosis activation assessment after unstable angina using ^{68}Ga-FAPI-04 PET/CT. Front. Cardiovasc. Med. 11:1332307. doi: 10.3389/fcvm.2024.1332307

Case Report: A case report of myocardial fibrosis activation assessment after unstable angina using ^{68}Ga-FAPI-04 PET/CT

Mimi Jiang†, Guolan Zhang†, Le Li, Yuanyuan He, Guo Li, Jinmei Yu, Jian Feng and Xing Liu*

Department of Cardiology, The Affiliated Hospital of Southwest Medical University, Luzhou, China

Myocardial ischemia may induce myocardial fibrosis, a condition that progressively leads to ventricular remodeling, heightening the risk of heart failure. The timely detection of myocardial fibrosis is crucial for intervention and improved outcomes. ^{68}Ga-FAPI-04 PET/CT shows promise in assessing fibroblast activation in patients with early myocardial infarction characterized by prolonged myocardial ischemia. However, there is a notable absence of data regarding patients with short-term myocardial ischemia, such as those experiencing unstable angina (UA). In this report, we evaluated a 49-year-old male with UA and severe stenosis in multiple coronary arteries using ^{68}Ga-FAPI-04 PET/CT. The results demonstrated tracer-specific uptake (SUVmax = 4.6) in the left anterior descending artery (LAD) territory, consistent with myocardial anterior wall ischemia indicated by the electrocardiogram. Following vascular recanalization therapy and regular medication treatment, the patient remained free of angina recurrence. A subsequent review at 2 months revealed a significant reduction in myocardial tracer uptake (SUVmax = 1.8). This case illustrates the validity of ^{68}Ga-FAPI-04 PET/CT in assessing the extent of early myocardial fibroblast activation in patients with UA. This approach offers valuable insights for early detection and visual evidence, providing information on disease progression and treatment response.

KEYWORDS
unstable angina, myocardial fibrosis, ventricular remodeling, ^{68}Ga-FAPI, PET-CT

Introduction

Unstable angina (UA) arises from a confluence of intricate factors that give rise to transient and reversible reductions in coronary blood flow. These contributing factors encompass vasoconstriction, transient platelet plugging, and transient thrombosis, collectively precipitating short-term myocardial ischemia (1). A subset of patients experiencing UA may undergo recurrent myocardial ischemia, potentially fostering pathological ventricular remodeling and an escalated risk of heart failure and arrhythmias (2, 3). Among these, fibrotic response plays a critical role in ventricular remodeling. In the context of myocardial ischemia-induced damage and inflammation, the release of TGF-β_1 by inflammatory cells serves to activate fibroblasts to differentiate into collagen-secreting myofibroblasts. They secrete increased amounts of cytokines and TGF-β_1 to regulate the deposition of matrix proteins, including fibronectin, type I and III collagen fibers, and proteoglycans. Excessive fibrosis and the persistence of active fibroblasts contribute to heightened left ventricular stiffness, thereby impacting diastolic

or systolic function (4, 5). However, current myocardial fibrosis imaging methods commonly used in clinical practice, like CMR-obtained LGE and post-contrast myocardial T1 techniques, have limitations as they primarily measure extracellular expansion rather than fibrosis itself (6). Therefore, noninvasive imaging of activated fibroblasts could provide the information of myocardial fibrosis in the initial stage and unique opportunities to monitor therapeutic interventions that aim to prevent a progressive decline of ventricular function.

Fibroblast activation protein (FAP), a marker for active fibroblasts, has been observed to be highly expressed in myofibroblasts in the hearts of rats with permanent myocardial infarction (MI) and in patients with acute MI (7). In vitro, FAP was induced by TGF-β_1 via the canonical SMAD2/SMAD3 pathway (7). Radiolabeled FAP inhibitors (FAPIs) for noninvasive imaging of FAP expression have been reported by Linder's group, used for diagnosis and treatment of tumor patients (8). Furthermore, in a small sample study by Diekmann et al. ($n = 34$), the non-invasive imaging method using ^{68}Ga-FAPI-04 PET/CT has shown feasibility in assessing activated fibroblasts in patients with MI following early reperfusion therapy and predicting the progression of contractile dysfunction (9). However, data on activated fibroblasts in patients with short-term myocardial ischemia and follow-up information on those with ischemic myocardial damage are currently lacking.

This case report demonstrates the feasibility of using ^{68}Ga-FAPI-04 PET/CT examination to assess early activated fibroblasts in a patient with UA and provides follow-up information.

Case presentation

A 49-year-old male was admitted with recurrent post-exertional chest pain. The pain occurred behind the sternum during brisk walking or stair climbing, occasionally radiating to the left shoulder, lasting a few minutes, and was relieved by rest. There was no persistent chest pain exceeding 30 min. The patient had a smoking history of 30 pack-years. He was diagnosed with hypertension 5 years ago and remained untreated until starting nifedipine controlled-release tablets at 30 mg daily when blood pressure was above 200/90 mmHg; it was then maintained around

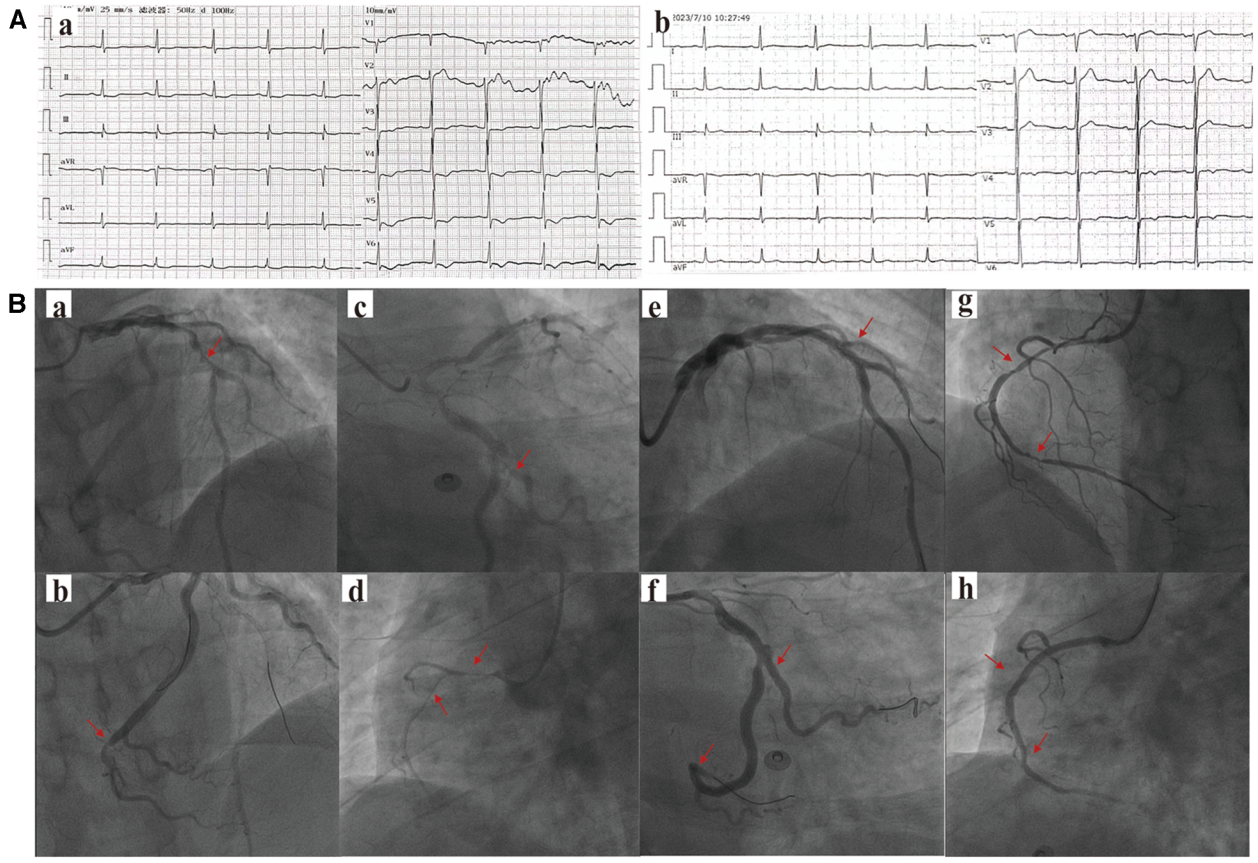

FIGURE 1
(A) The patient's (a) electrocardiogram at the time of hospital admission and (b) the electrocardiogram during the follow-up examination two months later. (B) The results of the patient's first coronary angiography are as follows: (a) The left anterior descending artery (LAD) mid-segment with approximately 95% stenosis, (b) The left circumflex artery (LCX) mid-distal segment with approximately 70% stenosis, (c) The dominant second obtuse marginal branch (OM2) proximal segment with approximately 90% stenosis, and (d) The right coronary artery (RCA) mid-segment with approximately 90% stenosis. The patient underwent the first-stage percutaneous coronary intervention (PCI) in the (e) LAD, (f) LCX, and OM2. A second-stage PCI was performed 7 days later, involving (g) the RCA mid-segment with approximately 90% stenosis, and (h) stents were implanted. The areas indicated by the arrows in the figure represent vascular stenosis or locations where stents have been implanted.

150/90 mmHg. Furthermore, he was diagnosed with primary hyperthyroidism 20 years ago and treated with radioactive iodine (I^{131}). However, his thyroid hormone levels were not rechecked.

Physical examination was normal except for high blood pressure (156/91 mmHg) and obesity (BMI = 34.37 kg/m^2). The results of the laboratory tests revealed that the patient has mild mix dyslipidemia (low-density lipoprotein 4.34 mmol/L, normal range:1–3.37 mmol/L; high-density lipoprotein 1.41 mmol/L, normal range:1.04–2.08 mmol/L; total cholesterol 7.64 mmol/L, normal range:2.9–5.18 mmol/L; triglycerides 3.66 mmol/L, normal range:0.4–1.7 mmol/L). Biochemical markers of myocardial injury included high-sensitivity troponin T (hs-TnT) mildly elevated (0.02 ng/ml, normal range <0.014), along with normal levels of creatine kinase isoenzymes (CK-MB) and myoglobin. Blood counts, serum electrolytes, fasting plasma glucose, glycated hemoglobin, liver and renal function tests, viral markers, a coagulation profile and were within normal limits. The electrocardiogram revealed ST-segment depression exceeding 0.05mv in leads II, V3-V6, accompanied by T-wave inversion (Figure 1A). Echocardiography indicated normal left ventricular systolic function but a slight decline in diastolic function with left atrial enlargement (Table 1).

Other laboratory investigations revealed decreased T3 (1.10 pg/ml, normal range: 1.8–3.8 pg/ml), decreased T4 (<0.1 ng/dl, normal range: 0.78–1.86 ng/dl), and elevated TSH (56.669 mIU/L, normal range: 0.38–5.57 mIU/L), accompanied by an increased level of thyroid peroxidase antibody. These findings suggest post-radioiodine hypothyroidism in the patient.

He underwent elective coronary angiography, which unveiled multi-vessel coronary artery stenosis by physician visual assessment (Figure 1B). The SYNTAX (Synergy Between Percutaneous Coronary Intervention with Taxus and Cardiac Surgery) score was 15, indicating a moderate level of complexity in the coronary artery disease. Subsequently, the patient agreed to undergo the first stage percutaneous coronary intervention (PCI) in the LAD and OM2. A second-stage PCI for the RCA was performed 7 days later (Figure 1B). The post-procedure hs-TnT measured 0.018 ng/ml, with normal CK-MB and myoglobin, and did not significantly change during the admission.

To evaluate the patient's myocardial fibrosis, a ^{68}Ga-FAPI-04 PET/CT examination was conducted the day following the first stage PCI (Figure 2A). The results revealed elevated FAPI uptake in the left ventricular myocardium, specifically in the apex,

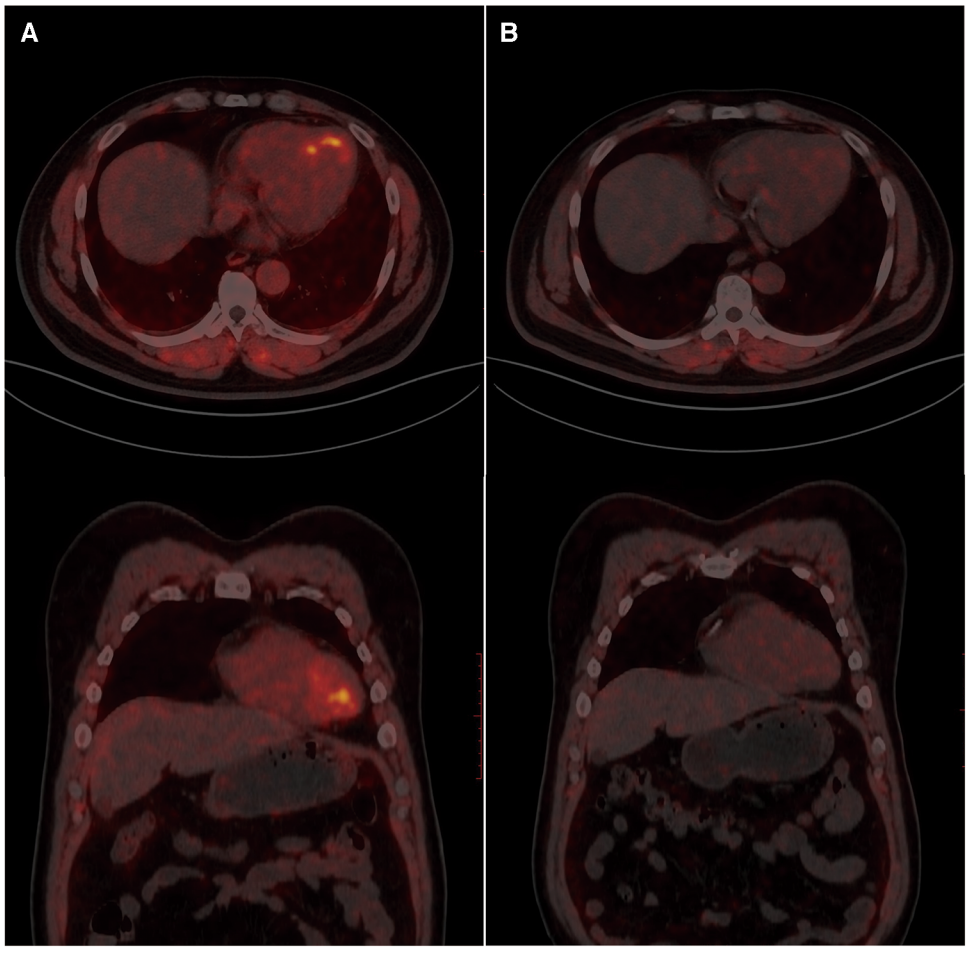

FIGURE 2
^{68}Ga-FAPI-04 PET/CT myocardial imaging. A. Examination results one day after postoperative PCI. B. Follow-up examination results after two months.

TABLE 1 Two-dimensional data from the echocardiogram.

	Upon admission	2 months later
LA (mm)	44	39
LVDd (mm)	43	52
LVDs (mm)	28	35
IVS (mm)	12	12
LVPW (mm)	10	12
RA (mm)	47 × 35	40 × 27
RV (mm)	21	24
LVEF (%)	65	62
E/e'	9.88	20

LA, left atrial diameter; LVDd, left ventricular end-diastolic diameter; LVDs, left ventricular end-diastolic diameter; IVS, interventricular septum; LVPW, left ventricular posterior wall at end-diastole; RA, suitable atrium diameter; RV, right ventricular diameter; LVEF, left ventricular ejection fraction; E/e', ratio of the early transmitral blood flow velocity to early diastolic velocity of the mitral annulus.

anterior wall, and septum, with an SUVmax (maximum standard uptake value) of approximately 4.6, consistent with the distribution of the LAD. Considering the link between ischemia and active fibroblast in pathophysiology, we hypothesize that the LAD is more likely to be the "culprit vessel" during the patient's angina attacks, while the RCA and LCX may be considered as "bystanders." Subsequently, the patient daily received aspirin 100 mg and ticagrelor 180 mg for antiplatelet aggregation therapy, atorvastatin 20 mg and hybutimibe 10 mg for hypolipidemic therapy, sacubitril/valsartan 100 mg for antihypertensive therapy, and levothyroxine sodium tablets 50 μg for thyroid hormone supplementation. During follow-up, the patient remained free of chest pain, adhered to medication, and maintained blood pressure within the range of 120–130/70–80 mmHg.

Two months later, the patient's ECG was normal (Figure 1A), cardiac injury markers and thyroid function were normal, and there was some improvement in dyslipidemia (low-density lipoprotein 1.36 mmol/L, high-density lipoprotein 1.06 mmol/L, total cholesterol 2.87 mmol/L, triglycerides 2.15 mmol/L). A follow-up ^{68}Ga-FAPI PET/CT examination (Figure 2B) revealed a slight increase in FAP expression in a smaller localized area of the left ventricular apex, with an SUVmax of approximately 1.8. The rest of the myocardium exhibited uniform tracer uptake similar to blood pool activity. Compared to the initial examination, the extent of ^{68}Ga-FAPI04 uptake in the left ventricular myocardium significantly decreased, and the SUVmax notably reduced. Meanwhile, echocardiographic measurements showed mild enlargement of the left ventricle within the normal range, with unaffected systolic function (Table 1).

Discussion

The radiotracer ^{68}Ga-FAPI-04 can selectively target FAP and visualize activated fibroblasts. In this case, the left ventricular myocardium displayed focal uptake of ^{68}Ga-FAPI-04 (SUVmax = 4.6), indicating the detection of active fibroblasts caused by transient myocardial ischemia was sensitive. Compared to previous studies on MI, the myocardial uptake in the UA patient was lower, potentially indicating a correlation with the extent of myocardial damage (10).

After a 2-month follow-up, a repeat ^{68}Ga-FAPI-04 PET/CT revealed a significant decrease in tracer uptake in the previously affected area, without new uptake sites. The echocardiogram revealed mild left ventricular enlargement at the same time. Notably, healthy myocardium and mature myocardial scars, lacking active fibroblasts, do not exhibit uptake of ^{68}Ga-FAPI-04 (11). This suggests that ^{68}Ga-FAPI-04 PET/CT can provide early information on myocardial fibrosis, and has a certain predictive effect on ventricular remodeling, serving as a supplementary tool to traditional exams. On the other hand, ^{68}Ga-FAPI-04 PET/CT provides insights into treatment efficacy by assessing activated fibroblasts. The patient underwent interventional therapy to address vascular narrowing and received pharmaceutical intervention for thrombosis prevention and the management of coronary risk factors, including hyperlipidemia, hypertension, andhypothyroidism. Upon reevaluation, the absence of newly activated fibroblasts suggested no recent myocardial ischemic damage, further supporting the treatment's effectiveness. In contrast, according to another study, it has been observed that a single case showed detectable high expression of FAP even 2 months after acute myocardial infarction. This difference may be associated with the distinct disease stages that the patients are in (acute phase and relatively stable phase) as well as the complete relief of myocardial ischemia (12). Therefore, more extensive cohort studies are warranted to explore further the degree, development, and outcome of myocardial fibrosis activated by different degrees of myocardial ischemia.

Furthermore, we observed concentrated ^{68}Ga-FAPI-04 uptake corresponding to the myocardial ischemia territory supplied by the LAD in this case. Historically, myocardial perfusion imaging was employed to assess myocardial ischemia by observing myocardial blood flow distribution. However, it was susceptible to physiological parameters such as heart rate during the examination. The imaging process was time-consuming, required pharmacologic stress, and was unsuitable for patients in danger (13). In contrast, the examination protocol for ^{68}Ga-FAPI-04 PET/CT is safer, being conducted an hour post-tracer injection (14). When referring to other molecular imaging, such as ^{18}F-FDG PET, determines viability of myocytes by visualizing uptake of radiolabelled glucose analogue, rather than fibrotic tissue in imaging (6). The ^{68}Ga-FAPI-04 PET/CT can not only conveniently provide areas of myocardial ischemia, but also provide fibrosis information, offering a potentially valuable means of detecting myocardial damage for patients who cannot tolerate traditional examinations and those with asymptomatic coronary artery disease.

Conclusion

We have demonstrated the feasibility of employing ^{68}Ga-FAPI-04 PET/CT to assess early myocardial fibrosis and pinpoint affected myocardium in patients with unstable angina (UA). FAP-targeted imaging holds promise as a novel biomarker for ventricular remodeling, complementing existing

techniques. Moreover, it offers potential guidance for future studies on anti-fibrotic interventions.

Data availability statement

The original contributions presented in the study are included in the article/Supplementary Material, further inquiries can be directed to the corresponding author.

Ethics statement

The studies involving humans were approved by Clinical Trial Ethics Committee, Affiliated Hospital of Southwest Medical University, Luzhou. The studies were conducted in accordance with the local legislation and institutional requirements. The participants provided their written informed consent to participate in this study. Written informed consent was obtained from the individual(s) for the publication of any potentially identifiable images or data included in this article.

Author contributions

MJ: Writing – original draft. GZ: Writing – original draft. LL: Writing – review & editing. YH: Writing – review & editing. GL: Investigation, Writing – original draft. JY: Investigation, Writing – original draft. JF: Writing – review & editing. XL: Funding acquisition, Writing – review & editing.

Funding

The author(s) declare financial support was received for the research, authorship, and/or publication of this article.

This work was supported by the Sichuan Science and Technology Program Joint Innovation Project (2022YFS0627-B1), and Doctoral Research Initiation Fund of Affiliated Hospital of Southwest Medical University, China (Grant No.20118).

Acknowledgments

The author wishes to acknowledge the laboratory and radiology staff for providing pertinent clinical information to the authors.

Conflict of interest

The authors declare that the research was conducted in the absence of any commercial or financial relationships that could be construed as a potential conflict of interest.

Publisher's note

References

1. Smitherman TC. Unstable angina pectoris: the first half century: natural history, pathophysiology, and treatment. *Am J Med Sci.* (1986) 292:395–406. doi: 10.1097/00000441-198612000-00013

2. Frantz S, Hundertmark MJ, Schulz-Menger J, Bengel FM, Bauersachs J. Left ventricular remodelling post-myocardial infarction: pathophysiology, imaging, and novel therapies. *Eur Heart J.* (2022) 43:2549–61. doi: 10.1093/eurheartj/ehac223

3. Agmadova ZM, Kallaeva AN. Special characteristics of progression of myocardial remodeling in patients with various forms of unstable angina. *Kardiologiia.* (2014) 54:9–16. doi: 10.18565/cardio.2014.7.9-16

4. Weber KT, Sun Y, Bhattacharya SK, Ahokas RA, Gerling IC. Myofibroblast-mediated mechanisms of pathological remodelling of the heart. *Nat Rev Cardiol.* (2013) 10:15–26. doi: 10.1038/nrcardio.2012.158

5. Varasteh Z, Mohanta S, Robu S, Braeuer M, Li Y, Omidvari N, et al. Molecular imaging of fibroblast activity after myocardial infarction using a ^{68}Ga-labeled fibroblast activation protein inhibitor, FAPI-04. *J Nucl Med.* (2019) 60(12):1743–9. doi: 10.2967/jnumed.119.226993

6. Barton AK, Tzolos E, Bing R, Singh T, Weber W, Schwaiger M, et al. Emerging molecular imaging targets and tools for myocardial fibrosis detection. *Eur Heart J Cardiovasc Imaging.* (2023) 24(3):261–75. doi: 10.1093/ehjci/jeac242

7. Tillmanns J, Hoffmann D, Habbaba Y, Schmitto JD, Sedding D, Fraccarollo D, et al. Fibroblast activation protein alpha expression identifies activated fibroblasts after myocardial infarction. *J Mol Cell Cardiol.* (2015) 87:194–203. doi: 10.1016/j.yjmcc.2015.08.016

8. Lindner T, Loktev A, Altmann A, Giesel F, Kratochwil C, Debus J, et al. Development of quinoline-based theranostic ligands for the targeting of fibroblast activation protein. *J Nucl Med.* (2018) 59(9):1415–22. doi: 10.2967/jnumed.118.210443

9. Diekmann J, Koenig T, Thackeray JT, Derlin T, Czerner C, Neuser J, et al. Cardiac fibroblast activation in patients early after acute myocardial infarction: integration with MR tissue characterization and subsequent functional outcome. *J Nucl Med.* (2022) 63(9):1415–23. doi: 10.2967/jnumed.121.263555

10. Xie B, Wang J, Xi XY, Guo X, Chen BX, Li L, et al. Fibroblast activation protein imaging in reperfused ST-elevation myocardial infarction: comparison with cardiac magnetic resonance imaging. *Eur J Nucl Med Mol Imaging.* (2022) 49(8):2786–97. doi: 10.1007/s00259-021-05674-9

11. Notohamiprodjo S, Nekolla SG, Robu S, Villagran Asiares A, Kupatt C, Ibrahim T, et al. Imaging of cardiac fibroblast activation in a patient after acute myocardial infarction using ^{68}Ga-FAPI-04. *J Nucl Cardiol.* (2022) 29(5):2254–61. doi: 10.1007/s12350-021-02603-z

12. Kessler L, Kupusovic J, Ferdinandus J, Hirmas N, Umutlu L, Zarrad F, et al. Visualization of fibroblast activation after myocardial infarction using 68Ga-FAPI PET. *Clin Nucl Med.* (2021) 46(10):807–13. doi: 10.1097/rlu.0000000000003745

13. Tamarappoo B, Hachamovitch R. Myocardial perfusion imaging versus CT coronary angiography: when to use which? *J Nucl Med.* (2011) 52:1079–86. doi: 10.2967/jnumed.110.081133

14. Zhou Y, Yang X, Liu H, Luo W, Liu H, Lv T, et al. Value of [^{68}Ga]Ga-FAPI-04 imaging in the diagnosis of renal fibrosis. *Eur J Nucl Med Mol Imaging.* (2021) 48(11):3493–501. doi: 10.1007/s00259-021-05343-x

frontiers | Frontiers in Cardiovascular Medicine

TYPE Case Report
PUBLISHED 24 January 2024
DOI 10.3389/fcvm.2024.1340406

OPEN ACCESS

EDITED BY
Grigorios Korosoglou,
GRN Klinik Weinheim, Germany

REVIEWED BY
Wolfgang Fehske,
Independent Researcher, Germany
Alexandros Kallifatidis,
St. Luke's Hospital, Greece

*CORRESPONDENCE
Kyle W. Klarich
klarich.kyle@mayo.edu

RECEIVED 17 November 2023
ACCEPTED 03 January 2024
PUBLISHED 24 January 2024

CITATION
Akiki E, Arghami A, Abbasi MA, El-Am EA, Ahmad A, Foley TA, Daly RC, Maleszewski JJ, Kurmann R and Klarich KW (2024) Case Report: A myxoma with a far reach. Front. Cardiovasc. Med. 11:1340406. doi: 10.3389/fcvm.2024.1340406

Case Report: A myxoma with a far reach

Elias Akiki, Arman Arghami, Muhannad A. Abbasi, Edward A. El-Am, Ali Ahmad, Thomas A. Foley, Richard C. Daly, Joseph J. Maleszewski, Reto Kurmann and Kyle W. Klarich*

Department of Cardiovascular Medicine, Mayo Clinic, Rochester, MN, United States

A 73-year-old woman presented to the emergency department with a syncopal episode and a history of dizzy spells. A transthoracic echocardiogram demonstrated a large left atrial mass extending into the right upper pulmonary veins. Subsequently, cardiac magnetic resonance imaging and coronary computed tomography angiography with three-dimensional reconstruction and printing of the heart and mass were performed, which demonstrated a high index of suspicion for an atypical left atrial myxoma. The mass was excised robotically, and the pathology report confirmed a diagnosis of myxoma.

KEYWORDS

atypical myxoma, multimodal imaging, 3D reconstruction, pulmonary veins, cardiac MRI (CMRI), cardiac CT, echocardiography

Introduction

Cardiac myxoma is one of the most common primary cardiac neoplasms in adults, second only to papillary fibroelastomas (1). Patients with cardiac myxomas can present with a variety of symptoms such as chest pain, shortness of breath, palpitations, and embolic phenomena. Malaise or syncope was reported in 14% of patients in a case series describing 112 cases of left atrial myxoma (2).

Case report

History of presentation

A 73-year-old woman presented to an outside clinic complaining of dizzy spells leading to a single syncopal episode. Following the syncopal episode, she was taken to the emergency department (ED). She was noted to have supraventricular tachycardia (SVT). An echocardiogram demonstrated a left atrial mass. However, she did not report any symptoms such as chest pain, dyspnea, orthopnea, paroxysmal nocturnal dyspnea, palpitations, or irregular heart rhythm. She was referred to our institution for further evaluation and treatment of the mass.

Abbreviations
3D, three-dimensional; CCTA, coronary computed tomography angiography; CMRI, coronary magnetic resonance imaging; CT, computed tomography; ED, emergency department; MRI, magnetic resonance imaging; SVT, supraventricular tachycardia.

Past medical history

The patient had a history of type 2 diabetes mellitus (on oral agents), well-controlled systemic hypertension, hyperlipidemia, and bronchial asthma.

Investigations

Her physical examination was unremarkable, as exemplified by the fact that her heart sounds were normal. A brain magnetic resonance imaging (MRI) did not show signs of ischemia or prior infarction. An echocardiogram in the ED demonstrated a left atrial mass with a broad base attachment to the atrial septum (Figure 1) that extended from the opening of the pulmonary veins to the mitral annulus. Subsequent investigation with coronary computed tomography angiography (CCTA) revealed a 41 mm × 27 mm × 33 mm broad-based lobulated mass in the left atrium that extended onto the mitral annulus (Figure 2). The mass was isointense on T1-weighted images and hyperintense on T2-weighted images and showed restricted diffusion (Supplementary Figure S1). There was heterogeneous enhancement on both early and late postcontrast images. The findings were compatible with a cardiac myxoma (Supplementary Video S1).

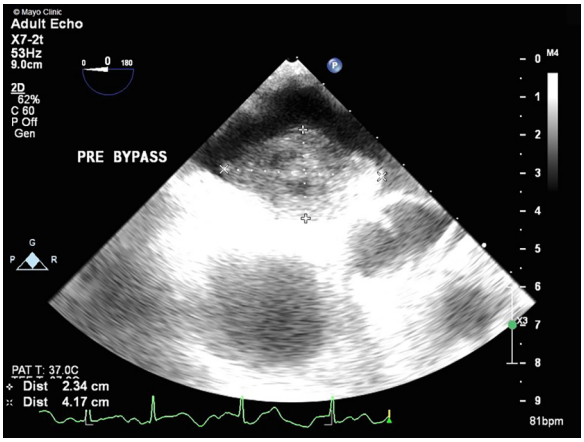

FIGURE 1
TEE showing a large mass (2.3 cm × 4.2 cm) with attachment to the left atrial side of the atrial septum.

Differential diagnosis

Cardiac myxoma; metastases from unknown primary; undifferentiated high-grade pleomorphic sarcoma; thrombus; leiomyosarcoma; lipoma.

Management

Following the reported imaging findings, a careful surgical plan was discussed with the multidisciplinary team for resection of the mass. A CCTA with a three-dimensional (3D) reconstruction of the mass, including a 3D-printed model of the patient's heart depicting the mass and relationship with adjacent structures, was obtained to help with surgical planning (Figure 3). The 3D CT model redemonstrated a polypoid, heterogeneously enhancing left atrial mass attached to the entire left side of the atrial septum and measuring approximately 44 mm × 28 mm × 40 mm. The appearance on the CCTA and the location were consistent with a cardiac myxoma. The mass occluded the right superior pulmonary vein ostium during the atrial systole phase. A large-caliber sinoatrial artery branch arising from the proximal segment

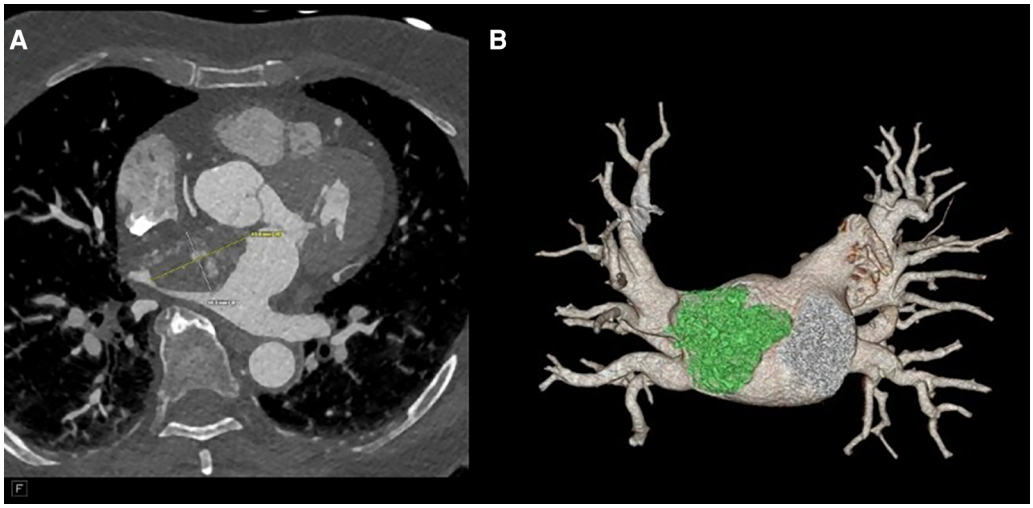

FIGURE 2
(A) CTA revealing a 41 mm × 27 mm × 33 mm broad-based lobulated mass in the left atrium that extends into the mitral annulus. (B) CTA reconstruction to show the mass extending to the right upper pulmonary vein (RUPV).

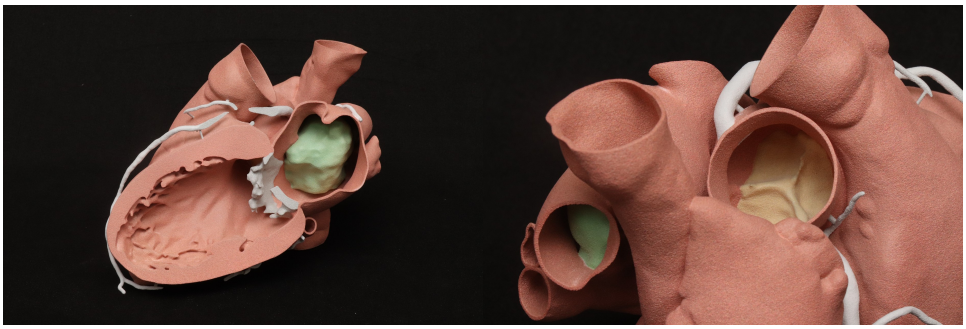

FIGURE 3
3D-printed models of the myxoma.

appeared to be the primary vascular supply to the mass. A transesophageal echocardiogram (TEE) was obtained, which confirmed that the mass was not adherent to the right superior pulmonary vein (Supplementary Videos S2, S3). Therefore, the patient was deemed to be a surgical candidate for a minimally invasive robotic approach given the location of the mass and the lack of adherence to the wall of the right superior pulmonary vein.

The patient underwent a robot-assisted minimally invasive mass resection. She was placed on cardiopulmonary bypass via the right femoral artery and vein. Access was obtained and the robot was docked to the right chest. After arresting the heart, we elected to access the left atrium via the right inferior pulmonary vein (as per visualization with the 3D-printed model), the point from which the tumor was furthest away. Upon entering the left atrium, a large tumor was identified, and care was taken not to disrupt the tumor. The mass was visualized and was easily separated from the atrial septum (Supplementary Video S4). A partial thickness of the atrial septum was resected along with the mass. The tumor had a gelatinous quality, consistent with that of a myxoma, and was sent to pathology for confirmation (Supplementary Figure S2). In the frozen section, the tumor was reported to be a highly undifferentiated malignant tumor that was adjacent to the line of resection. By the time the frozen section results became available, the atrium had been closed and the cross-clamp was removed, but the patient remained cannulated. With the findings of the pathology, it was decided to reinitiate the cardiopulmonary bypass and arrest the heart again, in order to resect the atrial septum at the foramen ovale, given the potential malignant nature of the tumor. The systemic margins alongside the septum were sent to pathology for evaluation, and the results were negative for malignancy. The atrial septum was closed with a bovine pericardial patch. The patient was extubated in the operating room and had an uncomplicated recovery in the hospital, following which she was discharged 5 days later. The final pathology report confirmed a cardiac myxoma with no malignancy (Supplementary Figure S3). The margins were uninvolved. The tumor cells were shown to be reactive with antibodies directed against PRKAR1A, in keeping with a non-syndromic cardiac myxoma. No complications were encountered by the patient in the postoperative phase.

Discussion

Cardiac myxomas usually (>90%) occur in an isolated fashion, but rarely, they can also occur in a syndromic context, as part of the Carney complex, an autosomal-dominant condition (3). Cardiac myxomas occurring as part of the Carney complex are termed "syndromic myxomas" and are associated with mutations in *PRKAR1A* (4). In addition to cardiac myxomas, the syndrome is associated with extracardiac myxomas, endocrinopathy, and spotty skin pigmentation (lentiginoses). Cardiac myxomas occurring in the Carney complex are more likely to occur in atypical (non-left atrial) locations, be multiple, and occur earlier in life. Immunohistochemical staining from our patient's myxoma showed positive results for PRKAR1A, but the patient did not have any dermatological manifestations associated with a Carney complex or a history of other tumors.

Myxomas are often initially diagnosed by echocardiography. The classic presentation is a mobile mass on a stalk arising from the atrial septum. In our patient, a TEE was done prior to surgery to assess hemodynamic function. A cavitated sessile mass arising from the atrial septum was seen. The mass did not have a stalk and exhibited contrast within the body of the tumor. The lack of a stalk from which the tumor arose and its cavitated appearance were atypical for a myxoma, warranting further investigation and planning prior to resection. The mass also extended upward into the right pulmonary veins, which is extremely uncommon. Cardiac MRI (CMRI) often complements echocardiography and offers improved tissue characterization, with cardiac myxomas typically demonstrating hypointensity on T1 images, hyperintensity on T2 images, and little to no perfusion or late enhancement (5). T1- and T2-weighted double-recovery sequences aid tissue characterization. Furthermore, cine cardiac imaging holds great importance in evaluating atrial myxomas because of their high mobility and their tendency to prolapse through the atrioventricular valve during diastole (6). Contrast-enhanced sequences are crucial in distinguishing myxomas from thrombus, as myxomas typically exhibit minimal or nil enhancement during first-pass perfusion, yet display a more heterogeneous enhancement pattern on late gadolinium enhancement (LGE) imaging (7). In our case, the patient's

cardiac MRI scan did show findings consistent with those of a myxoma, but it revealed more enhancement than is typical. Cardiac MRI has shown remarkable accuracy in identifying cardiac masses and effectively differentiating between benign and malignant tumors. However, relying solely on MRI has been associated with occasional instances of inaccurate diagnosis. Therefore, adopting a multimodal imaging approach comprising echocardiography, MRI, CT, and possibly positron emission tomography (PET) imaging offers an optimal approach for a comprehensive evaluation and stratification of cardiac masses (8). Given the atypical characteristics and location of our patient's left atrial mass, a CT angiogram with a 3D reconstruction of the heart depicting the mass was requested to guide the diagnosis and surgical planning. The mass was heterogeneously enhancing and polypoid in shape. The mass did not infiltrate or invade surrounding structures. This observation holds considerable significance as it reduces the likelihood of the tumor being a malignant one (9). However, it did extend to the ostium of the right superior pulmonary vein, occluding it during atrial systole. It is hard to ascertain whether the mass was the source of our patient's symptoms, but these findings could potentially explain the patient's orthostatic syncope and dizziness. A case report in the literature describes a patient presenting with syncope and dyspnea, who was found to have a left atrial myxoma extending into and occluding the left pulmonary veins and causing pulmonary infarction (10). However, in our patient, the mass did not extend or occlude the mitral valve, which made it feasible to adopt a robotic approach. Furthermore, the mass received blood supply from the small sinoatrial node branch of the right coronary artery. This was visualized precisely and with high spatial resolution on the 3D-printed model, which also showed the extent of expansion of the mass into the right upper pulmonary veins (Figure 4). The printed model also provided for visualization of the best approach to enter the left atrium without disruption of the mass. A possible implication of this occurrence is the formation of a fistula between the sinoatrial nodal artery and the right atrium after surgical resection of the atrial myxoma. For this reason, special attention should be paid to ligating neovascularized branches feeding myxomas during the surgical procedure (11).

FIGURE 4
A 3D-printed model showing blood supply to the myxoma in the RUPV.

Conclusion

This study described a peculiar and unique presentation of a left atrial myxoma extending into the right upper pulmonary veins. Multimodal imaging, including 3D reconstruction and printing of the heart and mass, guided the diagnostic approach and successful resection of the mass by robotic intervention.

Data availability statement

The original contributions presented in the study are included in the article/**Supplementary Material**, and further inquiries can be directed to the corresponding author.

Ethics statement

Written informed consent was obtained from the individual(s) for the publication of any potentially identifiable images or data included in this article.

Author contributions

EA: Writing – original draft, Writing – review & editing. AAr: Writing – review & editing. MA: Writing – review & editing. EE: Writing – review & editing. AAh: Writing – review & editing. TF: Writing – review & editing. RD: Writing – review & editing. JM: Writing – review & editing. RK: Writing – review & editing. KK: Writing – review & editing.

Funding

The authors declare that no financial support was received for the research, authorship, and/or publication of this article.

Conflict of interest

The authors declare that the research was conducted in the absence of any commercial or financial relationships that could be construed as a potential conflict of interest.

Publisher's note

All claims expressed in this article are solely those of the authors and do not necessarily represent those of their affiliated

organizations, or those of the publisher, the editors and the reviewers. Any product that may be evaluated in this article, or claim that may be made by its manufacturer, is not guaranteed or endorsed by the publisher.

Supplementary material

The Supplementary Material for this article can be found online at: https://www.frontiersin.org/articles/10.3389/fcvm.2024.1340406/full#supplementary-material

SUPPLEMENTARY FIGURE S1
Cardiac MRI images depicting (A) T1-weighted and (B) T2-weighted sequences.

SUPPLEMENTARY FIGURE S2
Gross photograph of a resected cardiac tumor. (A) The tumor has a lobulated morphology and (B) in the cut section has a gelatinous quality.

SUPPLEMENTARY FIGURE S3
Photomicrograph of a resected cardiac tumor. (A) Hematoxylin and eosin staining discloses bland spindle-shaped cells, occurring singly and in small clusters, proliferating in a myxoid background, consistent with a cardiac myxoma. (B) The neoplastic cells are reactive with antibodies directed against PRKAR1A, suggesting a non-syndromic tumor.

SUPPLEMENTARY VIDEO S1
A four-chamber view shows the entire left atrial septum being engulfed by the large mass and extending up and into the right upper pulmonary vein.

SUPPLEMENTARY VIDEO S2
A TEE of a myxoma four-chamber. (A) A demonstration of the entire left atrial septum being engulfed by the tumor mass. (B) A zoom view showing flow within the mass by a color Doppler.

SUPPLEMENTARY VIDEO S3
A TEE at 70°–88° showing the myxoma filling the right superior pulmonary vein (A); color (B) freely moving and color flow around the mass.

SUPPLEMENTARY VIDEO S4
A robot-assisted minimally invasive resection of an atypical left atrial myxoma.

References

1. Tamin SS, Maleszewski JJ, Scott CG, Khan SK, Edwards WD, Bruce CJ, et al. Prognostic and bioepidemiologic implications of papillary fibroelastomas. *J Am Coll Cardiol*. (2015) 65(22):2420–9. doi: 10.1016/j.jacc.2015.03.569

2. Pinede L, Duhaut P, Loire R. Clinical presentation of left atrial cardiac myxoma: a series of 112 consecutive cases. *Medicine (Baltimore)*. (2001) 80(3):159–72. doi: 10.1097/00005792-200105000-00002

3. Jain S, Maleszewski JJ, Stephenson CR, Klarich KW. Current diagnosis and management of cardiac myxomas. *Expert Rev Cardiovasc Ther*. (2015) 13 (4):369–75. doi: 10.1586/14779072.2015.1024108

4. Maleszewski JJ, Larsen BT, Kip NS, Castonguay MC, Edwards WD, Carney JA, et al. PRKAR1A in the development of cardiac myxoma: a study of 110 cases including isolated and syndromic tumors. *Am J Surg Pathol*. (2014) 38(8):1079–87. doi: 10.1097/PAS.0000000000000202

5. Kurmann R, El-Am E, Ahmad A, Abbasi MA, Mazur P, Akiki E, et al. Cardiac masses discovered by echocardiogram; what to do next? *Struct Heart*. (2023) 7 (4):100154. doi: 10.1016/j.shj.2022.100154

6. Abbas A, Garfath-Cox KA, Brown IW, Shambrook JS, Peebles CR, Harden SP. Cardiac MR assessment of cardiac myxomas. *Br J Radiol*. (2015) 88(1045):20140599. doi: 10.1259/bjr.20140599

7. Fussen S, De Boeck BW, Zellweger MJ, Bremerich J, Goetschalckx K, Zuber M, et al. Cardiovascular magnetic resonance imaging for diagnosis and clinical management of suspected cardiac masses and tumours. *Eur Heart J*. (2011) 32 (12):1551–60. doi: 10.1093/eurheartj/ehr104

8. Giusca S, Kelle S, Korosoglou G. When tissue and outcomes are the issue. Cardiac magnetic resonance for patients with suspected cardiac tumours. *Eur Heart J*. (2021) 43(1):81–3. doi: 10.1093/eurheartj/ehab625

9. Avranas K, Eisenbach C, Flechtenmacher C, Korosoglou G. Diagnostic pathway from incidental mass to metastatic melanoma. *JACC Case Rep*. (2024) 29(1):102146. doi: 10.1016/j.jaccas.2023.102146

10. Stevens LH, Hormuth DA, Schmidt PE, Atkins S, Fehrenbacher JW. Left atrial myxoma: pulmonary infarction caused by pulmonary venous occlusion. *Ann Thorac Surg*. (1987) 43(2):215–7. doi: 10.1016/S0003-4975(10)60401-8

11. Roth JE, Conner WC, Porisch ME, Shry E. Sinoatrial nodal artery to right atrium fistula after myxoma excision. *Ann Thorac Surg*. (2006) 82(3):1106–7. doi: 10.1016/j.athoracsur.2006.01.067

frontiers | Frontiers in Cardiovascular Medicine

TYPE Case Report
PUBLISHED 13 February 2024
DOI 10.3389/fcvm.2024.1344975

OPEN ACCESS

EDITED BY
Riccardo Liga,
Pisana University Hospital, Italy

REVIEWED BY
Vermes Emmanuelle,
Centre Hospitalier Universitaire (CHU) d'Amiens, France
Giulia Iannaccone,
Catholic University of the Sacred Heart, Rome, Italy

*CORRESPONDENCE
Fang Liu
fliu2084@126.com

RECEIVED 27 November 2023
ACCEPTED 25 January 2024
PUBLISHED 13 February 2024

CITATION
Kong L-Y, Cui X-Z, Xiang W, Wang X-J and Liu F (2024) Case report: Primary pericardial angiosarcoma, a rare cause of cardiac tamponade.
Front. Cardiovasc. Med. 11:1344975.
doi: 10.3389/fcvm.2024.1344975

Case report: Primary pericardial angiosarcoma, a rare cause of cardiac tamponade

Ling-Yun Kong, Xiao-Zheng Cui, Wei Xiang, Xiu-Juan Wang and Fang Liu*

Cardiovascular Center, School of Clinical Medicine, Beijing Tsinghua Changgung Hospital, Tsinghua University, Beijing, China

Primary pericardial angiosarcoma is a rare malignancy of the pericardium with variable clinical features and imaging characteristics. Herein, we report a case of histopathologically confirmed pericardial angiosarcoma in a 66-year-old man. The patient developed cardiac tamponade in a short time period. The transthoracic echocardiography showed the presence of multiple irregular echodensities, heterogeneous in echogenicity, encasing the apex of both ventricles in the pericardial space, initially misinterpreted as pericardial effusion. The patient died of cardiogenic shock despite undergoing a surgical pericardiectomy. Pericardial angiosarcoma can manifest as a mass obliterating the pericardial sac, rather than the typical pericardial effusion observed on echocardiography. Multimodality imaging studies aid in diagnosing primary pericardial angiosarcoma, but the final diagnosis relies on tissue histopathology.

KEYWORDS

pericardial neoplasm, pericardial angiosarcoma, cardiac tamponade, echocardiography, outcome

Introduction

Primary pericardial angiosarcoma is a rare malignancy of the pericardium. Its clinical features and imaging characteristics are variable. We report a case of an adult male who developed primary pericardial angiosarcoma, diagnosed 3 years after resection of colon carcinoma, and describe the multimodality imaging findings including unusual characteristics on echocardiography.

Case presentation

A 69-year-old male exhibited symptoms of fever, dry cough, and dyspnoea for a duration of 3 weeks. His past medical history included an uneventful surgery for a well-differentiated carcinoma of the colon (T1bN0M0, stage IA) 3 years ago, as well as hypertension and hyperlipidaemia. He quit cigarette smoking 20 years ago. No particular social history or family history of cancer was reported. A physical examination at admission revealed a body temperature of 37.6°C, a pulse rate of 109 beats per minute, a respiratory rate of 25 breaths per minute, and a blood pressure of 108/75 mmHg. The physical exam was otherwise unremarkable, except for tachycardia and muffled heart sounds. The laboratory findings showed leucocytosis (9.94×10^9/L) with neutrophilia (77.8%), an elevated C-reactive protein level (108.12 mg/L), and an elevated erythrocyte sedimentation rate (89 mm/h). The level of hypersensitivity cardiac troponin-T was

mildly elevated at 0.04 ng/ml (reference range 0–0.024 ng/ml). The electrocardiogram showed sinus tachycardia. Transthoracic echocardiography demonstrated a normal left ventricular ejection fraction (63%) and bi-atrial enlargement. Heterogeneous echodensities in the apical pericardial space were noted (Figures 1A,B). Chest computed tomography (CT) after admission revealed newly developed pulmonary and hepatic lesions compared with the CT findings 1 year prior, when he had regular post-operation follow-up for colon cancer. The CT scan also revealed a heterogeneous mass located on the right side, lateral to the pericardium, which is larger than that observed 2 weeks prior on the outpatient CT scan (Figures 1C,D). Enhanced abdominal magnetic resonance imaging revealed multiple lesions in the liver and vertebral bodies (Figures 1E,F), which also included part of the heart and revealed ill-defined solid lesions involving the pericardial sac. The patient developed worsening dyspnoea, hypotension, and tachycardia and subsequently underwent a surgical pericardiectomy 25 days after admission. The pericardial space was found to be severely constricted by the haemorrhagic tumour tissues, but no pericardial effusion was present (Figure 1G). A palliative partial pericardiectomy was performed as the tumour had already infiltrated the myocardium and was unresectable. The diagnosis of pericardial angiosarcoma was confirmed through post-operative pathology of the pericardial tissue (Figure 1H), characterized by vimentin (+), AE1/AE3 (−), CD31 (+), CD34 (+), EMA (−), D2-40 (partially+), calretinin (−), and Ki-67 (25%+) on immunohistochemistry. Unfortunately, the patient died on the 12th day after the surgery due to cardiogenic shock and cardiac arrest. Table 1 lists the timeline and clinical course of the patient.

TABLE 1 Timeline of the patient.

Timepoint	Event
3 years ago	The patient received an uneventful surgery for a well-differentiated carcinoma of the colon (T1bN0M0, stage IA).
1 year ago	The patient was asymptomatic and underwent chest CT for colon cancer surveillance.
3 weeks ago	The patient developed recurrent fever, cough and dyspnea.
Day 1 (hospital presentation)	The patient was admitted for fever, cough, and dyspnoea. Empirical treatment with antibiotics was ineffective. He underwent echocardiography, chest computed tomography, and enhanced abdominal magnetic resonance imaging examinations.
Day 25	The patient underwent partial pericardiectomy as the tumor was inseparable from the myocardium, and no pericardial effusion was found.
Day 37	The patient died of cardiogenic shock.

Discussion

Angiosarcomas are the most commonly reported primary malignant cardiac tumours, but primary pericardial angiosarcomas are extremely rare (1). Pericardial angiosarcoma has an insidious but aggressive nature. It is often diagnosed at a late stage. In our case, the pericardial angiosarcoma was diagnosed by surgical histopathology. Due to the patient's history of colon cancer and newly diagnosed metastatic lesions involving the liver and vertebrae, metastatic pericardial malignancy from colon cancer was at the top of our differential diagnoses. However, the pathological analysis showed no evidence of colon cancer metastasis but primary angiosarcoma involving the pericardium. The metastatic lesions

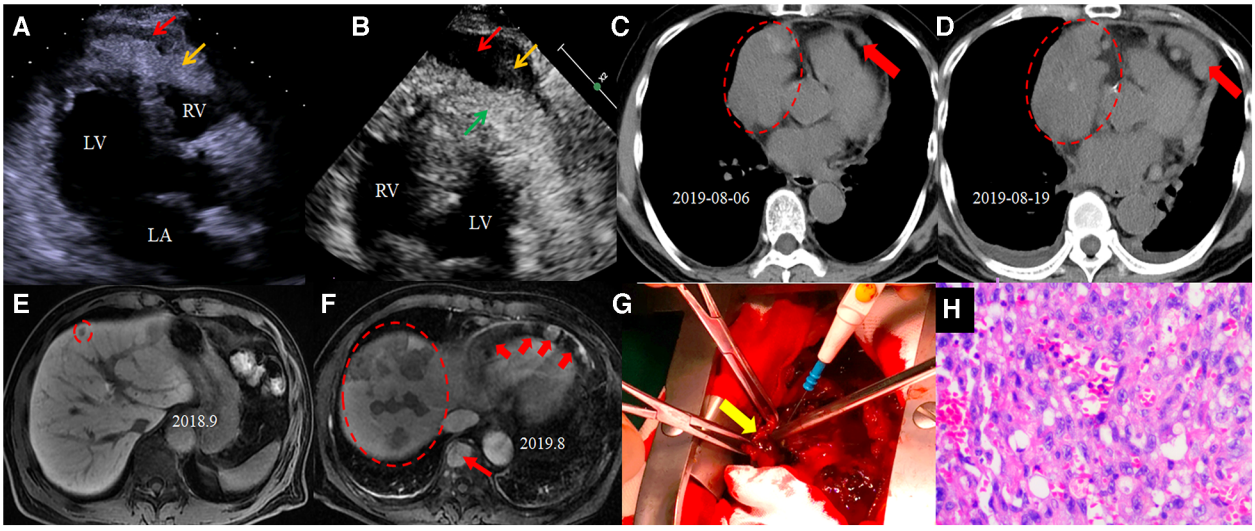

FIGURE 1
Iconography of the patient. The echocardiogram shows an echolucency (red arrow) and heterogeneous echodensities (yellow arrow) in the pericardial space in parasternal long axis view (A) and in apical four-chamber view (B) Chest CT (C) before admission reveals a heterogeneous mass (dotted ellipse) and pericardial nodules (red arrow). The repeat CT after admission (D) reveals an enlarged pericardial mass (dotted ellipse) and nodules (red arrow). The abdominal magnetic resonance hepatobiliary phase 1 year ago shows a low-signal nodule in the liver (dotted ellipse) on T2 weighted image. The magnetic resonance after this admission (F) shows multiple lesions involving the liver (dotted ellipse), spine (thin arrow), and pericardium (thick arrow). The gross specimen (G) shows a haemorrhagic solid tumour (yellow arrow) infiltrating the ventricular myocardium, and only partial pericardiectomy was performed. Histopathology (H) examinations confirmed the pericardial tissue to be angiosarcoma.

in the liver and the vertebrae could possibly come from the pericardial angiosarcoma, although no autopsy report is available to confirm this.

Pericardial angiosarcomas often manifest as pericardial effusions rather than a visible mass, posing a diagnostic challenge due to the possibility of other cardiac abnormalities also causing pericardial effusions (2, 3). Pericardial mesothelioma can also masquerade as pericardial effusion (3). Echocardiography is a readily available imaging modality for evaluating pericardial effusion (4). In our case, the primary pericardial angiosarcoma was echocardiographically characterized by pericardial effusion mixed with heterogeneous echodensities due to a tumour encasing the heart. The tumour growth into the pericardial space may be misinterpreted as a pericardial fat pad, which is a benign condition. Multimodality imaging is warranted (5, 6).

Conclusions

Pericardial angiosarcoma is a rare malignant pericardial neoplasm. It may manifest as a mass obliterating the pericardial sac, rather than pericardial effusion as usually seen on echocardiography. Multimodality imaging studies can assist in the diagnosis of primary pericardial angiosarcoma, but the final diagnosis relies on tissue histopathology.

Data availability statement

The raw data supporting the conclusions of this article will be made available by the authors, without undue reservation.

Ethics statement

The studies involving humans were approved by the Institutional Review Board of Beijing Tsinghua Changgung Hospital. The studies were conducted in accordance with the local legislation and institutional requirements. The participants provided their written informed consent to participate in this study.

Author contributions

L-YK: Conceptualization, Funding acquisition, Writing – original draft, Writing – review & editing. X-ZC: Conceptualization, Methodology, Validation, Visualization, Writing – review & editing. WX: Data curation, Resources, Validation, Writing – review & editing. X-JW: Data curation, Methodology, Validation, Writing – review & editing. FL: Supervision, Validation, Writing – review & editing.

Funding

The author(s) declare financial support was received for the research, authorship, and/or publication of this article.

This work was sponsored by Beijing Tsinghua Changgung Hospital Startup Foundation for Young Scientist (No. 12021C1004) and Beijing Hospitals Authority Youth Programme (No. QML20230901).

Acknowledgments

The authors thank the patient's family for granting permission to publish this report. We also thank Dr. Ruihai Zhou (Division of Cardiology, University of North Carolina at Chapel Hill) for his medical writing support.

Conflict of interest

The authors declare that the research was conducted in the absence of any commercial or financial relationships that could be construed as a potential conflict of interest.

Publisher's note

Supplementary material

The Supplementary Material for this article can be found online at: https://www.frontiersin.org/articles/10.3389/fcvm.2024.1344975/full#supplementary-material

SUPPLEMENTARY VIDEO S1
The apical four-chamber view shows heterogeneous echodensities in the pericardial space.

SUPPLEMENTARY VIDEO S2
The apical two-chamber view shows echolucency and heterogeneous echodensities in the pericardial space resembling effusion.

References

1. Guo Y, Liu Q, Wu H. Primary cardiac tumor: a case report of right atrial angiosarcoma and review of the literature. *Front Oncol*. (2023) 13:1164153. doi: 10.3389/fonc.2023.1164153

2. Schusler R, Meyerson SL. Pericardial disease associated with malignancy. *Curr Cardiol Rep*. (2018) 20(10):92. doi: 10.1007/s11886-018-1040-5

3. Kong L, Li Z, Wang J, Lv X. Echocardiographic characteristics of primary malignant pericardial mesothelioma and outcomes analysis: a retrospective study. *Cardiovasc Ultrasound*. (2018) 16(1):7. doi: 10.1186/s12947-018-0125-z

4. Adler Y, Charron P, Imazio M, Badano L, Barón-Esquivias G, Bogaert J, et al. 2015 ESC guidelines for the diagnosis and management of pericardial diseases: the task force for the diagnosis and management of pericardial diseases of the European Society of Cardiology (ESC) endorsed by the European Association for Cardio-Thoracic Surgery (EACTS). *Eur Heart J*. (2015) 36(42):2921–64. doi: 10.1093/eurheartj/ehv318

5. Zhao Y, Tian F, Ge Z, Pan C, Shu X. Multimodality imaging for the diagnosis of primary pericardial angiosarcoma. *Circ J*. (2023) 87(9):1250. doi: 10.1253/circj.CJ-23-0397

6. Senthil Kumaran S, Asif AA, Hussain H, Chatterjee T. Pericardial angiosarcoma: a diagnostic challenge. *Cureus*. (2021) 13(5):e15350. doi: 10.7759/cureus.15350

Frontiers in
Cardiovascular Medicine

Innovations and improvements in cardiovascular treatment and practice

Focuses on research that challenges the status quo of cardiovascular care, or facilitates the translation of advances into new therapies and diagnostic tools.

Discover the latest Research Topics

See more →

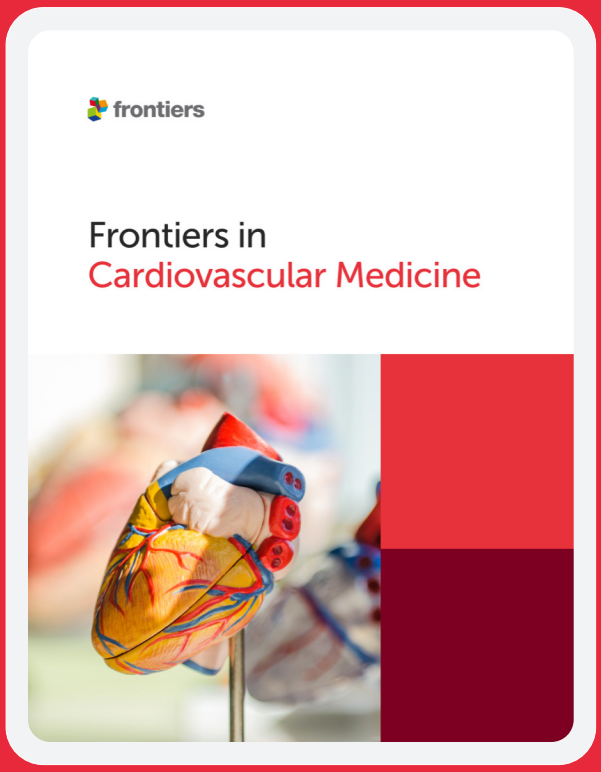

Frontiers

Avenue du Tribunal-Fédéral 34
1005 Lausanne, Switzerland
frontiersin.org

Contact us

+41 (0)21 510 17 00
frontiersin.org/about/contact